AD-A148 757 EXPLORATORY DEVELOPMENT OF ADVANCED SURFACE FLAW DETECTION METHODS(U) SOUTHWEST RESEARCH INST SAN ANTONIO TX R E BEISSNER ET AL. SEP 84 SWRI-15-7106 1/2

UNCLASSIFIED AFWAL-TR-84-4121 F33615-82-C-5020 F/G 21/5 NL

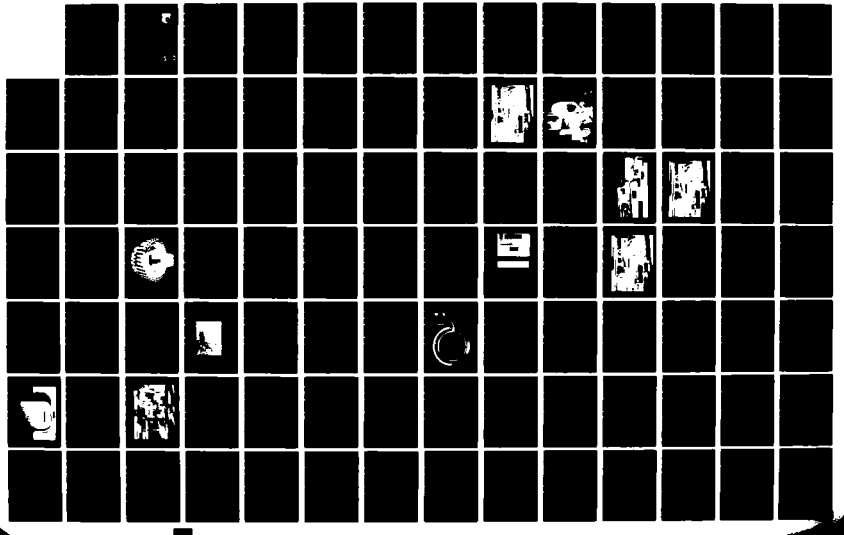

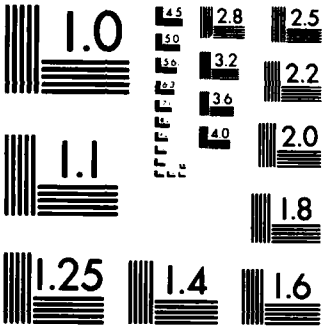

AFWAL-TR-84-4121

EXPLORATORY DEVELOPMENT OF ADVANCED SURFACE FLAW DETECTION METHODS

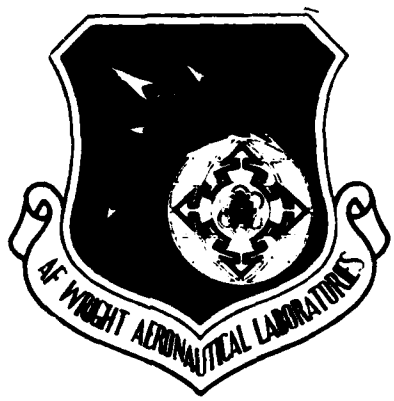

Robert E. Beissner
Gary L. Burkhardt
Felix N. Kusenberger

Southwest Research Institute
P.O. Drawer 28510
San Antonio, Texas 73284

September 1984

Final Report for Period 1 June 1982—31 October 1984

Approved for public release; distribution unlimited

MATERIALS LABORATORY
AIR FORCE WRIGHT AERONAUTICAL LABORATORIES
AIR FORCE SYSTEMS COMMAND
WRIGHT-PATTERSON AIR FORCE BASE, OHIO 45433

NOTICE

When Government drawings, specifications, or other data are used for any purpose other than in connection with a definitely related Government procurement operation, the United States Government thereby incurs no responsibility nor any obligation whatsoever; and the fact that the government may have formulated, furnished, or in any way supplied the said drawings, specifications, or other data, is not to be regarded by implication or otherwise as in any manner licensing the holder or any other person or corporation, or conveying any rights or permission to manufacture use, or sell any patented invention that may in any way be related thereto.

This report has been reviewed by the Office of Public Affairs (ASD/PA) and is releasable to the National Technical Information Service (NTIS). At NTIS, it will be available to the general public, including foreign nations.

This technical report has been reviewed and is approved for publication.

THOMAS J. MORAN
Nondestructive Evaluation Branch
Metals and Ceramics Division

FOR THE COMMANDER

D. M. FORNEY, JR., Chief
Nondestructive Evaluation Branch
Metals and Ceramics Division

"If your address has changed, if you wish to be removed from our mailing list , or if the addressee is no longer employed by your organization please notify AFWAL/MLLP, W-PAFB, OH 45433 to help us maintain a current mailing list".

Copies of this report should not be returned unless return is required by security considerations, contractual obligations, or notice on a specific document.

Unclassified

SECURITY CLASSIFICATION OF THIS PAGE *(When Data Entered)*

REPORT DOCUMENTATION PAGE

READ INSTRUCTIONS BEFORE COMPLETING FORM

1. REPORT NUMBER: AFWAL-TR-84-4121	2. GOVT ACCESSION NO.
3. RECIPIENT'S CATALOG NUMBER	
4. TITLE *(and Subtitle)*: Exploratory Development of Advanced Surface Flaw Detection Methods	5. TYPE OF REPORT & PERIOD COVERED: Final, 1 June 1982 - October 31, 1984
6. PERFORMING ORG. REPORT NUMBER: 15-7106	
7. AUTHOR(s): R.E. Beissner, G.L. Burkhardt and F.N. Kusenberger	8. CONTRACT OR GRANT NUMBER(s): F33615-82-C-5020
9. PERFORMING ORGANIZATION NAME AND ADDRESS: Southwest Research Institute, P.O. Drawer 28510, San Antonio, TX 78284	10. PROGRAM ELEMENT, PROJECT, TASK AREA & WORK UNIT NUMBERS
11. CONTROLLING OFFICE NAME AND ADDRESS: AFWAL/MLLP, Air Force Systems Command, Wright-Patterson AFB, Ohio 45433	12. REPORT DATE: September 1984
	13. NUMBER OF PAGES: 137
14. MONITORING AGENCY NAME & ADDRESS *(if different from Controlling Office)*	15. SECURITY CLASS. *(of this report)*: Unclassified
	15a. DECLASSIFICATION/DOWNGRADING SCHEDULE

16. DISTRIBUTION STATEMENT *(of this Report)*

Approval for public release, distribution unlimited

17. DISTRIBUTION STATEMENT *(of the abstract entered in Block 20, if different from Report)*

18. SUPPLEMENTARY NOTES

19. KEY WORDS *(Continue on reverse side if necessary and identify by block number)*

Nondestructive Evaluation (NDE)
Surface-Crack Detection
Eddy-Current Testing

20. ABSTRACT *(Continue on reverse side if necessary and identify by block number)*

Development of the electric current perturbation (ECP) method for application to surface flaw detection in the retirement-for-cause (RFC) inspection system is described. Physical constraints imposed by material properties and complex geometrical features of F100 engine parts are discussed as background for the selection and preparation of specimens for experimental optimization of ECP probe design. A laboratory breadboard system, which features a computer-controlled scanning mechanism and data acquisition system is also described and shown to be compatible with RFC system requirements. Experimental flaw

DD FORM 1 JAN 73 1473 EDITION OF 1 NOV 65 IS OBSOLETE

Unclassified

SECURITY CLASSIFICATION OF THIS PAGE *(When Data Enter*

20.

detection data are presented for simple laboratory specimens, specimens designed to simulate complex geometry features of concern in F100 engine inspection, and, finally, for actual engine parts. Specific features investigated were antirotation windows in the second-to-third stage fan seal, and scallops and blade slots in the first stage fan disk. Results demonstrate that the detection of flaws even smaller than 0.010 in. long by 0.005 in. deep is possible in blade slots. Also, from experimental data obtained in blade slot scans, preliminary estimates of the probability of detection as a function of flaw size are provided. Based on data reported here, it is concluded that the ECP method has been demonstrated with the breadboard system to have the inherent sensitivity and repeatability to meet RFC requirements regarding flaw detection capability and system compatibility, and is now ready for more extensive evaluation in an actual inspection environment.

PREFACE

This report describes work performed by Southwest Research Institute under Contract No. F33615-82-C-5020, SwRI Project No. 15-7106, "Exploratory Development on Advanced Surface Flaw Detection Methods". The contract period was June 1, 1982 through October 31, 1984. Project Manager at SwRI was Dr. R.E. Beissner.

TABLE OF CONTENTS

TABLE OF CONTENTS (Cont'd.)

LIST OF ILLUSTRATIONS

LIST OF ILLUSTRATIONS (Cont'd.)

LIST OF ILLUSTRATIONS (Cont'd.)

LIST OF TABLES

SECTION I

INTRODUCTION AND SUMMARY

1. Background

The retirement-for-cause (RFC) inspection system currently under development by the Air Force must reliably detect very small defects in complex geometry features of gas turbine engine components made of titanium alloys and nickel base alloys. The computer controlled, automated RFC inspection system will initially utilize conventional eddy current and ultrasonic nondestructive evaluation (NDE) techniques. However, advanced NDE methods are also being evaluated which may be incorporated later into the RFC system to improve reliability and sensitivity. One of these advanced methods is electric current perturbation (ECP) which was investigated in the present program as a possible surface flaw detection method for RFC.

The principle by which ECP detects flaws is illustrated in Figure 1. An electric current $\vec{j}_o$ is introduced in the region to be inspected, thus producing an associated magnetic flux density $\vec{B}_o$ above the surface of the piece as indicated in Figure 1a. If a flaw is present the current is perturbed by the flaw, Figure 1b, and the flux density is changed by an amount $\Delta\vec{B}$. Flaw detec-detection is accomplished by sensing this change in flux density $\Delta\vec{B}$, with a magnetic field sensing device.

In most applications the ECP method makes use of an induction coil, much like that of a conventional eddy current probe, to provide the unperturbed current density $\vec{j}o$ in the region to be inspected. However, unlike conventional eddy current, the use of a coil to induce an alternating current is not essential. As is documented in Appendix C, experiments have, in fact, been performed with direct current injection with results similar to those obtained by induction.

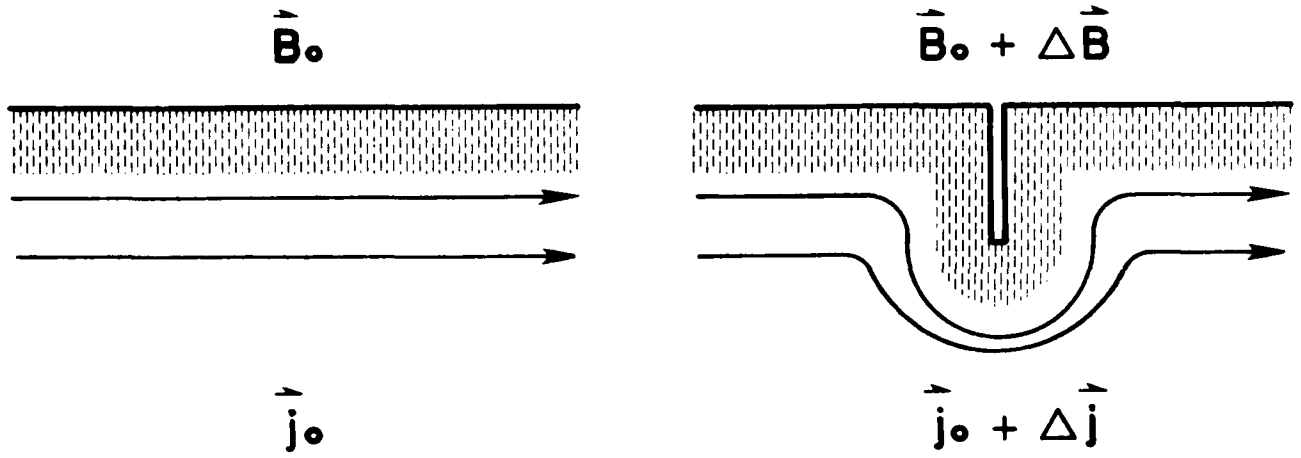

FIGURE 1. PRINCIPLE OF ELECTRIC CURRENT PERTURBATION FLAW DETECTION

Another similarity between the conventional eddy current and ECP methods is in the use of a coil, or a pair of coils, to measure the magnetic flux perturbation. Again, however, with the ECP method other types of sensors may be used. The data presented in Appendix C demonstrate the use of Hall effect sensors for magnetic field measurements and show, once again, that results are similar to those obtained with sensor coils.

In practice, one noticeable difference between the ECP and conventional eddy current methods is that the frequencies employed with ECP are almost always much lower. Thus, while many eddy current probes are designed for frequencies of several hundred kHz, ECP probes are normally used at frequencies less than about 100 kHz.

However, the most important difference between the ECP and conventional eddy current methods lies in the design of the sensor. ECP uses separate coils for the induction of current in the piece and for sensing magnetic field perturbations, with the sensor coil oriented in such a way as to minimize the influence of the unperturbed field B_o. In this way probe-to-surface coupling is minimized, and sensitivity to probe liftoff variations, which is a major source of noise with probes using conventional eddy current coil orientations, is greatly reduced. The end result is that ECP probes have excellent signal-to-noise characteristics which makes them well-suited to the detection of small surface flaws.

The ECP method has been under development at Southwest Research Institute for several years and has been the subject of extensive experimental and theoretical research[1-5]. It has been successfully applied to many complex inspection problems, often producing meaningful results where more conventional methods had failed. The ECP method is, therefore, a well-researched

technique of proven capability, and this is the principal reason it was chosen as a candidate method for the difficult inspection problems posed by RFC.

2. Objectives

The overall objective of this program was to develop the ECP surface flaw detection method to the stage where it is ready for incorporation into a prototype instrument for application to generic problems of the type encountered in engine disk RFC. The end-product is a laboratory breadboard instrument which was designed and built with the requirements of the automated RFC/NDE System under development by Systems Research Laboratory (SRL) and associated contractors as a guide.

Specific objectives were to:

1. Improve the reliability of detection of surface or near surface defects in complex geometry locations of engine components, for example antirotation windows, blade slots, boltholes, etc., as well as in uniform areas of regular geometry.
2. Provide a capability for high reliability detection of surface cracks 0.010 in. long by 0.005 in. deep or larger.

The principal tasks of the SwRI technical approach to accomplishing the program objectives were as follows:

Task I. Optimize Method

Determine the physical constraints imposed by the complex geometry and the materials in the inspection environment on the development of the ECP method and prepare specimens necessary for the optimization of inspection sensitivity and reliability under these physical constraints.

Task II. Construct and Evaluate Breadboard

Design and assemble a laboratory breadboard of an advanced ECP surface flaw detection system.

Task III. Demonstrate Breadboard

Evaluate and demonstrate the breadboard system.

3. Summary of Principal Results

Optimization of the ECP method for surface flaw detection is exemplified by the experimental results shown in Figure 2. These data wre obtained by scanning an ECP probe over a flat plate containing small artificial flaws. The prominent signal obtained from flaw No. 3 is typical of results obtained from flaws with dimensions somewhat greater than the RFC target flaw size. A more important point is, however, illustrated by the signals from flaws 1 and 2. These data show that the optimized ECP probe has the inherent sensitivity to detect flaws even smaller than the RFC target size. Thus, flaw detection capability is more than adequate to meet RFC program objectives.

The flaw areas noted in Figure 2 are interfacial areas, i.e. the planar areas that would be exposed if the specimen were fractured. These areas are listed in the figure because the ECP signal amplitude is directly proportional to flaw area. Both analytical modelling investigations and experimental observations[2], some of which are reported in Appendix C, have confirmed this proportionality. This is an important feature for RFC because it means that the ECP method can be used not only to detect, but also to determine the size and approximate configuration of small surface breaking cracks.

Figure 3 illustrates the capability of the ECP breadboard system to detect small flaws in actual engine parts. In this case the part is an F100 first stage fan disk, shown in Figure 4, and the flaws are located in blade slots.

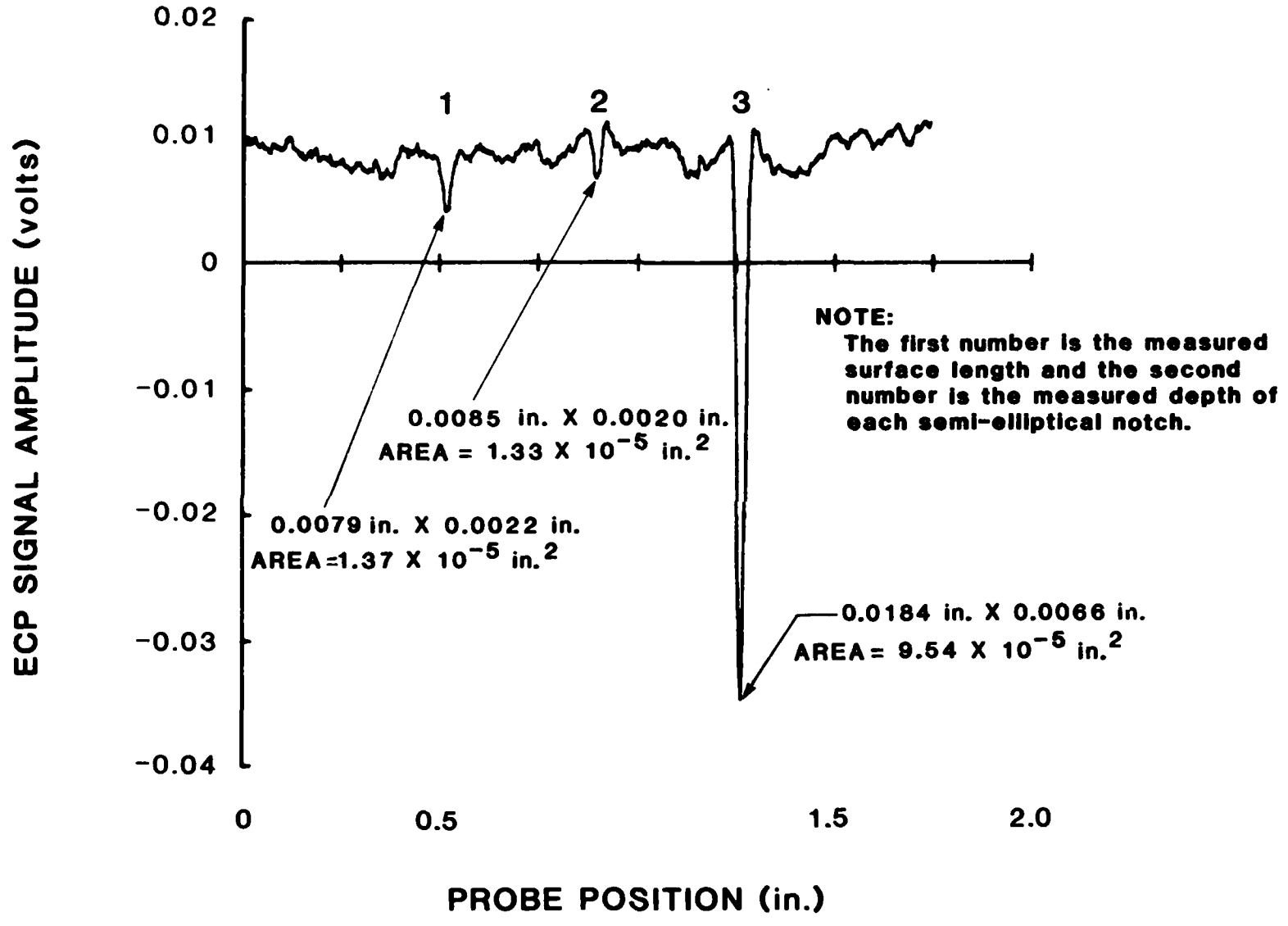

FIGURE 2. ECP SIGNALS FROM SMALL SURFACE EDM SLOTS IN TI 6-4 SPECIMEN

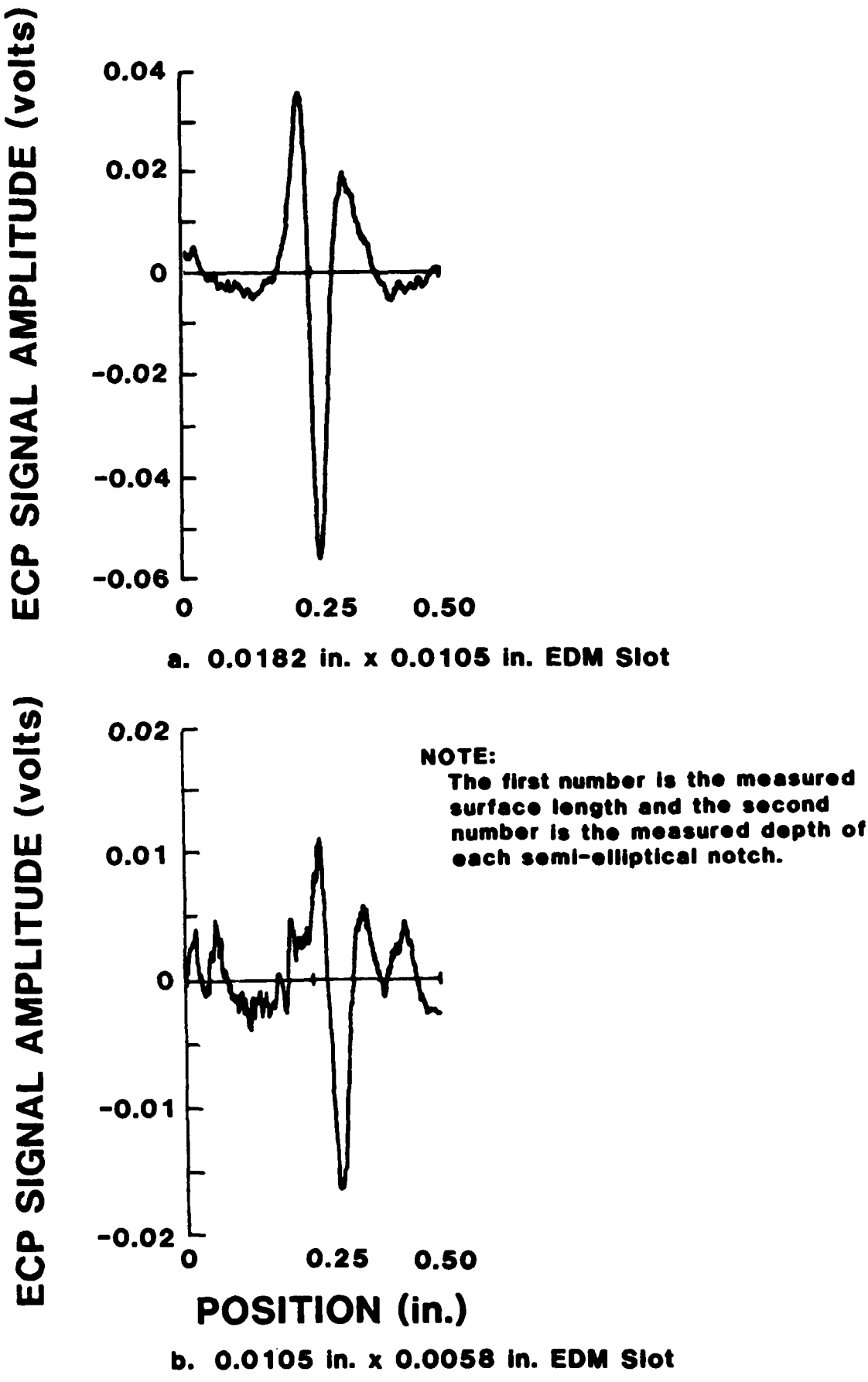

FIGURE 3. ECP SIGNALS FROM EDM SLOTS IN F100 FIRST STAGE FAN DISK BLADE SLOTS

Additional data for blade slots, balance flange scallops and antirotation windows in the F100 first stage fan disk and 2nd to 3rd stage seal are presented in Section II.6. The results of these tests, on components which include many of the more difficult inspection problems posed by the F100 engine, show that the ECP method is capable of flaw detection in such complex geometrical features.

The ECP laboratory breadboard system shown in Figure 4 was designed and assembled under the present program. The automated scanning system has three degrees of freedom and is computer controlled in much the same way as systems being designed for RFC. Digital data acquisition and storage in the computer memory is also automatic.

The breadboard system was designed to be fully compatible with anticipated RFC requirements. Further details on the design and operation of the breadboard system can be found in Section II.4; compatibility with RFC is discussed in Section II.8 and in Appendix B.

The versatility of the breadboard system is illustrated by its application to inspection of a J85 second stage turbine disk, which is shown in Figure 5. The wheel shown here was retired from service and is known to contain fatigue cracks around the snap diameter, though the number of cracks and their sizes are not known. Part of an ECP scan of the region containing cracks is shown in Figure 6. The changes in background level are periodic and are caused by the geometry of the part, while the very prominent deviations from background level are crack indications. As is evident from these data, the ECP breadboard system, though designed and optimized for the inspection of certain F100 engine parts can be applied with confidence to a variety of inspection problems.

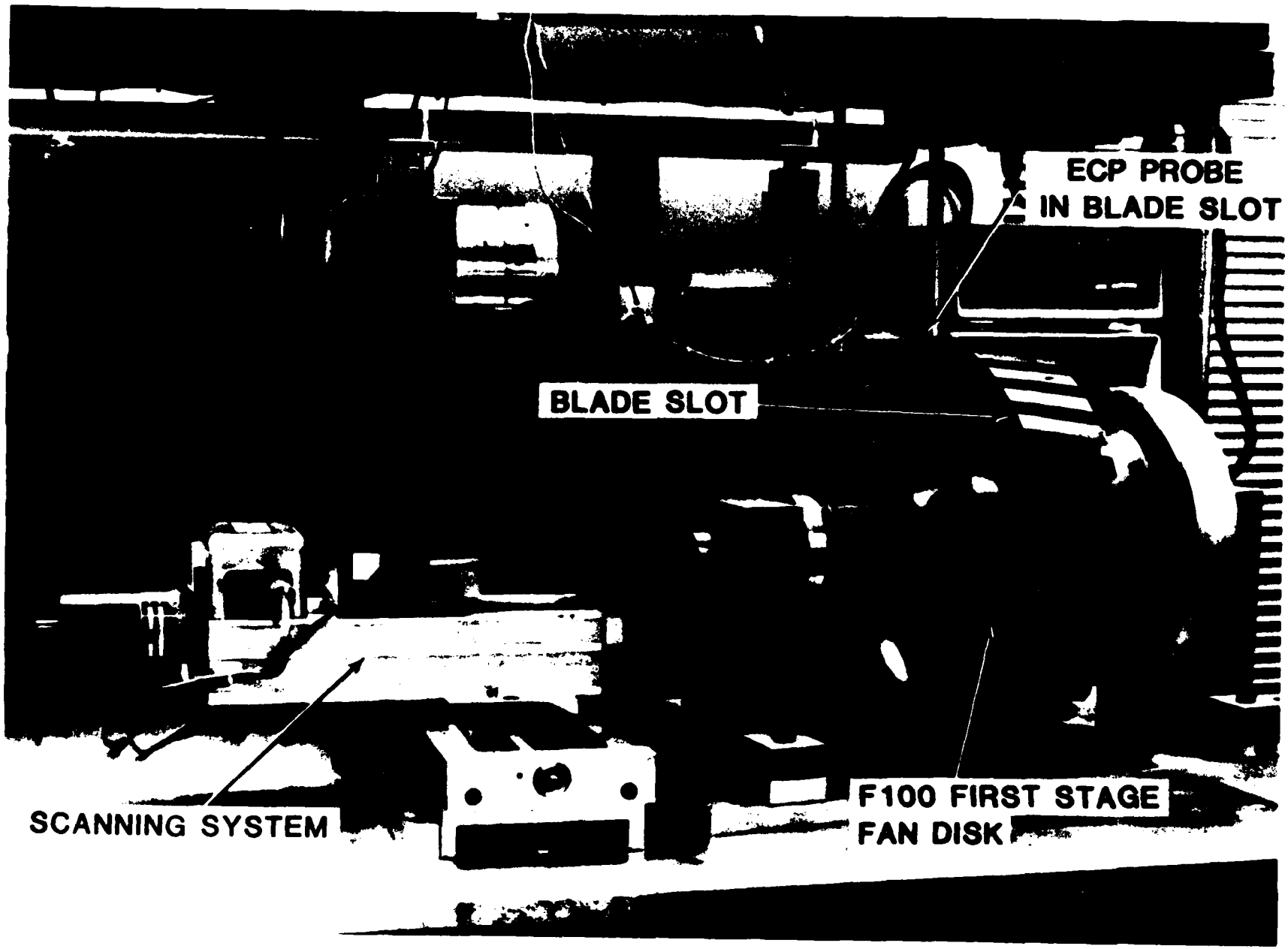

FIGURE 4. ECP LABORATORY BREADBOARD SCANNING SYSTEM WITH F100 FIRST STAGE FAN DISK IN PLACE

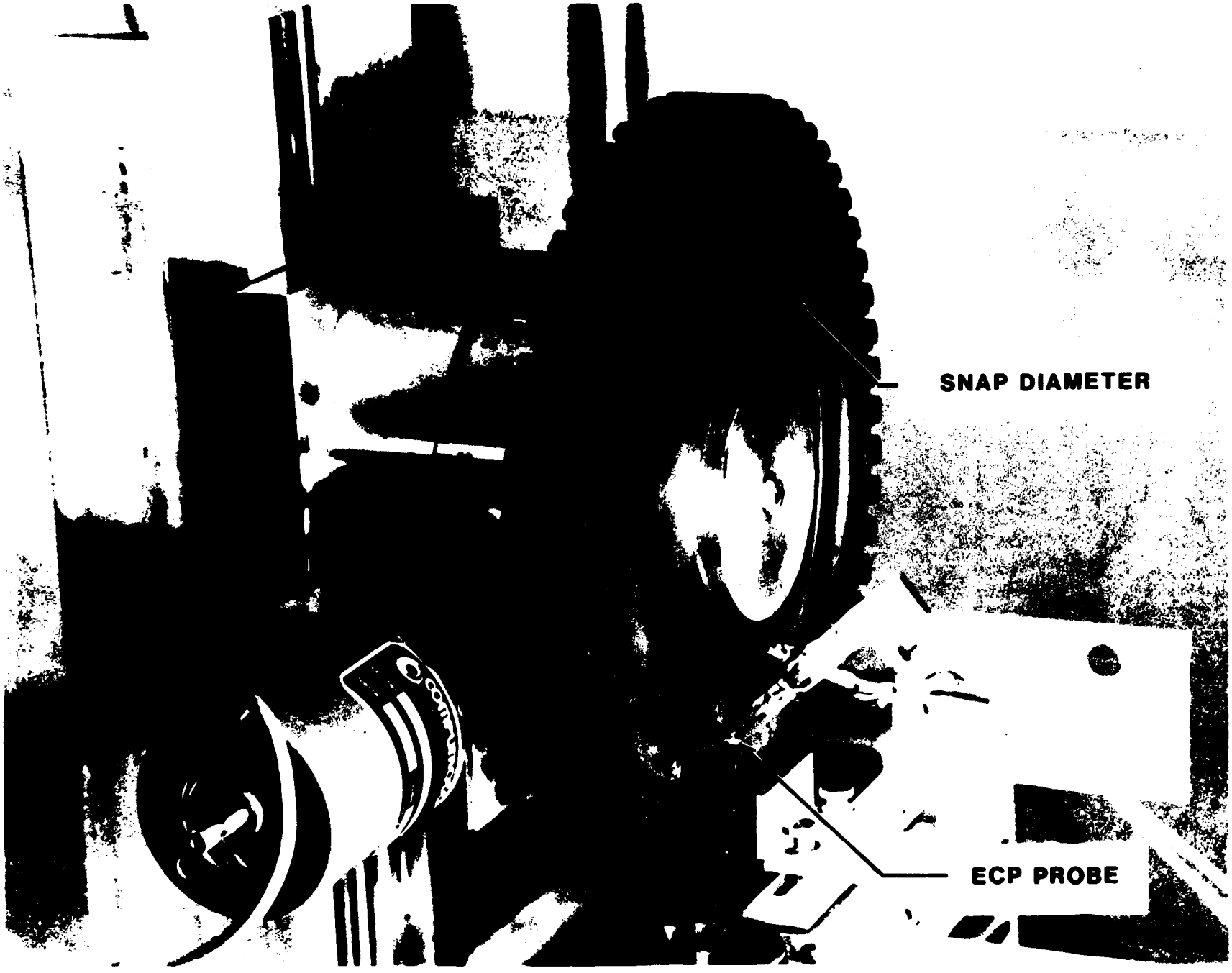

FIGURE 5. J85 SECOND STAGE TURBINE DISK INSTALLED IN ECP LABORATORY BREADBOARD SYSTEM

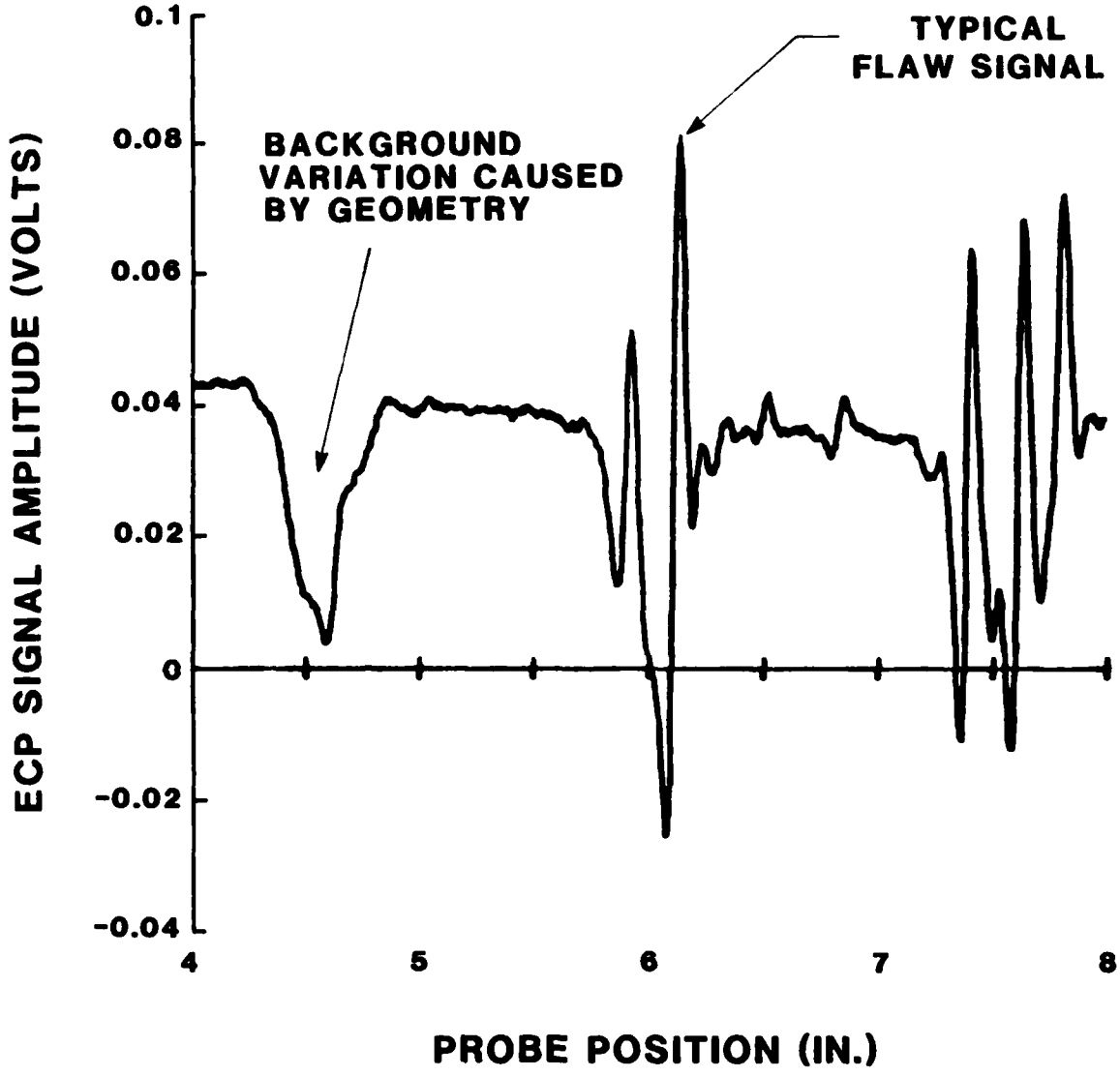

FIGURE 6. ECP SIGNALS FROM FATIGUE CRACKS IN SNAP DIAMETER OF J85 SECOND STAGE TURBINE DISK

Although a complete analysis of flaw detection reliability was not within the scope of this exploratory development program, sufficient data were obtained from flaws in blade slots to make preliminary estimates of the probability of detection (POD) as a function of flaw size. The results are summarized in Figure 7 where data corresponding to four different false alarm probabilities, ranging from 10^{-6} to 10^{-3} are plotted on the same graph. The main points to note here are that POD curves rise very rapidly in the vicinity of the RFC target flaw size, and that the curves corresponding to different false alarm rates are very closely spaced. Thus, regardless of the false alarm rate, a very small increase in flaw length, of the order of 0.001 in., results in a dramatic increase in the POD. This means that for flaws only slightly larger than the target flaw, detection is virtually certain and the probability of errors, through missed flaws or false alarms, is almost negligible. Though much more data are needed for an accurate statistical assessment, these preliminary results indicate that the ECP method should provide a highly reliable and efficient flaw detection capability for RFC.

- In summary, then, the principal results of this program are:
  optimization of the ECP method to obtain sensitivity and repeatability such that flaws even smaller than the RFC target flaw size can be detected;
- the design and assembly of an ECP breadboard system;
  demonstration of the system in the detection of flaws in F100 engine parts;
- a preliminary assessment of the reliability of the ECP system as an RFC inspection technique.

The exploratory phase of ECP development has, therefore, reached a successful conclusion. The method is now ready for more extensive evaluation in the context of actual inspection problems.

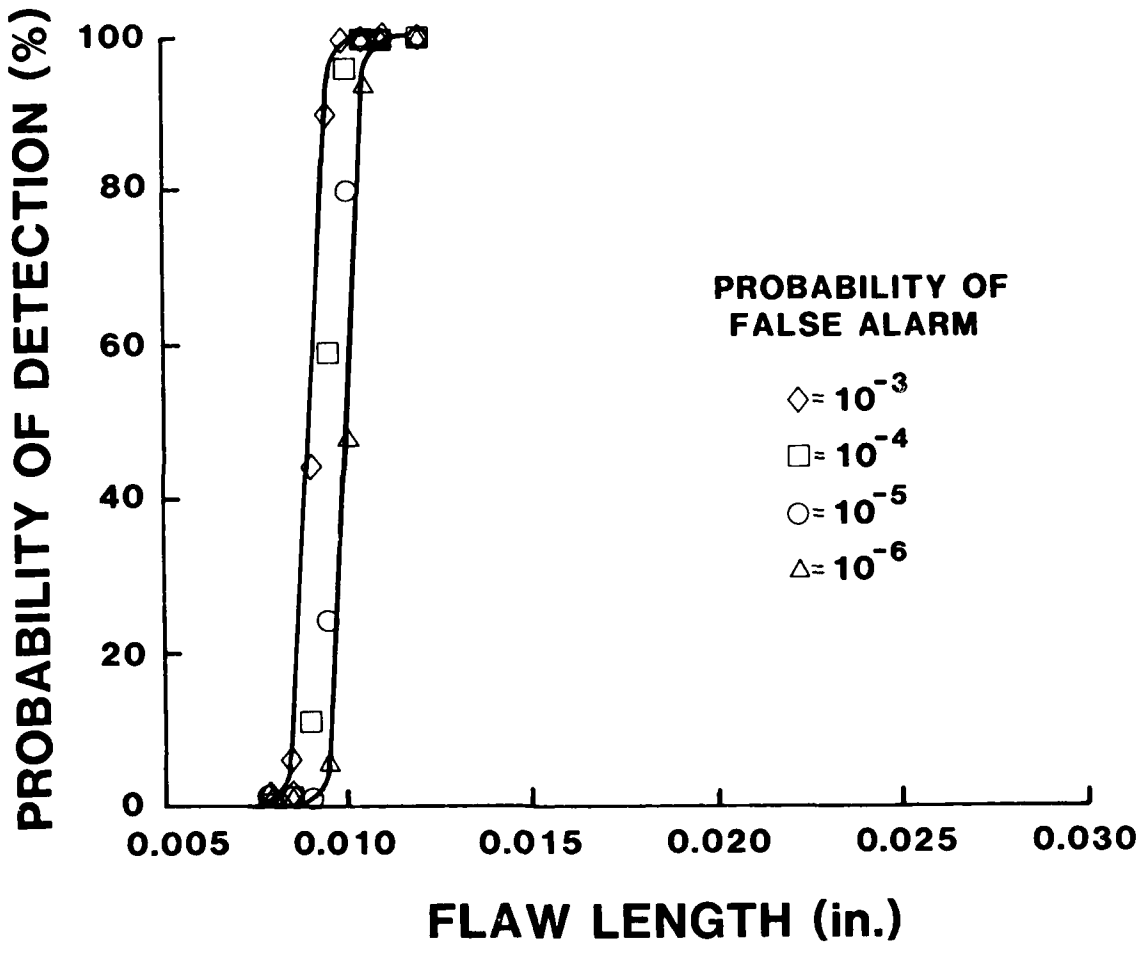

FIGURE 7. PROBABILITY OF DETECTION FOR FLAWS IN BLADE SLOTS OF AN F100 ENGINE FIRST STAGE FAN DISK

SECTION II

RESULTS AND DISCUSSION

Project accomplishments are presented and discussed in this section. The first subsection is a summary of tasks in outline form, and is intended primarily as a guide to the technical subsections that follow. These include discussions of the physical constraints associated with F100 engine part inspection, the selection and acquisition of specimens and the development of a laboratory breadboard system. Experimental procedure and results are then presented, followed by an analysis of probability of detection and a discussion of potential for RFC. Conclusions and recommendations are summarized in Section III.

1. Summary of Tasks

Task I - Determine Constraints and Optimize ECP Method

1. Identify Constraints - Constraints imposed by material properties and complex geometry features are discussed in Section II.2.
2. Prepare Specimens - The choice of materials and geometrical features to be inspected, as well as the fabrication and acquisition of specimens are summarized in Section II.3.
3. Optimize ECP Method - Optimization efforts are described in subsections specific to the type of inspection, i.e., blade slots are discussed in Section II.6.a, antirotation windows in II.6.b, and scallops in II.6.c.

Task II - Design, Assemble and Evaluate an ECP Breadboard System

1. Design and Assemble Breadboard - The ECP breadboard system is described in Section II.4, with engineering drawings in Appendix D.

2. Monitor Compatibility - The plan followed to ensure compatibility with RFC, and answers to specific questions concerning compatibility are presented in Appendices A and B, respectively.

3. Evaluate Breadboard - Data pertaining to the evaluation of the breadboard system are presented and discussed in Sections II.6.a.3 (blade slots), II.6.b.3 (antirotation windows), and II.6.c.3 (scallops). The discussion of probability of detection in Section II.7 also pertains to evaluation of the breadboard.

4. Assess Potential for RFC - Results pertinent to potential RFC applications of the ECP method are summarized in Section II.8.

Task III - Demonstrate Breadboard

A formal demonstration of the breadboard system was conducted for Air Force personnel at Southwest Research Institute on May 24, 1984. Experimental data presented in this report also serve to demonstrate and document the flaw detection capabilities of the ECP system.

2. Constraints

The physical constraints imposed by the materials and complex geometry of the F100 engine components are significant factors in the application of the ECP methodology to the RFC program. The materials identified are Ti 6-2-4-6 and IN100 and many of the features of interest are illustrated in Figures 8 and 9. One material, Ti 6-2-4-6, and two geometries, antirotation windows and blade slots, were selected as worst-case conditions. The titanium alloy was chosen because, based on prior experience, the background noise resulting from material characteristics is expected to be greater for titanium alloys than

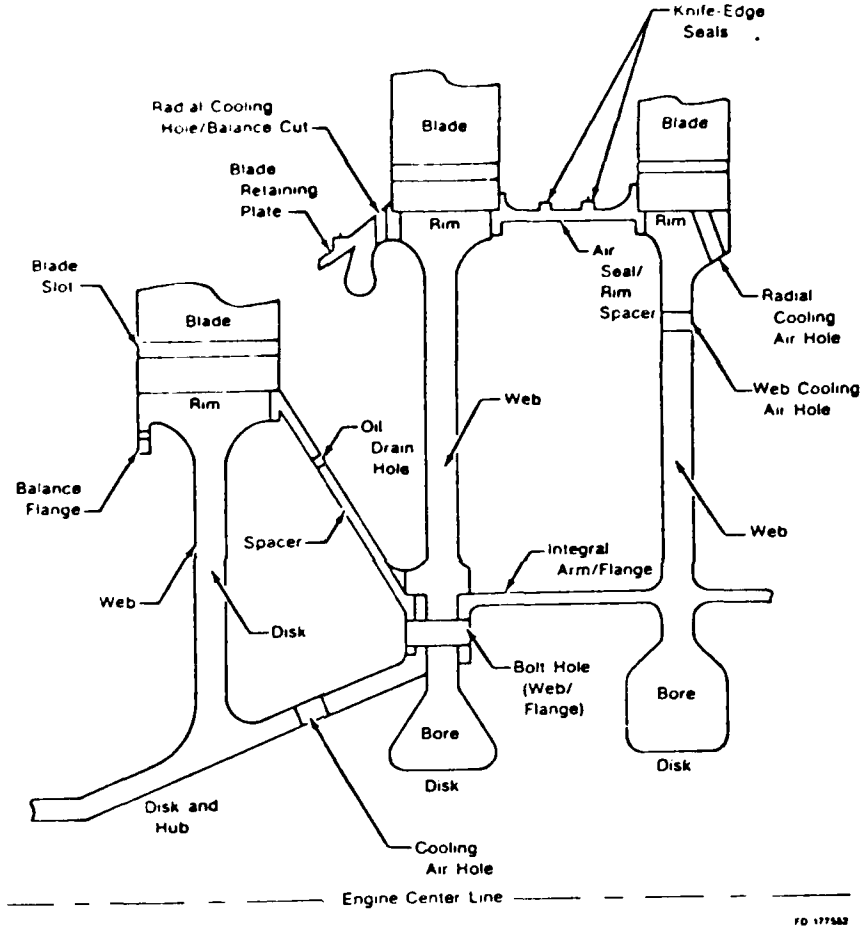

FIGURE 8. COMPOSITE SKETCH OF TYPICAL F100 ROTOR COMPONENTS AND CRITICAL LOCATIONS (Not All Features of All Parts) Reference 6

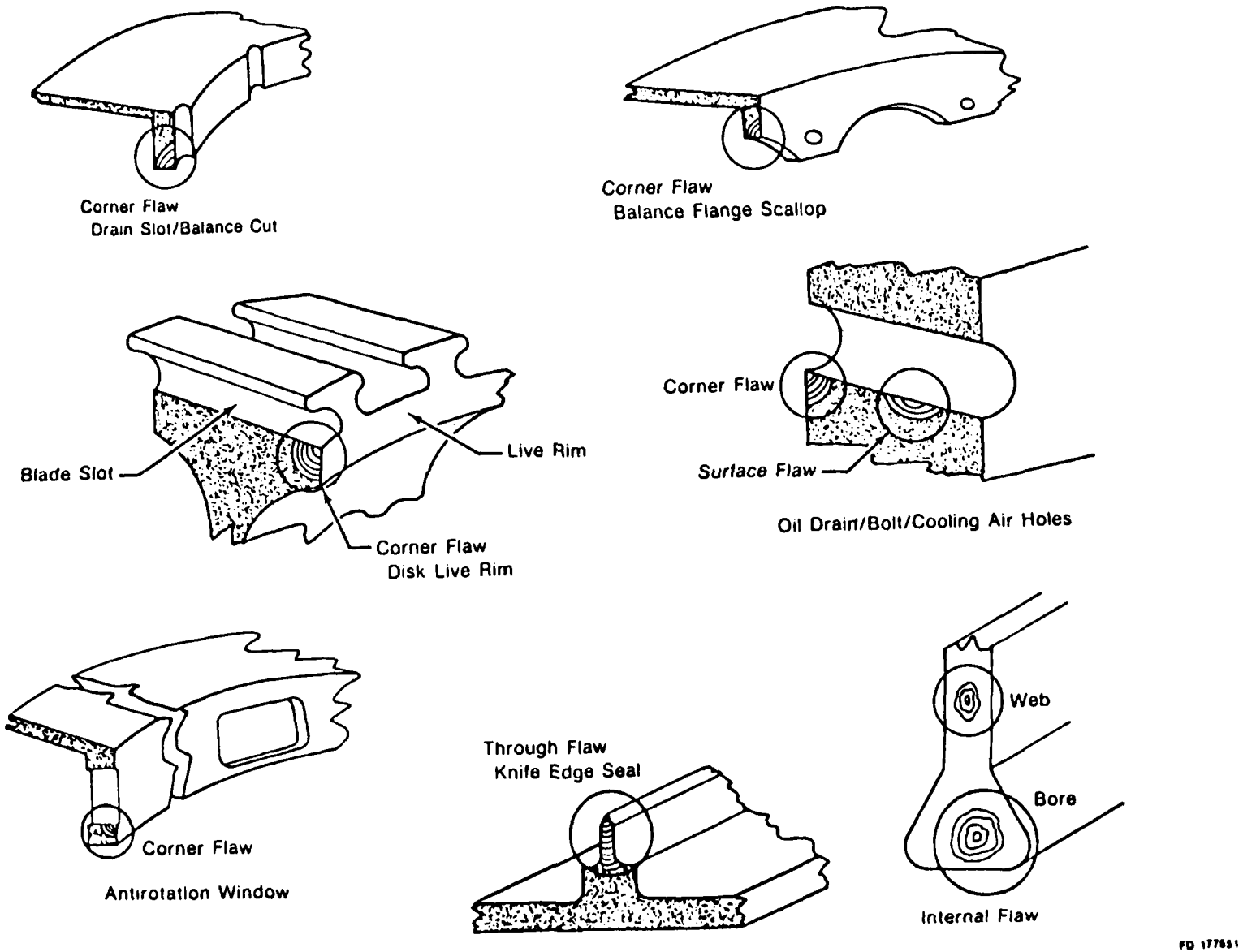

FIGURE 9. COMPOSITE SKETCH OF TYPICAL FLAW LOCATIONS (Not All Features on All Parts)
Reference 6

for the IN100 alloy. Antirotation windows and blade slots were chosen as the worst-case geometries for ECP because techniques developed to accommodate these geometries would permit essentially all other geometries illustrated in Figures 8 and 9 to be inspected.

From the above considerations, a comprehensive list of potential constraints on the ECP method was prepared early in the program. This list was subsequently refined based on discussions with Mr. C. M. Elias, AFWAL/ MLLP, Project Engineer, and Mr. W. D. Rummel, Martin Marietta Corp., Denver Aerospace, consultant, and on visual examination of F100 compressor disks and seals at San Antonio ALC. Further refinement of the constraints list has been possible through analysis of data acquired in optimization of the ECP methodology.

From the above identified sources and based on SwRI's prior background and experience in the application of the ECP method to practical inspection problems, Table 1, Constraints Significant to ECP Inspection, was prepared. This table identifies the geometry, material and inspection parameters which are significant to the successful development of the ECP method for potential application to the RFC/NDE System. Comments are included in Table 1 which address the various parameters in terms of their anticipated influence on the ECP inspection method. The paragraph below summarizes the actual influence of the constraints on the ECP methodology based on experimental results.

Table 1 confirms the significant influence of part geometry on the ECP inspection methodology for both antirotation windows and blade slots. As discussed in greater detail in Section II.5, ivnvestigative efforts were initiated on the window problem and much of what was learned was directly applicable to blade slot inspection. Background signals resulting from the material and

TABLE 1

CONSTRAINTS SIGNIFICANT TO ECP INSPECTION

Parameter	Comments
I. Geometry	
A. Antirotation Window	- Windows produce a signature (hereafter referred to as gradient) as a result of the geometry even when no flaw is present. Gradients can significantly influence the discrimination or detection of flaws in the vicinity of the window. Small corner radii could significantly constrain the size of the probe.
• Geometry effects because of window shape and proximity part edge.	
• Accommodation of small corner radii in window.	
B. Blade Slot	
• Geometry effects when inspecting near disk edge.	- Slots also produce a gradient even when no flaw is present. Comments are the same as above.
• Accommodation of small radii in slot.	
II. Dimensional Variations	
A. Antirotation Window	
• Variation of corner radii.	- Effect on gradient.
• Smoothness of transition into radius.	- False signal or reduced flaw sensitivity due to increased background signal.
• Variation in edge blending.	- Effect on gradient or reduced sensitivity.

TABLE 1 (Cont'd)

Parameter	Comments
B. Blade Slot	
• Variable radii.	- Tracking of probe over varying radii. Reduced sensitivity due to variation in liftoff.
• Smoothness of transition into radius.	- False signals or reduced sensitivity due to liftoff.
• Variation in edge blending.	- Effect on gradient or reduced sensitivity.
III. Surface Conditions	
• Surface Finish.	- Modified background signal. Results indicate only a minor influence.
• Galling, erosion, FOD or handling damage.	- Increased background or interfering signals. ECP method should detect and discriminate this surface damage.*
• Coating or foreign material on surface.	- Non-uniform sensitivity due to variation in liftoff. Thorough overhaul cleaning procedures make this an unlikely problem. Also, ECP method is not strongly liftoff sensitive.
IV. Flaw (Crack) Conditions	
• Crack opening. • Residual stress, plastic zone. • Crack filled with foreign material. • Metal smeared over crack at surface.	- From limited experimental results, these factors appear to have a negligible effect on ECP method. All are of considerable concern with other NDE methods such as penetrant, ultrasonics and in some cases, eddy current.
• Crack profile/orientation.	- Can influence ECP sensitivity. Greatest sensitivity for relatively planar crack interface which is oriented perpendicular to excitation current in part, but ECP method can give information on orientation.

*See Section II.6.a for an example encountered in blade slot inspection.

TABLE 1 (Cont'd)

Parameter	Comments
V. Material	
• Variations in conductivity.	- Possible reduced sensitivity due to local variations or increased background signal.
• Other material characteristics, i.e. grain size, compositional variations, etc.	- Same as above for conductivity variations.
• Forming processes or service-induced changes (via heating).	- No significant influence anticipated unless conductivity or permeability significantly affected or localized changes introduced.
VI. Inspection Environment	
• EMI, temperature, vibration, etc.	- Factors are basically instrumentation considerations and are accommodated by adequate consideration in prototype design.

surface conditions influence flaw detection sensitivity to the extent that background noise is the principal constraint on probability of detection of small flaws in blade slots. Still, the problem is not serious and flaws of the RFC target size are detectable, even in blade slots. On the other hand, dimensional variations, noted in some of the simulated window specimens can significantly reduce flaw detection.

3. Specimen Preparation

Specimen selection was based on worst-case geometric features and materials as discussed in the previous section. Accordingly, antirotation windows and blade slots were selected as the two features on which the ECP method would be optimized with emphasis on titanium alloy material. The specimen set which incorporated these features consisted of the following:

Type I - Government-Furnished Specimens

Type II - Supplementary Geometry Specimens

Type III - Fatigue Crack Specimens

a. Type I Specimens

The Type I Government-furnished specimens were actual engine parts, which were used to demonstrate the ECP method on production engine hardware.

The selection of candidate engine parts was based on the two critical geometric features, antirotation windows and blade slots, and the material, Ti 6-2-4-6. With these constraints, part selection falls within the fan/compressor section of the F100 engine which limits the candidates to the first three fan disks (for blade slots) and the first seal between the second and third stage fan disk (for antirotation windows). Unfortunately, both blade slots and antirotation windows do not exist in a single part; therefore, the following parts were selected as Type I Specimens:

Part No.	Item	Geometric Feature	Material
4047301	First stage fan disk	Blade slot	Ti 6-2-4-6
4049087	2nd to 3rd stage fan seal	Antirotation window (open slot)	Ti 6-2-4-6

Two disks and two seals were obtained from scrap parts available at Kelly AFB. Details as to the types and locations of flaws introduced in these specimens are provided in Section II.6.

b. Type II Specimens

The supplementary geometry specimens (Type II) were orginally intended to serve as substitutes for the Type I specimens if both antirotation windows and blade slots were not available in actual engine hardware. Early in the program, however, specimens were required in order to proceed with optimization of the ECP method. Since the Type I and Type III specimens would not be available for some time, a Type II specimen was fabricated from Ti 6-4. This specimen, which contains simulated antirotation windows, is described in Section II.6.b.1. An existing Ti 6-4 flat bar specimen containing three surface EDM slots was also used as a Type II specimen (Section II.6.a.1).

c. Type III Specimens

Type III specimens are those in which actual fatigue cracks were generated. These specimens were of a size and shape which facilitates ease and economy of fatigue crack generation. After generation of each crack, an EDM slot was placed in the vicinity* of the fatigue crack. It was intended that the relative responses between the fabricated flaws and the fatigue cracks in the simple geometry specimen would be used to establish correlation between the two types of flaws and to infer the sensitivity and reliability of fatigue

*But not so close as to influence the signal from the fatigue crack.

crack detection when the actual part geometry is present. Details are presented in Section II.6.a.3 and II.6.b.3.

4. ECP Laboratory Breadboard Inspection System

An ECP laboratory breadboard inspection system was designed and built with the requirements of the automated RFC/NDE system under development by Systems Research Laboratory (SRL) and associated contractors as a guide. The breadboard system demonstrates adaptability of the ECP method to computer supervised scanning control and data acquisition as required by RFC. The breadboard features a three axis, computer controlled scanning mechanism and analog to digital converter for digitization of the ECP data.

An overall view of the breadboard system as configured for scanning simple geometry specimens is shown in Figure 10, while Figure 11 shows elements of the scanner system with an F100 engine fan disk in place. A block diagram of the system is shown in Figure 12. The scanner has the capability of incrementally or continuously scanning along two perpendicular axes with rotation about a third axis using micro-stepper motor drive technology. The equipment provides digitized (spatially sampled) data with permanent data storage on magnetic disks. The range of spatial sampling resolution (manually selectable)available along the x and y axes is 10^{-3} in. to 10^{-2} in. per sample and for the rotational axis is 0.1° to 2° of angle per sample. The scanner is controlled by a computer (Tektronix 4052) and can negotiate a pre-programmed scan pattern in any or all three of the axes. The computer is interfaced to the stepper motor controllers by an IEEE-488 (GPIB) interface. Sampling of the ECP signal by the analog to digital converter (digital oscilloscope) is controlled by dividing the stepper motor drive pulses by the appropriate

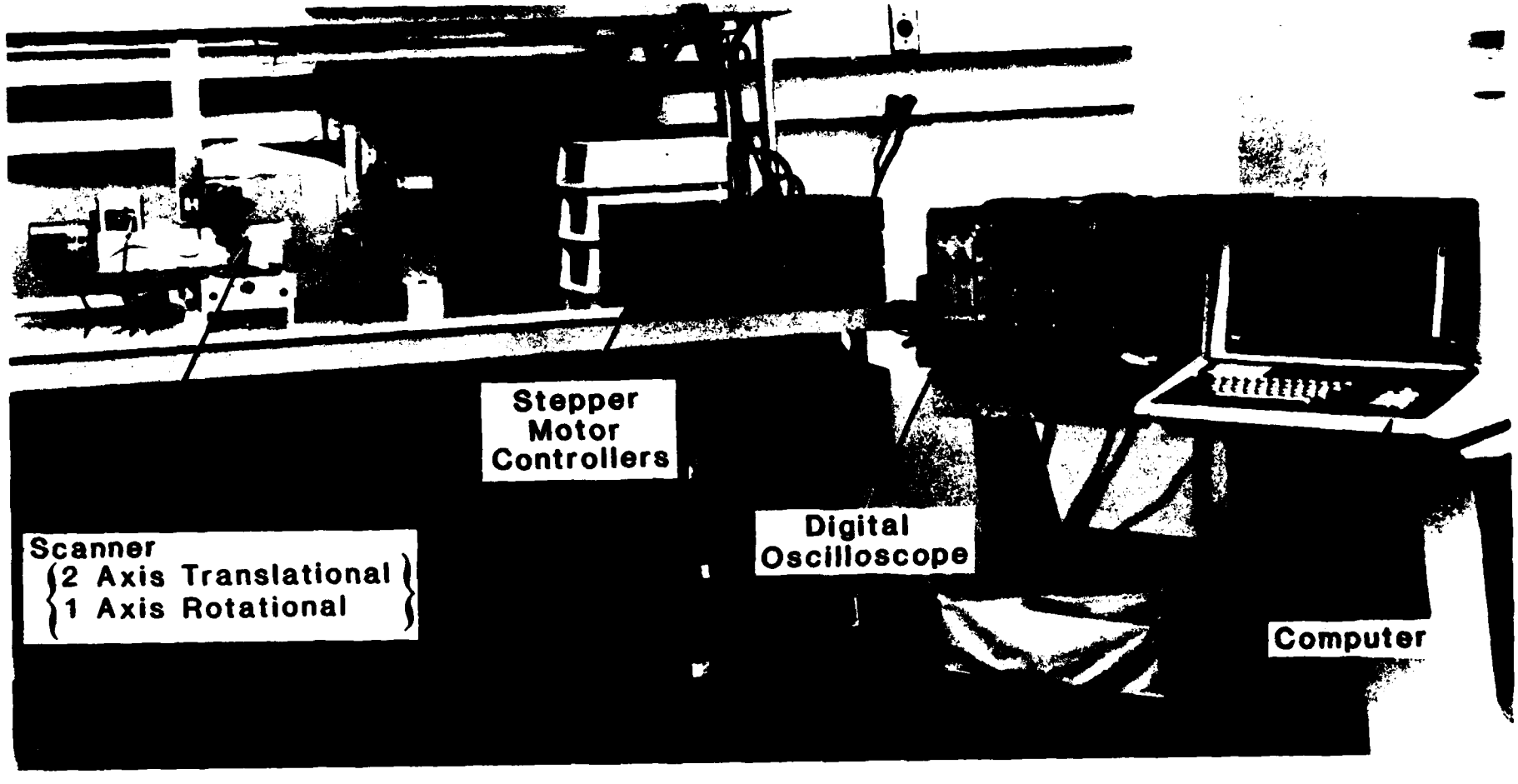

FIGURE 10. OVERALL VIEW OF ECP LABORATORY BREADBOARD SCANNING SYSTEM

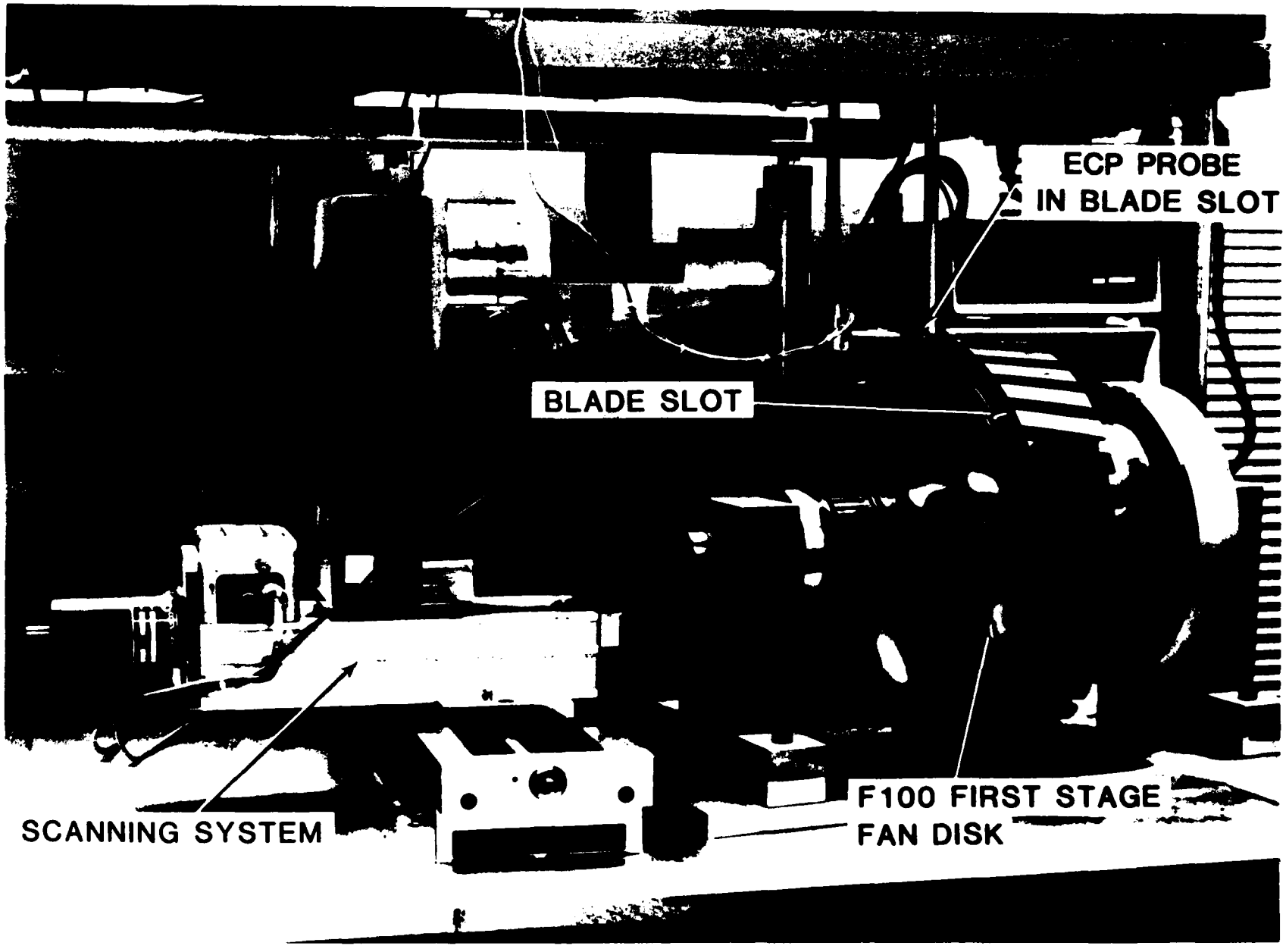

FIGURE 11. ECP LABORATORY BREADBOARD SCANNING SYSTEM WITH F100 FIRST STAGE FAN DISK IN PLACE

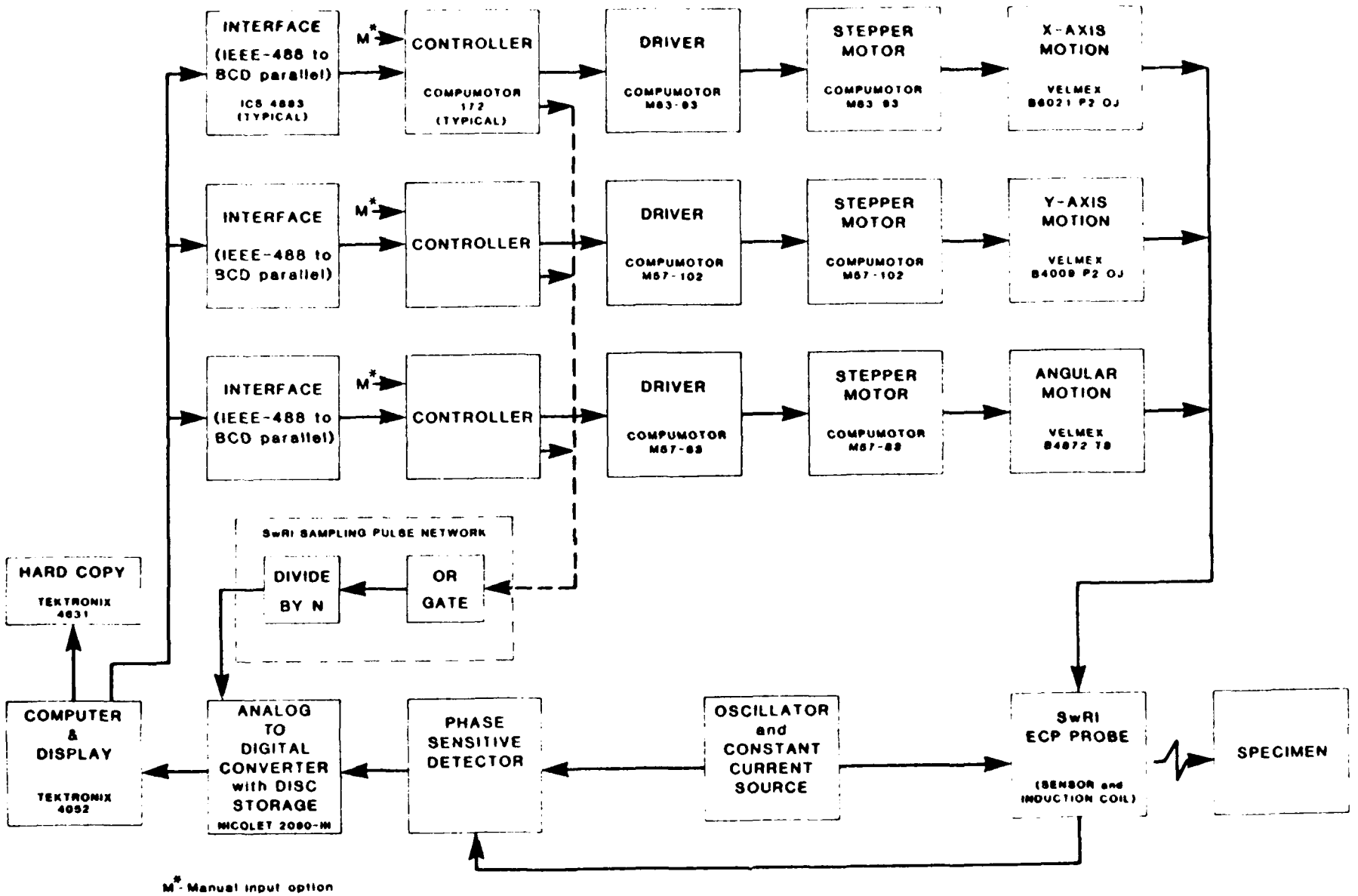

FIGURE 12. BLOCK DIAGRAM OF ECP LABORATORY BREADBOARD SYSTEM

factor to achieve the desired sampling resolution. Linear scanning is accomplished by lead screw slide assemblies driven by stepper motors. Rotary motion is accomplished by a stepper motor driven rotary table.

The induction coil in the ECP probe is driven by an oscillator/current source, and the signal from the the ECP probe sensor output is input to a phase sensitive detector. The analog output from the phase sensitive detector is sampled by the analog to digital converter and may be stored on flexible magnetic disks. The data may then be transferred to the computer for plotting and/or signal processing.

5. Experimental Procedure

Experiments were designed to optimize the ECP method for high realiability detection of surface cracks having a target size of 0.010 in. surface length x 0.005 in. depth in typical complex geometry locations of engine components. Two types of flaws were of interest: (1) corner flaws which would be expected in engine component features such as antirotation windows and balance flange scallops and (2) surface flaws which would be expected in features such as blade slots. Initial experiments were performed on simple geometry specimens so that the ECP response to small flaws could be determined without the influence of the complex geometries present in actual engine components. Initially, EDM slots were used to simulate fatigue cracks. Experiments were then extended to specimens having blade slot, antirotation window, and balance flange scallop geometries to determine the influence of specimen configuration on the ECP signal. Finally, ECP data were obtained on laboratory grown fatigue cracks so that the equivalence of the ECP response to EDM slots and fatigue cracks could be demonstrated.

Optimization of the ECP method involved investigation of a number of parameters including probe design (induction coil and sensor), excitation frequency, positioning of the probe with respect to the part, probe scanning configurations, signal processing etc. Probe design was guided by previous experience and by an existing theoretical model[2]. Emphasis was placed on miniaturization of the overall probe size so that the complex geometry engine component features could be accommodated. Several different probe configurations were fabricated and evaluated on both the antirotation window and blade slot configurations. Probe evaluations included the size and shape of induction coils, size and spacing of the differential sensor coils, and various shielding arrangements to reduce stray magnetic coupling between the induction coil and sensor and to reduce the spread of the induced currents in the part. Three final probe designs resulted. One design was used for blade slot inspection, the second design was used for linear scans past the antirotation windows, and the third design was used to inspect the inside of the antirotation windows and balance flange scallops using a contour scan to track the part geometry. A description of these designs is presented in Appendix F.

Previous experience had shown that excitation frequencies of the order of 100 KHz provided high sensitivity to flaws in low conductivity materials such as the titanium and superalloys used in engine components. Limited investigations of operating frequency in this program confirmed this finding.

Optimization investigations of probe positioning and probe scanning configurations showed that for blade slots, a linear scan along the blade slot length was optimum; however, for antirotation windows, tradeoffs existed in flaw sensitivity and sensitivity to part geometry variations, depending on whether linear scans or contour scans were used.

Investigations of signal processing were very limited; however, in some cases such as antirotation windows, a strong gradient signal is obtained from part geometry and the flaw signal can be more easily recognized by digitially subtracting an unflawed window signal from a flawed window signal. In the case of blade slots, a digital high pass filtering operation was used to reduce slowly varying background signals.

Signal processing was limited to these very simple operations because, in most cases, signal-to-background ratios were quite large and further signal enhancement through digital processing was not needed. However, it should be noted that signal processing may extend the minimum flaw size that can be reliably detected.

The data presented in the following sections were obtained using the optimized probe designs and other parameters described above.

6. Experimental Results

a. Blade Slots

(1) Specimens

The Type I specimen consisted of an F100 engine first stage fan disk (Figure 13) which is fabricated from Ti 6-2-4-6. The blade slot configuration in this disk is shown in Figure 14. The blade slot contains several different radii which blend together as shown in the figure. The large radius (0.350 in.) blends into a flat area on the bottom of the blade slot and the primary area of interest for surface flaw detection is at the tangency point of this radius. Half-penny shaped EDM slots were therefore machined in two blade slots at the tangency point for use as target flaws. EDM slot dimensions are 0.0182 in. L. x 0.0105 in. D. and 0.0105 in. L. x 0.0058 in. D.

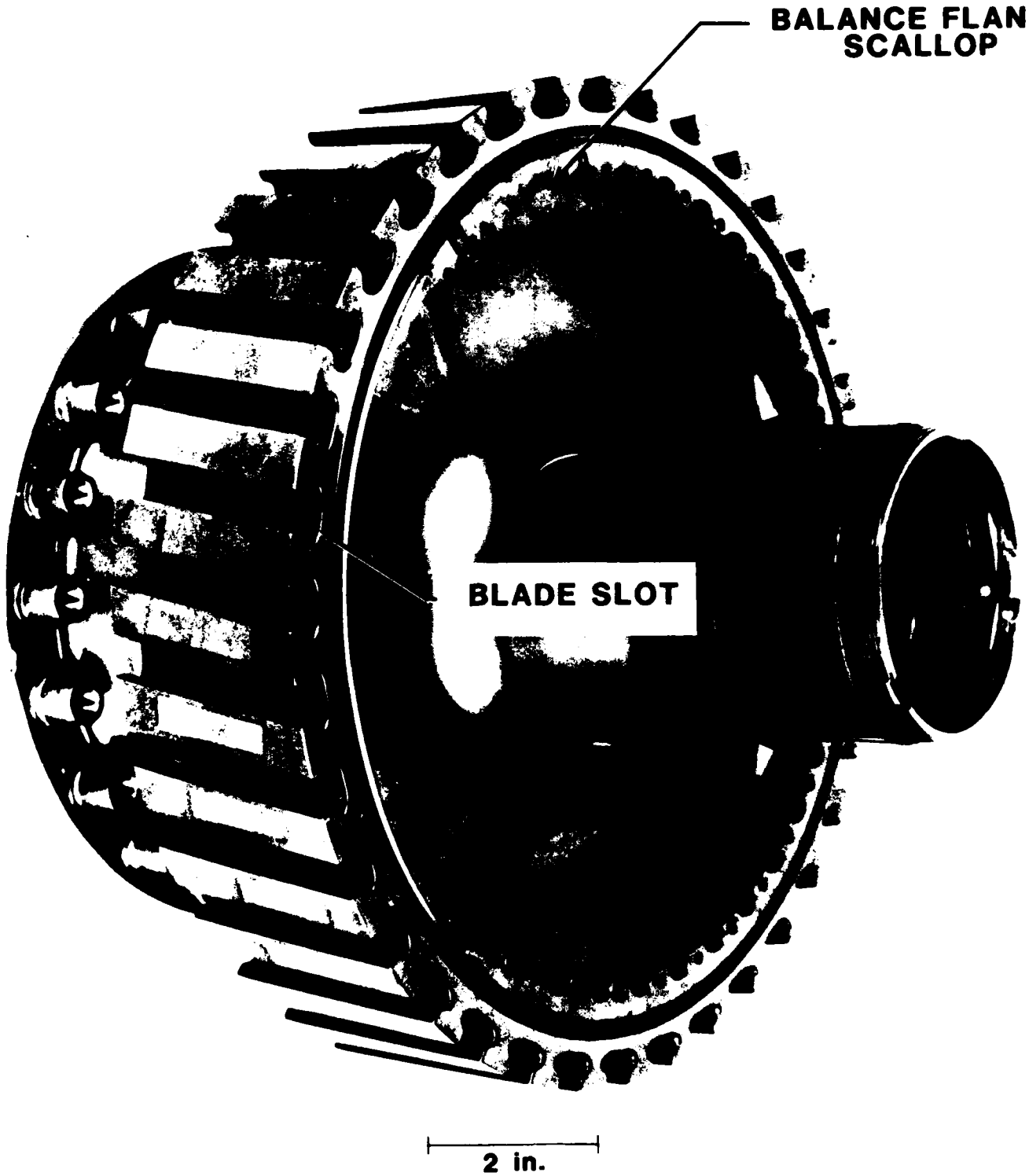

FIGURE 13. F100 FIRST STAGE FAN DISK

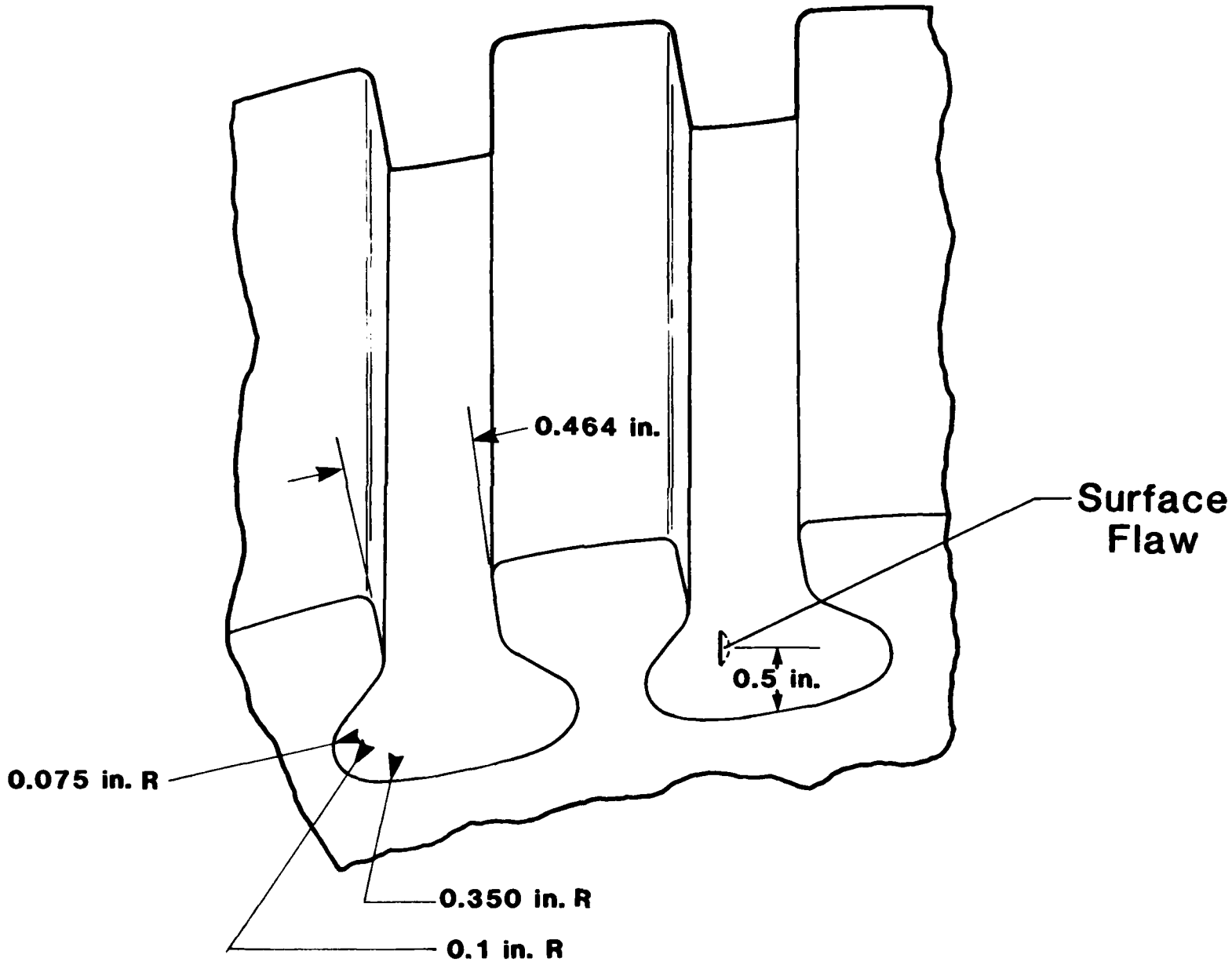

FIGURE 14. F100 FIRST STAGE FAN DISK BLADE SLOT CONFIGURATION

The Type II specimen was a flat-bar specimen of Ti 6-4 (Figure 15) and was used for initial tests. This specimen contained three semi-elliptical shaped EDM slots.

The Type III specimen set consisted of a total of six specimens having the configuration shown in the sketch in Figure 16. Both EDM slots and fatigue cracks were introduced at the tangency point of the 0.350 in. radius. Three specimens were fabricated from Ti 6-2-4-6 material which was cut from a scrap F100 engine third stage fan disk, and three IN-100 specimens were cut from a scrap F100 engine first stage turbine disk. Specimen blanks were machined at SwRI and final machining and introduction of EDM slots and fatigue cracks was subcontracted to Martin Marietta.

Dimensions of the surface flaws which were introduced into these specimens are shown in Table 2. It was anticipated that the fatigue cracks would have a semicircular shape with approximately a 2 to 1 aspect ratio i.e., depth = length/2. In order to measure the actual crack depth, specimen TR-2 was metallurgically sectioned. A photomicrograph of the top view of the crack on the surface of the specimen is shown in Figure 17a, and locations where sections were taken are designated by arrows. A photomicrograph of the crack cross section near the midpoint is shown in Figure 17b. The surface length of the crack is 0.0218 in., and the depth near the midpoint is 0.0058 in. which is much shallower than anticipated. The aspect ratio is thus 3.7 to 1. The depth measured from the section on the left is approximately the same as at the midpoint, while the depth on the right is 0.0077 in., or slightly deeper than at the center. From these results it is apparent that the crack profile differs significantly from a semicircular shape.

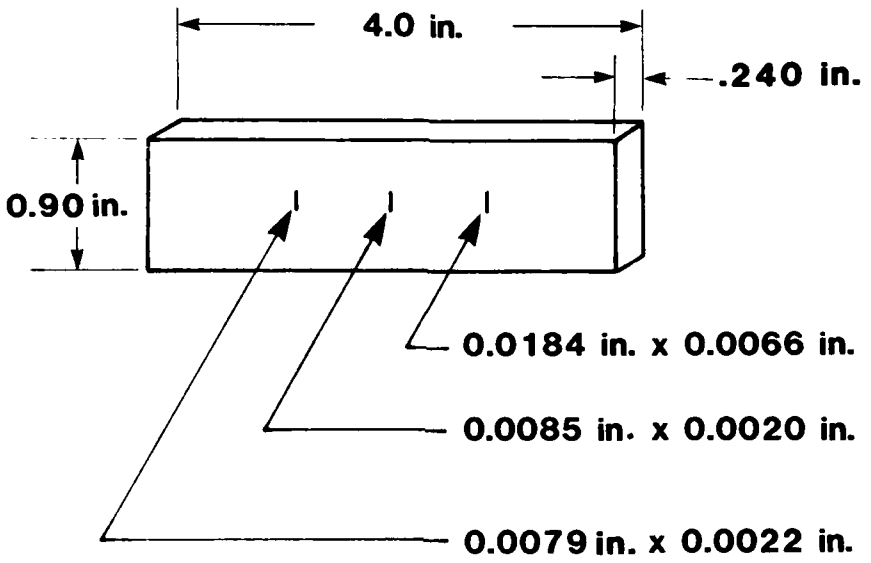

DIMENSIONS SHOWN ARE LENGTH AND DEPTH OF SEMI-ELLIPTICAL SHAPED EDM SLOTS.

FIGURE 15. TYPE II SPECIMEN WITH SURFACE EDM SLOTS

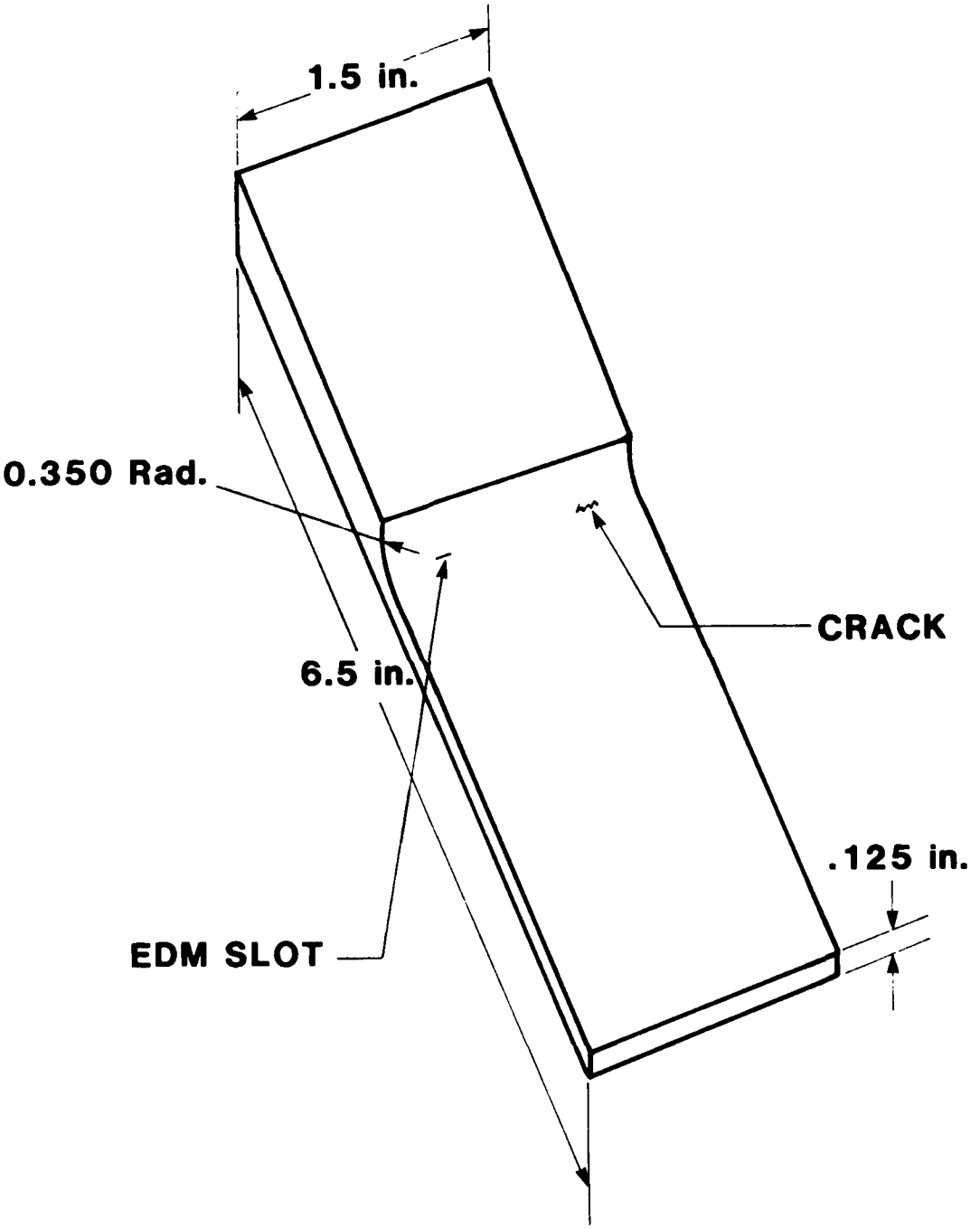

FIGURE 16. SIMULATED BLADE SLOT GEOMETRY IN TYPE III SPECIMENS

TABLE 2

SURFACE FLAW DIMENSIONS* IN TYPE III SPECIMENS WITH SIMULATED BLADE SLOTS

SPECIMEN NUMBER	SPECIMEN MATERIAL	CRACK SURFACE LENGTH (in.)	ESTIMATED CRACK DEPTH** (in.)	EDM SLOT SURFACE LENGTH (in.)	EDM SLOT DEPTH (in.)
TR-1	Ti 6-2-4-6	0.0087	0.0024	0.0094	0.0034
TR-2	Ti 6-2-4-6	0.0216	0.0058	0.0210	0.0096
TR-3	Ti 6-2-4-6	0.0448	0.0121	0.0456	0.0170
IR-1	IN100	0.0082	0.0022	0.0113	0.0009
IR-2	IN100	0.0155	0.0042	0.0156	0.0044
IR-3	IN100	0.0193	0.0052	0.0206	0.0074

* Measured from replicas and photomicrographs.
** Crack depth estimated using 3.7:1 aspect ratio determined by sectioning specimen TR-2.

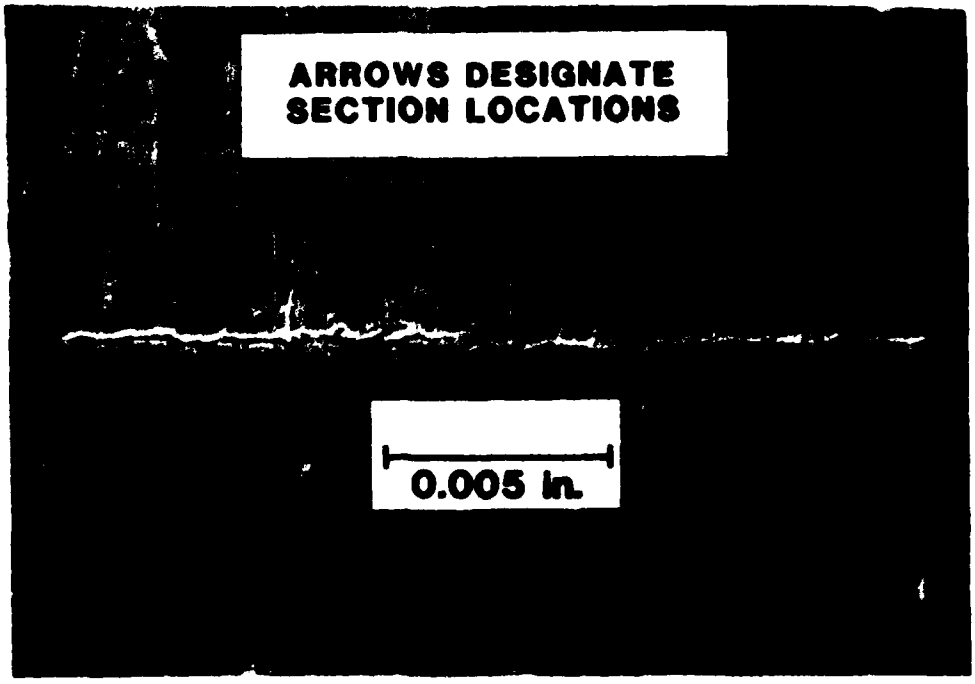

a. Top View of Crack

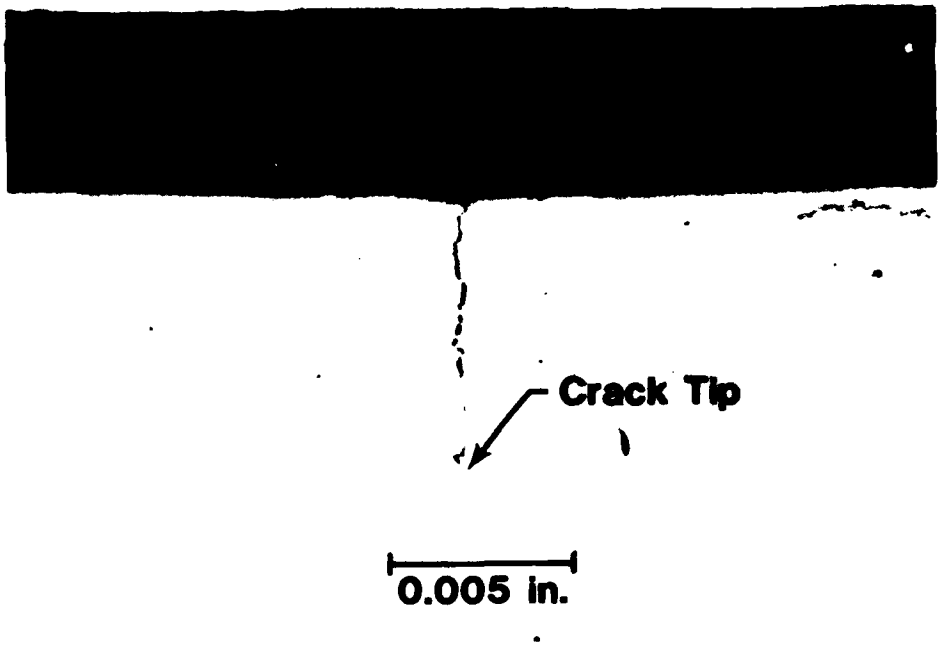

b. Cross Section of Crack
Near Midpoint

FIGURE 17. PHOTOMICROGRAPHS OF CRACK IN TYPE III SIMULATED BLADE SLOT SPECIMEN TR-2

(2) Experimental Setup

The laboratory breadboard scanning system was used to obtain ECP data from all of the blade slot specimens. Figure 18 shows the first stage fan disk mounted in the scanning system. The ECP probe was mounted on an air bearing which allowed the probe to be scanned without physical contact with the surface of the specimen. Evaluations on the Type I and Type III specimen used a linear scan along the length of the blade slot as shown in Figure 19. The initial tests on the Type II specimens used a scan which was perpendicular to the direction of the flaws and parallel with the length of the specimen.

(3) Experimental Results

Initial optimization of the ECP probes for detection of surface flaws in the blade slots was performed on the Type II simple geometry specimen shown previously in Figure 15. The probe was scanned linearly past all three EDM slots and the results obtained with the optimized probe configuration are shown in Figure 20. These data were obtained by averaging data from eight separate scans so that the electronic noise (normally on the order of 3 mV) is reduced and the background signal is that caused by the inhomogeneity of the specimen material. The 0.0184 in. x 0.0066 in. slot in this specimen gives a prominent ECP signal. More importantly, recognizable signals are also obtained from the two small slots. The smallest slot, which measures 0.0085 in. x 0.0020 in., has an interfacial area which is approximately one-third that of the RFC target flaw size of 0.010 in. x 0.005 in. From these data, the inherent sensitivity of the ECP method for detection of flaws smaller than the RFC target size was established.

Data were then obtained from the blade slots in the first stage fan disk (Type I specimen) to demonstrate detection of flaws in an actual

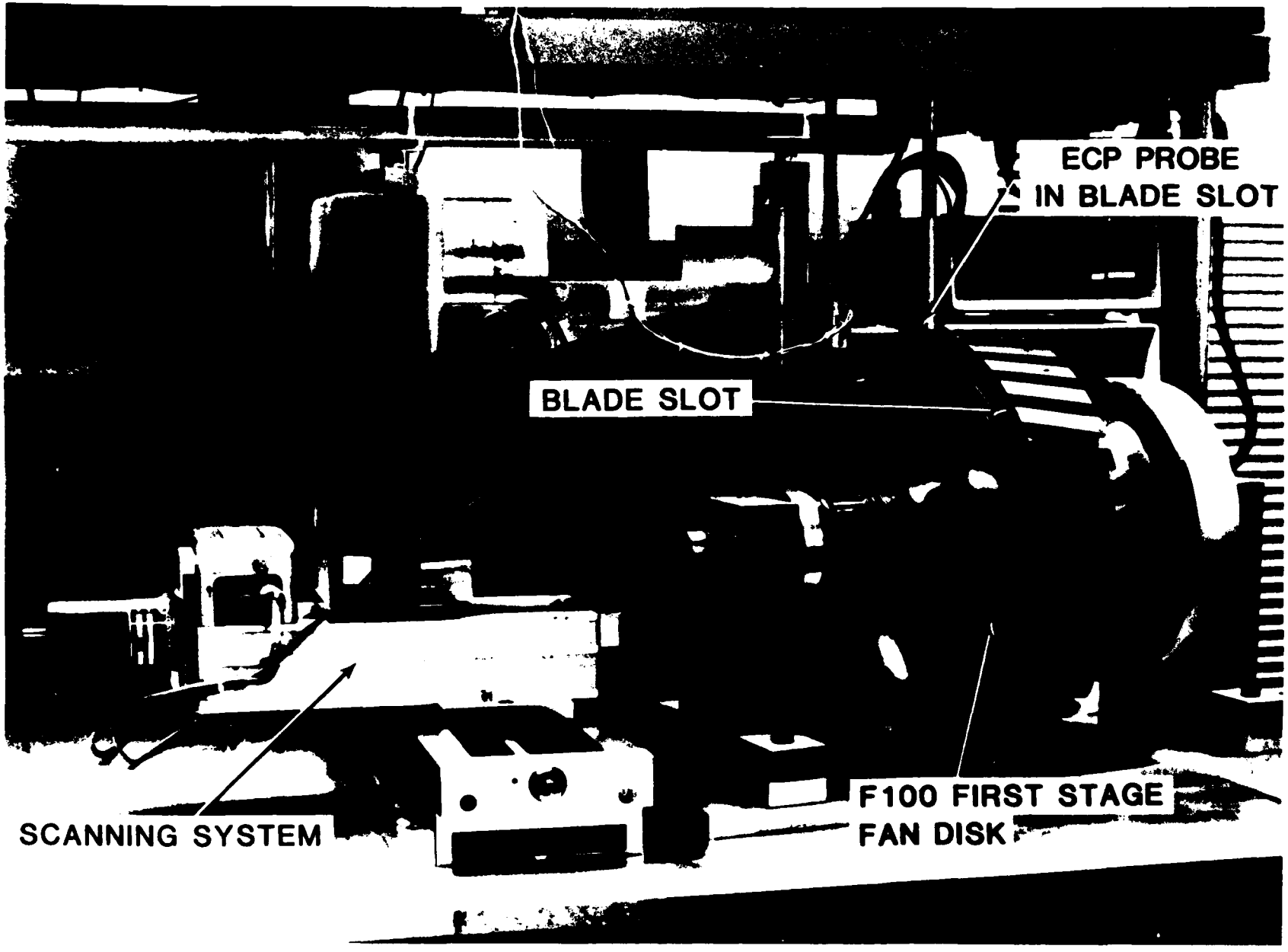

FIGURE 18. ECP LABORATORY BREADBOARD SCANNING SYSTEM WITH F100 FIRST STAGE FAN DISK IN PLACE

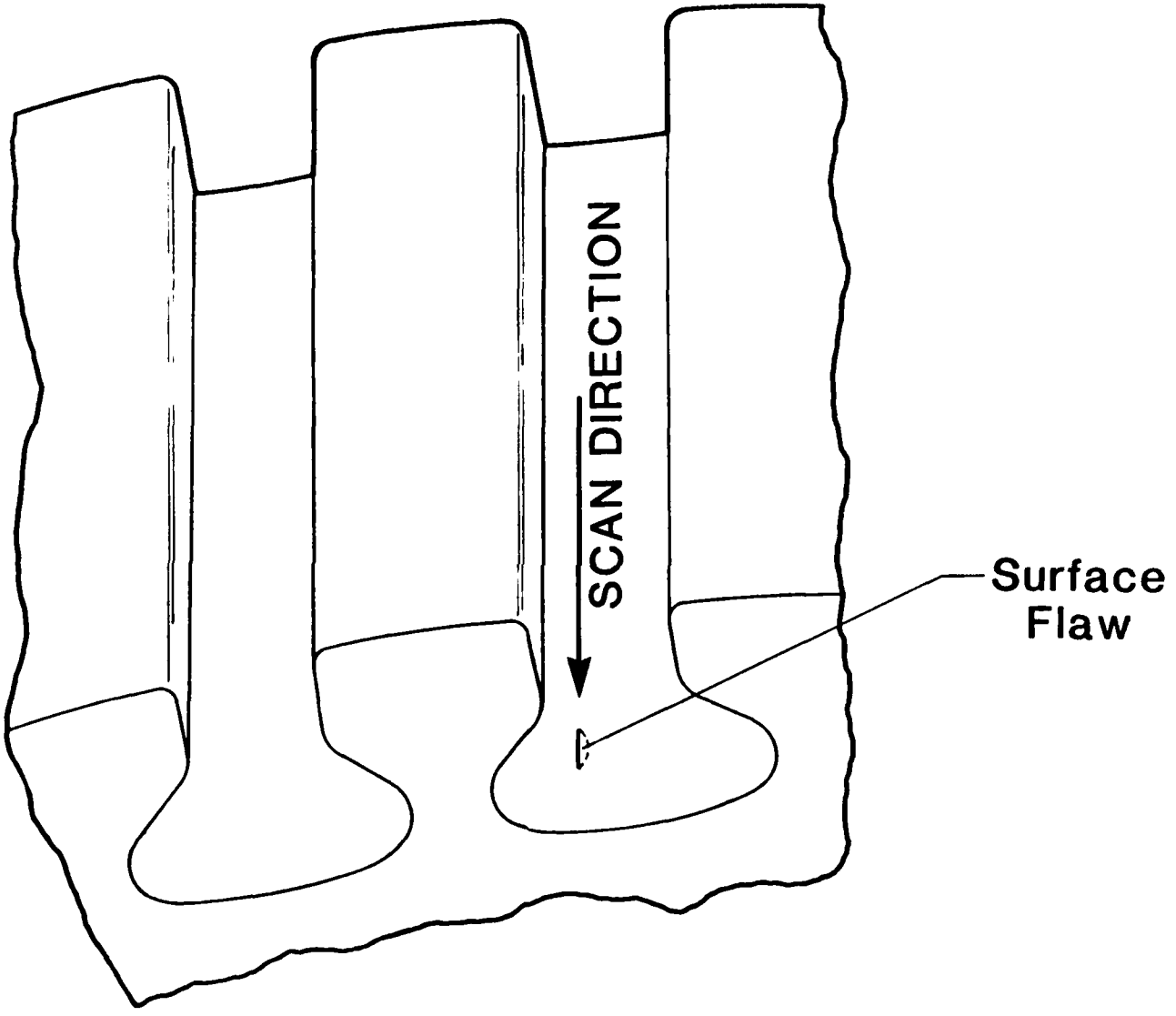

FIGURE 19. BLADE SLOT SCAN CONFIGURATION.

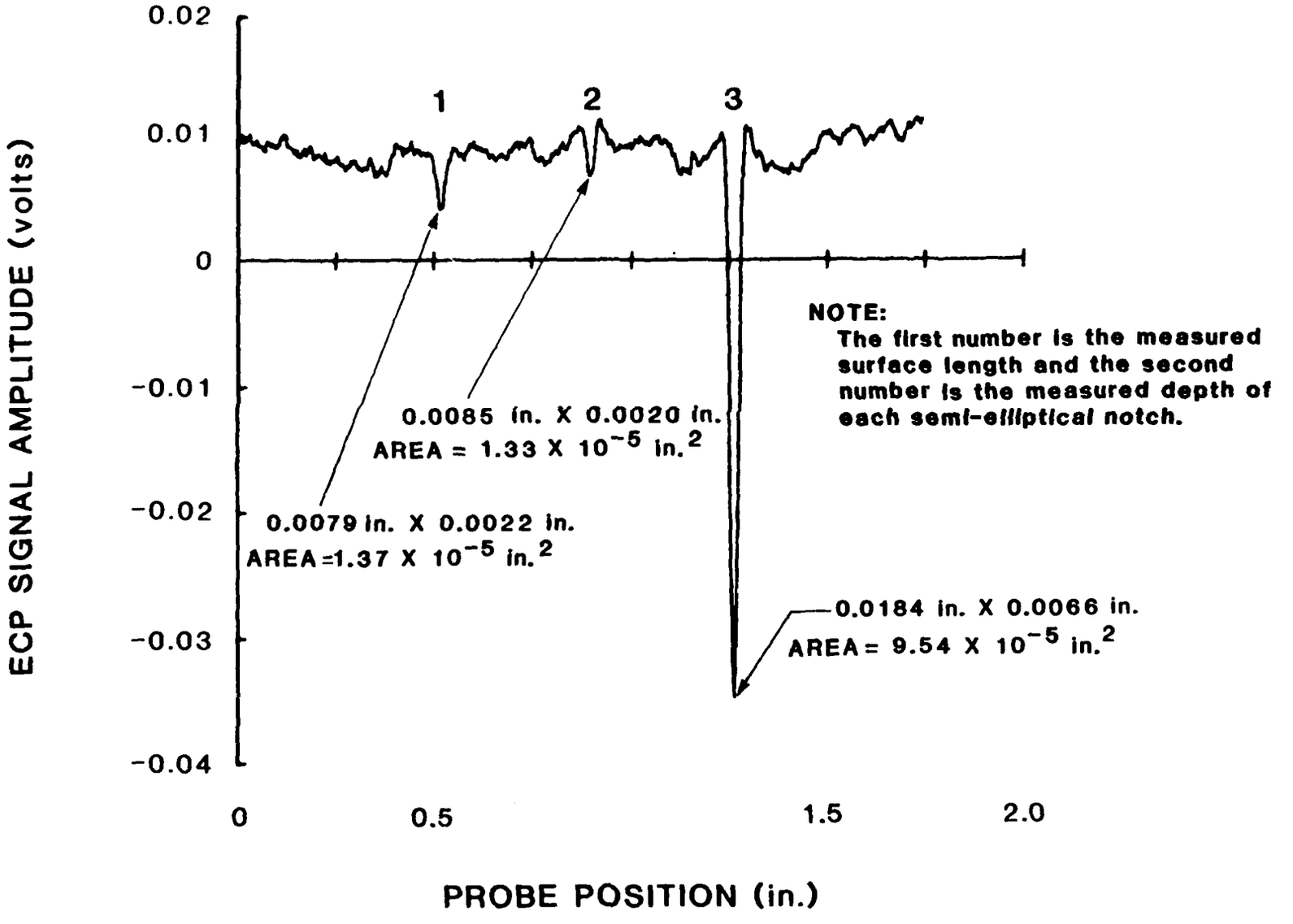

FIGURE 20. ECP SIGNALS FROM SURFACE EDM SLOTS IN TYPE II SPECIMEN

engine component. The blade slots were scanned with the probe scan path positioned directly in line with each EDM slot. ECP signals from the two blade slots which contained surface EDM slots measuring 0.0182 in. x 0.0105 in. and 0.0105 in. x 0.0058 in. are shown in Figure 21a and 21b. Prominent signatures are obtained from both the larger EDM slot and the 0.0105 in. x 0.0058 in. EDM slot, which is nominally equivalent to the RFC target flaw size. Additional scans were made with the probe scan path positioned on either side of the flaws to determine the effect of probe position on signal amplitude. These data were used in the probability of detection calculations as discussed in Section II.7.

All blade slots in the fan disk were also scanned to determine the variation in signal background level. These data were also used in the probability of detection calculations (Section II.7). Figure 22 shows a scan of one blade slot which has a typical background signal level with the exception of the area designated "signal from foreign material". It is emphasized that the background signal obtained from the blade slot is greater than that obtained from the Type II flat bar specimen (Figure 20). The larger background signal is apparently caused by the rougher peened surface on the blade slot. Since the features of the background signal reproduce when the scan is repeated, they are caused by the characteristics of the material and/or the material surface.

Because the characteristics of the ECP signal in the area designated "signal from foreign material" appear similar to those which would be expected from a flaw, this area of the blade slot surface was examined in further detail by replicating the surface and examining the replica in a scanning electron microscope (SEM). A photomicrograph of the area from which this

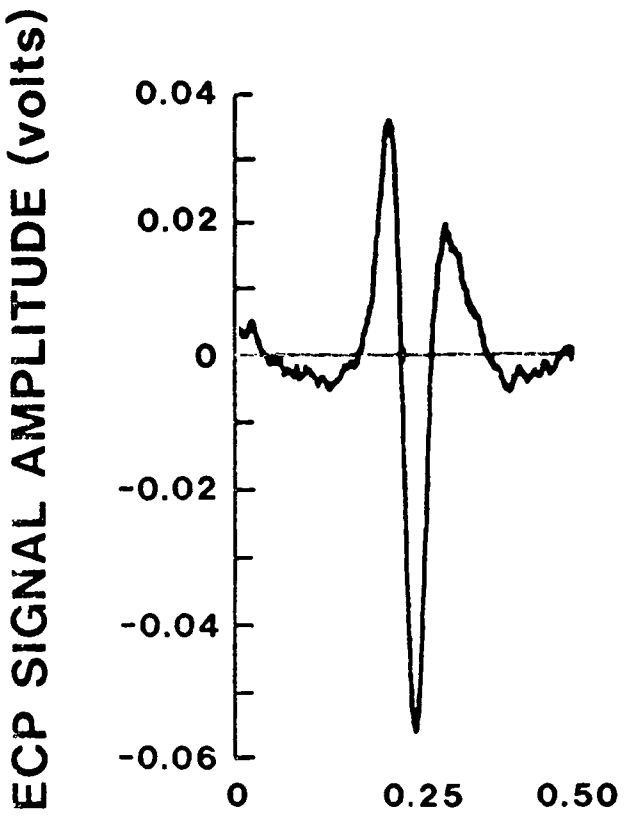

a. 0.0182 in. x 0.0105 in. EDM Slot

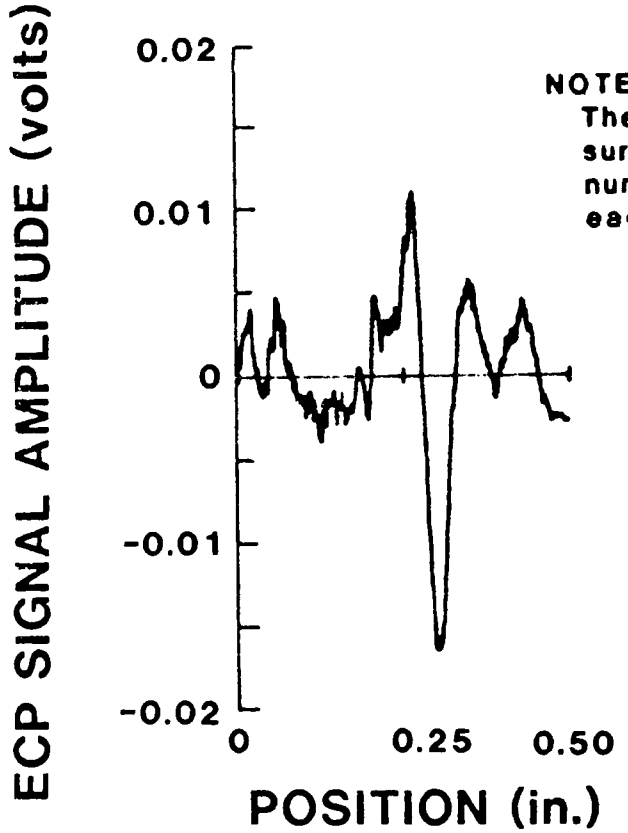

NOTE:
The first number is the measured surface length and the second number is the measured depth of each semi-elliptical notch.

b. 0.0105 in. x 0.0058 in. EDM Slot

FIGURE 21. ECP SIGNALS FROM EDM SLOTS IN F100 FIRST STAGE FAN DISK BLADE SLOTS

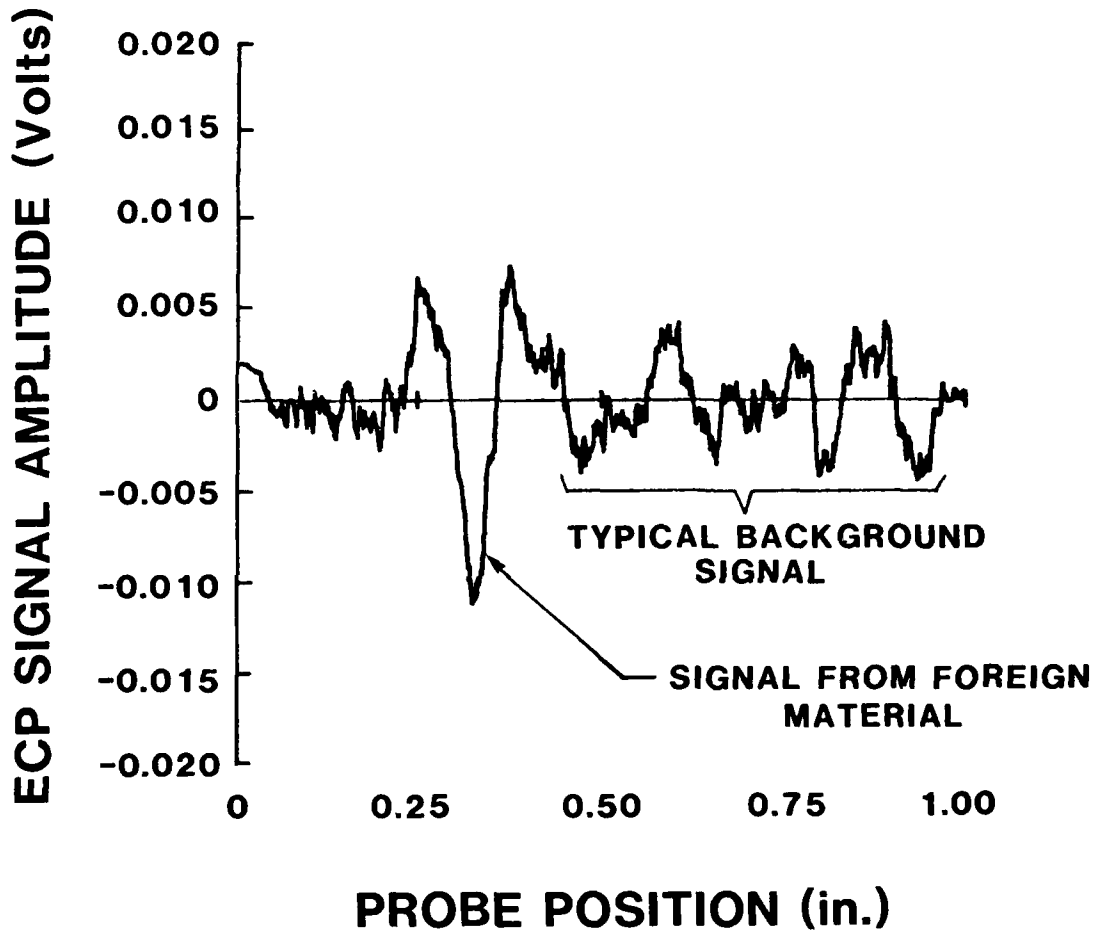

FIGURE 22. ECP SIGNAL FROM FIRST STAGE FAN DISK BLADE SLOT SHOWING TYPICAL BACKGROUND SIGNAL AND SIGNAL FROM FOREIGN MATERIAL IN SURFACE

signal was obtained is shown in Figure 23. It appears that the flaw shown in the photomicrograph is a particle of foreign material which is imbedded in the blade slot surface. It is possible that the foreign material could be a piece of glass from the glass bead peening operation to which this part was subjected during manufacture.

Using the linear scan along the length of the blade slots produces an edge effect in the ECP signal as the probe approaches the end of the blade slot. Initially this edge effect, which produces a large upswing in the signal, prevented flaws from being detected within approximately 0.2 in. of the edge of the blade slot. A limited evaluation of probe shielding showed that the use of a rudimentary shield allowed the probe to be scanned up to 0.12 in. from the edge of the slot before the edge effect became severe. It is likely that the use of more effective shielding arrangements and/or signal processing would allow the edge effect to be reduced even further.

ECP data were also obtained from EDM slots and fatigue cracks in all six of the Type III specimens. It was initially intended that a direct comparison would be made of the ECP signals from EDM slots and fatigue cracks of nominally the same size. Such a direct comparison was not possible, however, because of uncertainties in crack sizes. As was noted in Section II.6.a.1, one of the fatigue cracks was sectioned in an attempt to determine the geometrical shape of the crack tip, which determines the area of the crack face. It was found, however, that sectioning results did not conform to any simple geometrical shape, i.e., crack shape, based on depth data at three points along the length of the crack, appeared to be quite irregular. Given this result, and knowing that the shapes of small fatigue cracks grown from starter notches can be very dependent on crack size as well as starter notch

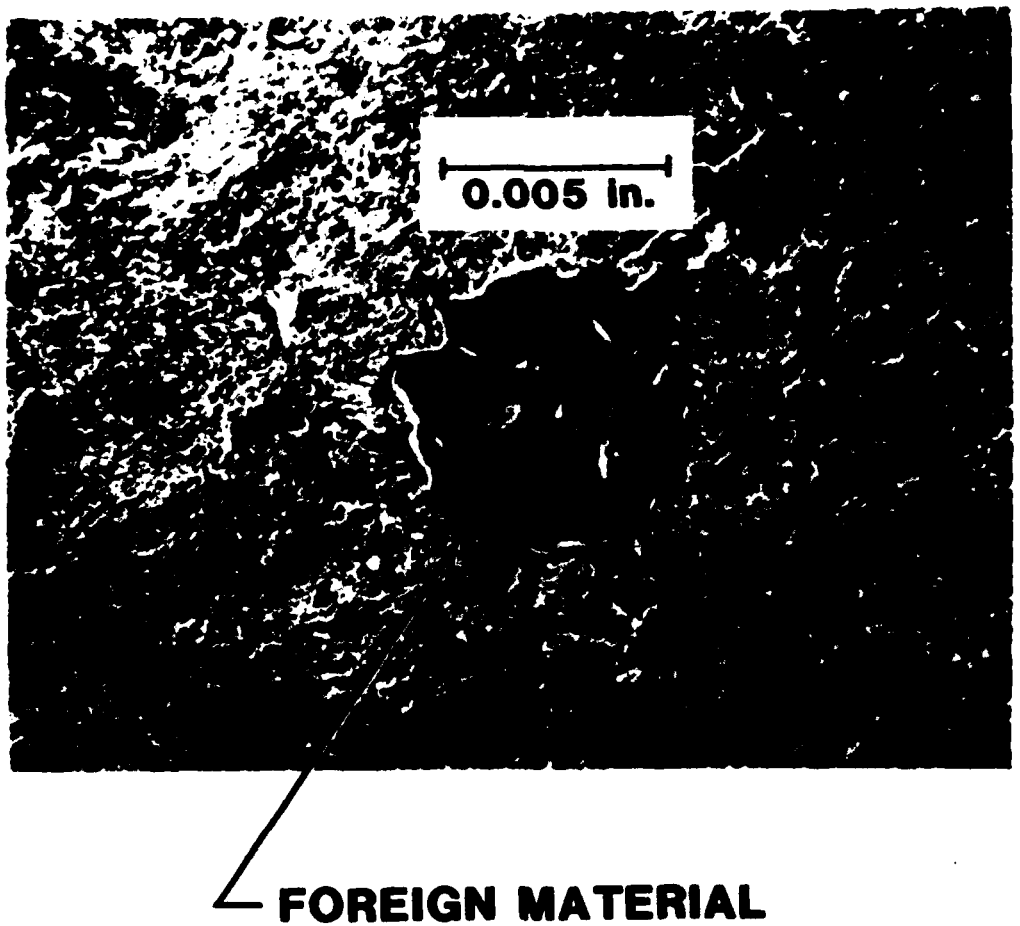

FIGURE 23. SEM PHOTOMICROGRAPH OF REPLICA TAKEN FROM A BLADE SLOT IN FIRST STAGE FAN DISK

size and shape, it was necessary to make some rather questionable assumptions regarding crack shape in order to make comparisons with EDM slot data on the basis of flaw area. Thus, for lack of better data, it was assumed that all fatigue cracks had a 3.7 to 1 aspect ratio, based on the sectioning result at the center of one crack, and were of semi-elliptical shape. This assumption forms the bases for the amplitude/area relationship for fatigue cracks shown in Figure 24 as circled points.

Data for EDM slots, which are subject to much less uncertainty in the determination of flaw area, are shown as triangles in Figure 24. These data show the expected linear relationship between signal amplitude and flaw area in agreement with previous experience. The least squares fit, shown as a solid straight line in the figure, is based on EDM slot data for all but the largest slot because, for the largest slot, probe dimensions were comparable to flaw length and under such conditions, the linear amplitude/area relationship can be expected to fail. It should be noted that, in spite of considerable uncertainty in crack areas, the amplitude/area relationship for fatigue cracks (the circles in Figure 24) agree surprisingly well with the data for small EDM notches.

However, because of uncertainties in crack areas, demonstration of the equivalence of EDM slots and fatigue cracks, based on data obtained under the present program, cannot be considered satisfactory. For this reason, additional data obtained from previous experiments are presented in Appendix C to demonstrate equivalence. These data include an amplitude/area plot, much like that in Figure 24, and plots of ECP signal amplitude vs. position along the lengths of an EDM slot and a crack of the same size. The latter plots show point-by-point equivalence of slot and crack signals and

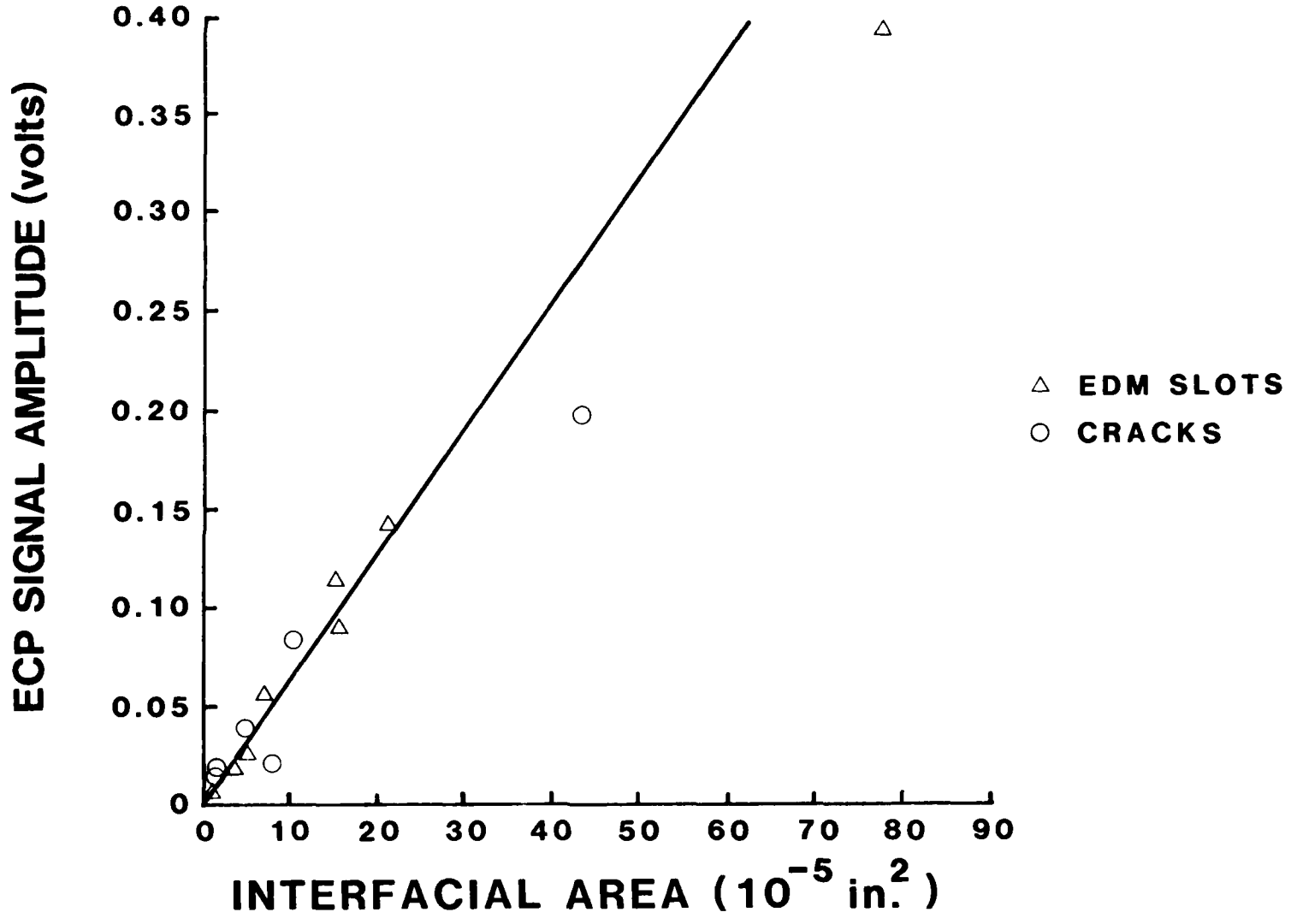

FIGURE 24. ECP SIGNAL AMPLITUDE VS. INTERFACIAL AREA FOR EDM SLOTS AND CRACKS IN TYPE I AND TYPE III SPECIMENS. CRACK AREA ESTIMATED FROM 3.7 TO 1 ASPECT RATIO OF SECTIONED CRACK.

thus provide convincing evidence that ECP response to cracks and slots are essentially the same.

In conclusion, it has been shown that the ECP method is very sensitive to surface flaws and that flaws as small as 0.0085 in. L. x 0.0020 in. D. with approximately one-third the interfacial area of the RFC flaw size of 0.010 in. L. x 0.005 in. D. are detectable in Titanium alloy material. Flaws of the nominal RFC target size are also readily detectable in the blade slots in an F100 engine first stage fan disk, even in the presence of the higher background noise produced by the material and surface conditions in the disk. The presence of what appears to be a piece of foreign material in the surface of one of the blade slots was also detected by the ECP method. ECP data from the Type I and Type III specimens showed that a linear relationship exists between the amplitude of the ECP signal and the interfacial area of the flaws. Although it was not possible to obtain a measurement of the depths of all of the fatigue cracks in the Type III specimens, projections made from sectioning results on one fatigue crack showed that the ECP responses from EDM slots and fatigue cracks having the same interfacial area are nominally equivalent.

b. Antirotation Windows

(1) Specimens

The Type I antirotation window specimen consisted of an F100 second-to-third stage fan seal as shown in Figure 25. Basically the antirotation window is a notch with a radius in each corner. Window dimensions are shown in Figure 26. A 0.063 in. radius is shown in Figure 26 and was used in the Type II specimens; however, the manufacturing drawings for the seal allow a radius dimension of 0.060 in. to 0.080 in. The seal material is Ti 6-2-4-6.

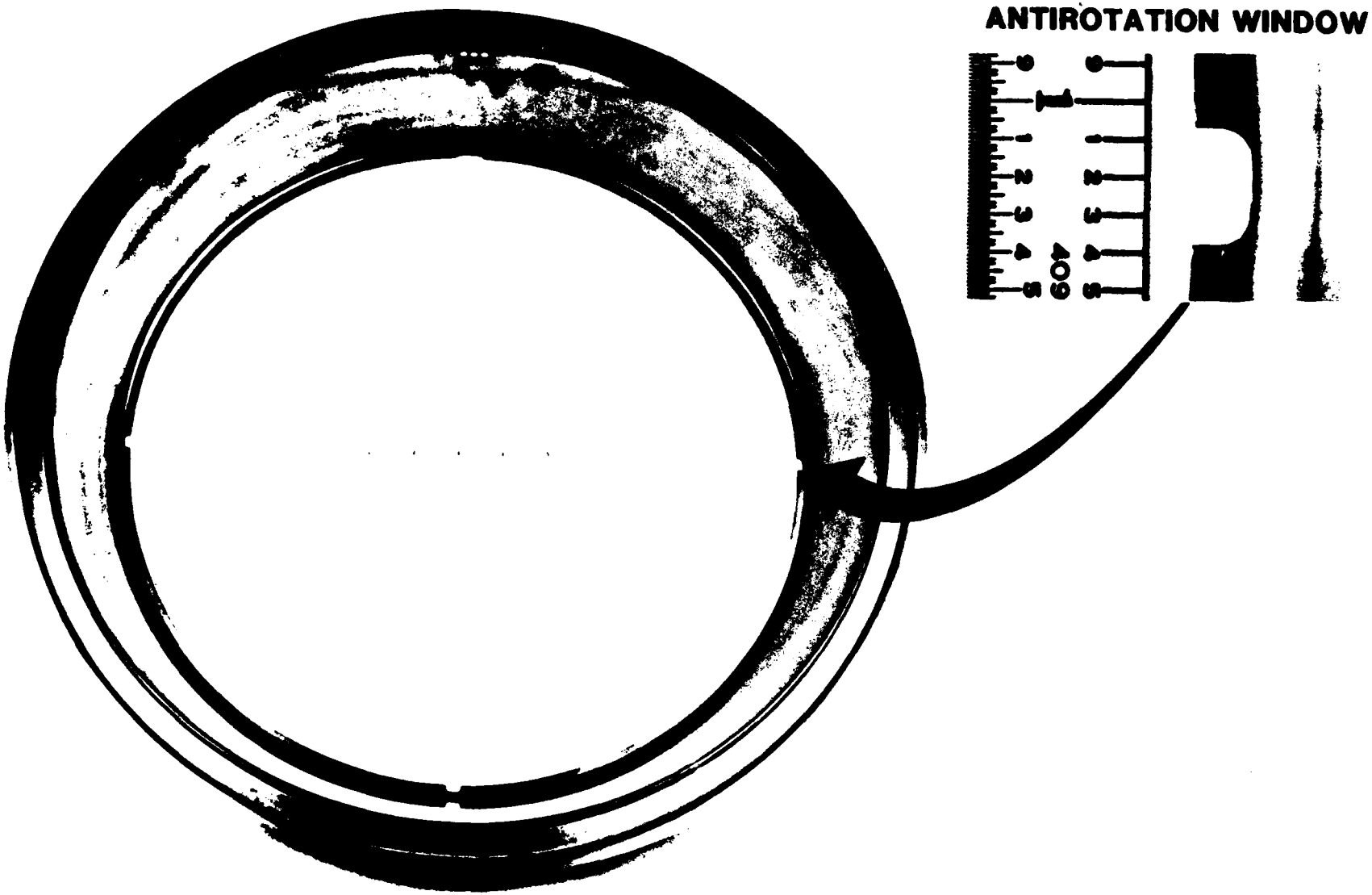

FIGURE 25. F100 ENGINE SECOND-TO-THIRD STAGE FAN SEAL WITH ANTIROTATION WINDOWS

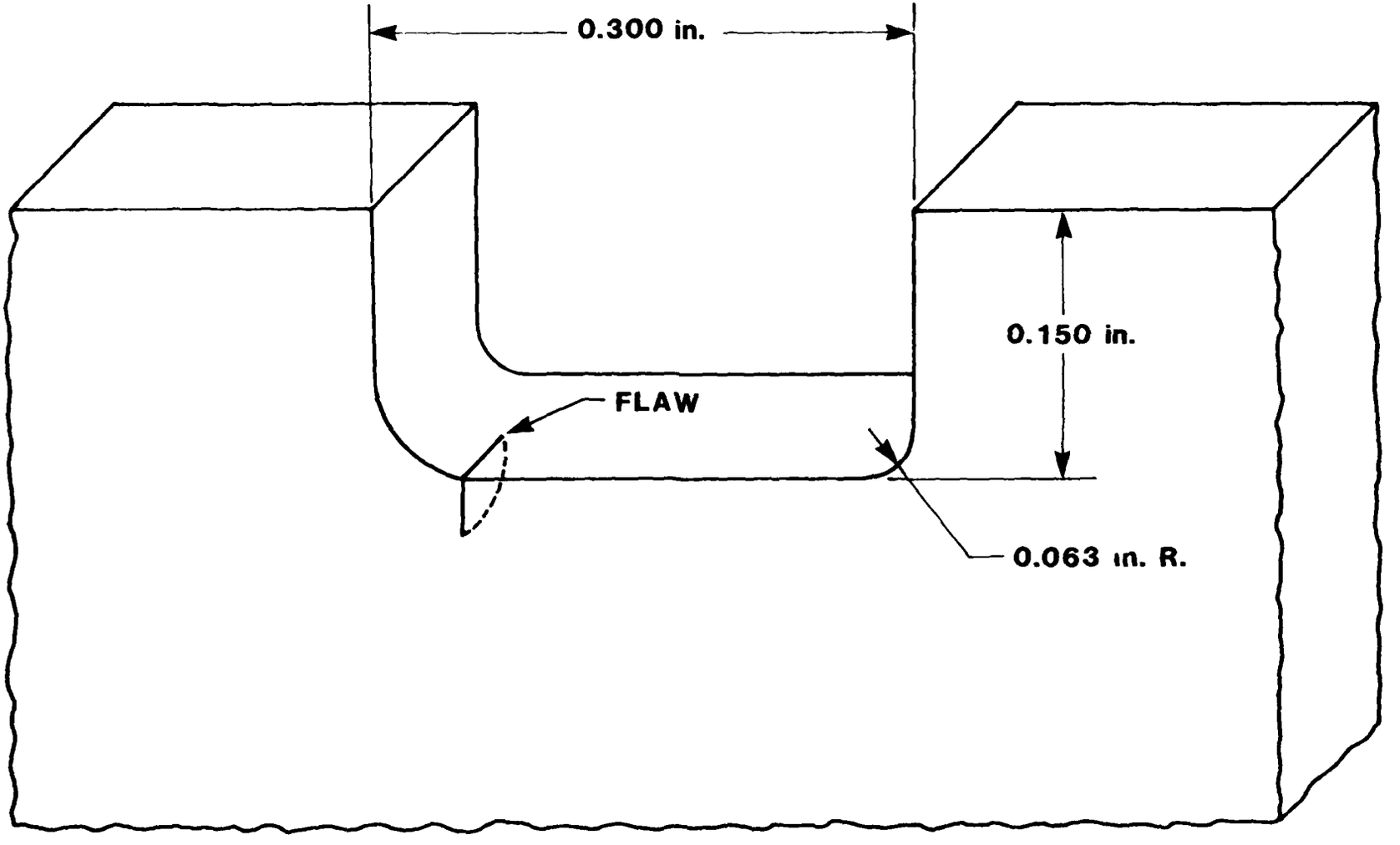

FIGURE 26. ANTIROTATION WINDOW CONFIGURATION IN F100 SECOND-TO-THIRD STAGE FAN SEAL

Corner fatigue cracks are expected to grow at the window radius tangency point. EDM slots (quarter penny shape) were therefore machined in two of the four antirotation windows of the seal as shown in Figure 26. The two EDM slot radii were 0.015 in. and 0.020 in.

The Type II specimen is shown in Figure 27. This specimen contains flaws on a straight edge for initial tests, as well as simulated 2nd to 3rd stage seal antirotation windows with and without flaws. The flaws are triangular EDM slots of the sizes shown in Table 3. The simulated antirotation window dimensions are the same as those shown in Figure 26. Since Ti 6-2-4-6 material was not readily available, the specimen was fabricated from Ti 6-4.

The Type III specimen set consisted of three specimens containing simulated antirotation windows into which fatigue cracks and EDM slots were introduced. Each of the three specimens had the configuration shown in the sketch of Figure 28. Specimen material (Ti 6-2-4-6) was cut from a scrap F100 third stage fan disk obtained from Kelly AFB. A fatigue crack was grown on one edge of each simulated antirotation window, and an EDM slot of nominally the same dimension was machined in the opposite edge. Fabrication of the rectangular specimen blanks was performed at SwRI; machining of the simulated antirotation windows, fatigue cracks, and EDM slots was subcontracted to Martin Marietta. Flaw sizes are shown in Table 4.

Although the antirotation window dimensions desired were nominally those shown in Figure 26, some of the specimens deviated from this configuration. Generally, the curved surfaces in the radius regions were not circular and the average radii were generally larger than the 0.063 in. specified. Figure 29 is a photograph of one specimen with a 0.063 in. radius

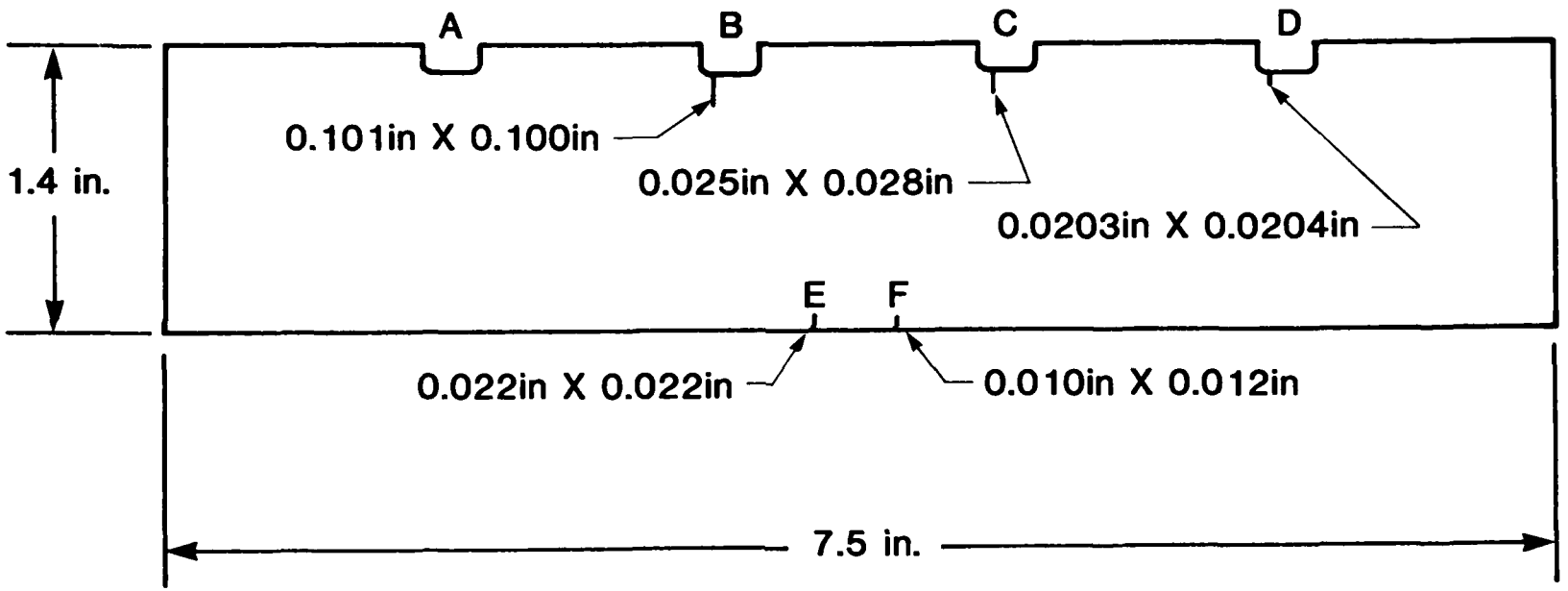

FIGURE 27. TYPE II ANTIROTATION WINDOW SPECIMEN

TABLE 3

EDM SLOT DIMENSIONS IN TYPE II SPECIMENS WITH SIMULATED ANTIROTATION WINDOWS

DESIGNATION	LOCATION	DIMENSION ON SPECIMEN FACE (in.)	DIMENSION ON SPECIMEN EDGE (in.)	WIDTH (in.)
B	Window B	0.101	0.100	0.005
C	Window C	0.025	0.028	0.005
D	Window D	0.0203	0.0204	0.005
E	Straight Edge	0.010	0.012	0.0041
F	Straight Edge	0.022	0.022	0.0042

Note: Window A is unflawed

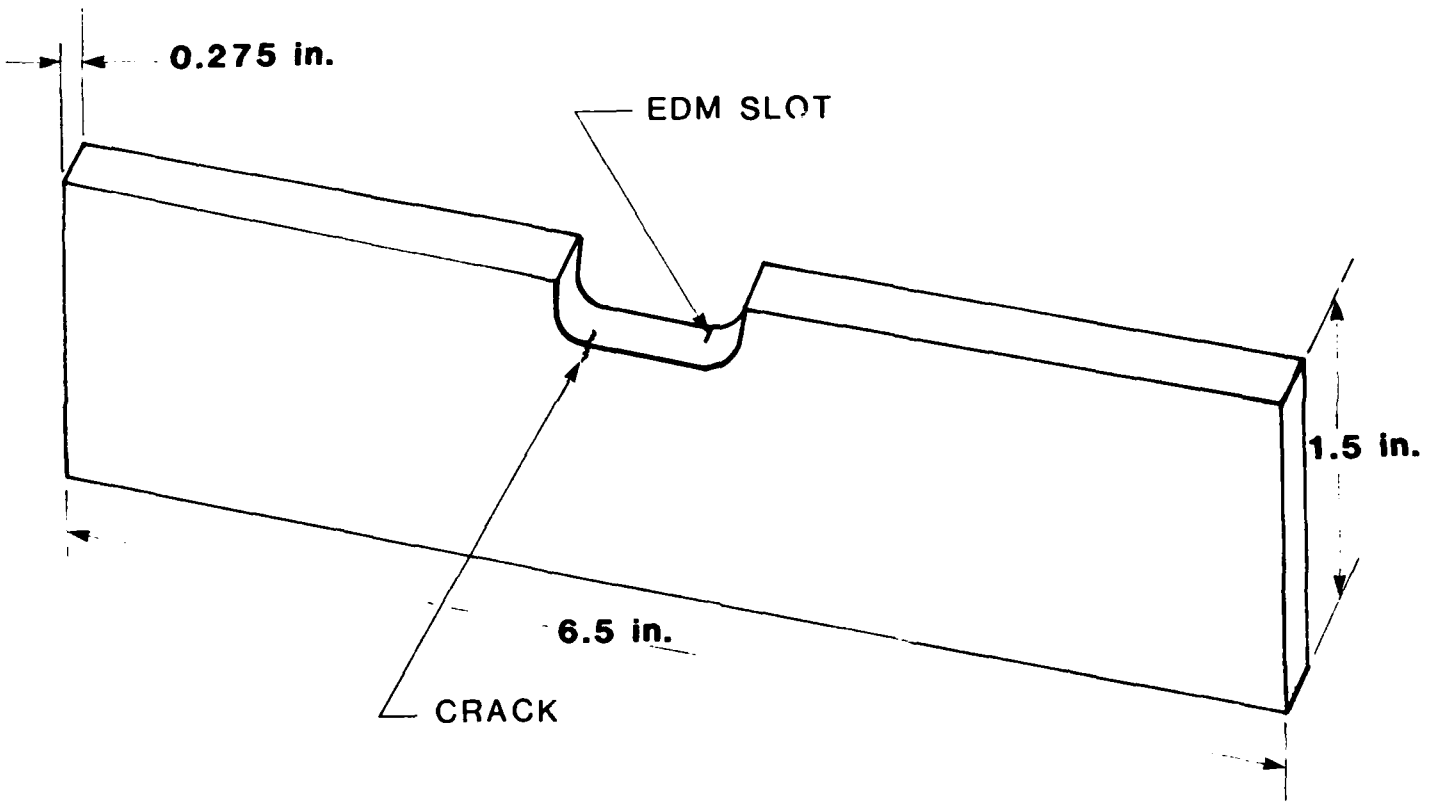

FIGURE 28. SIMULATED ANTIROTATION WINDOW GEOMETRY IN TYPE III SPECIMENS

TABLE 4

CORNER FLAW DIMENSIONS* IN TYPE III SPECIMENS WITH SIMULATED ANTIROTATION WINDOWS

SPECIMEN NUMBER	SPECIMEN MATERIAL	CRACK SURFACE LENGTH (in.)		EDM SLOT SURFACE LENGTH (in.)	
		On Face of Specimen	On Edge of Specimen	On Face of Specimen	On Edge of Specimen
S-1	Ti 6-2-4-6	0.0073	**	0.0247	0.0195
S-2	Ti 6-2-4-6	0.0085	**	0.0170	0.0165
S-3	Ti 6-2-4-6	0.0100*** 0.0200	** 0.033	0.0252	0.0201

* Measured from replicas and photomicrographs

** Crack is not visible

*** Two crack indications are present in specimen S-3

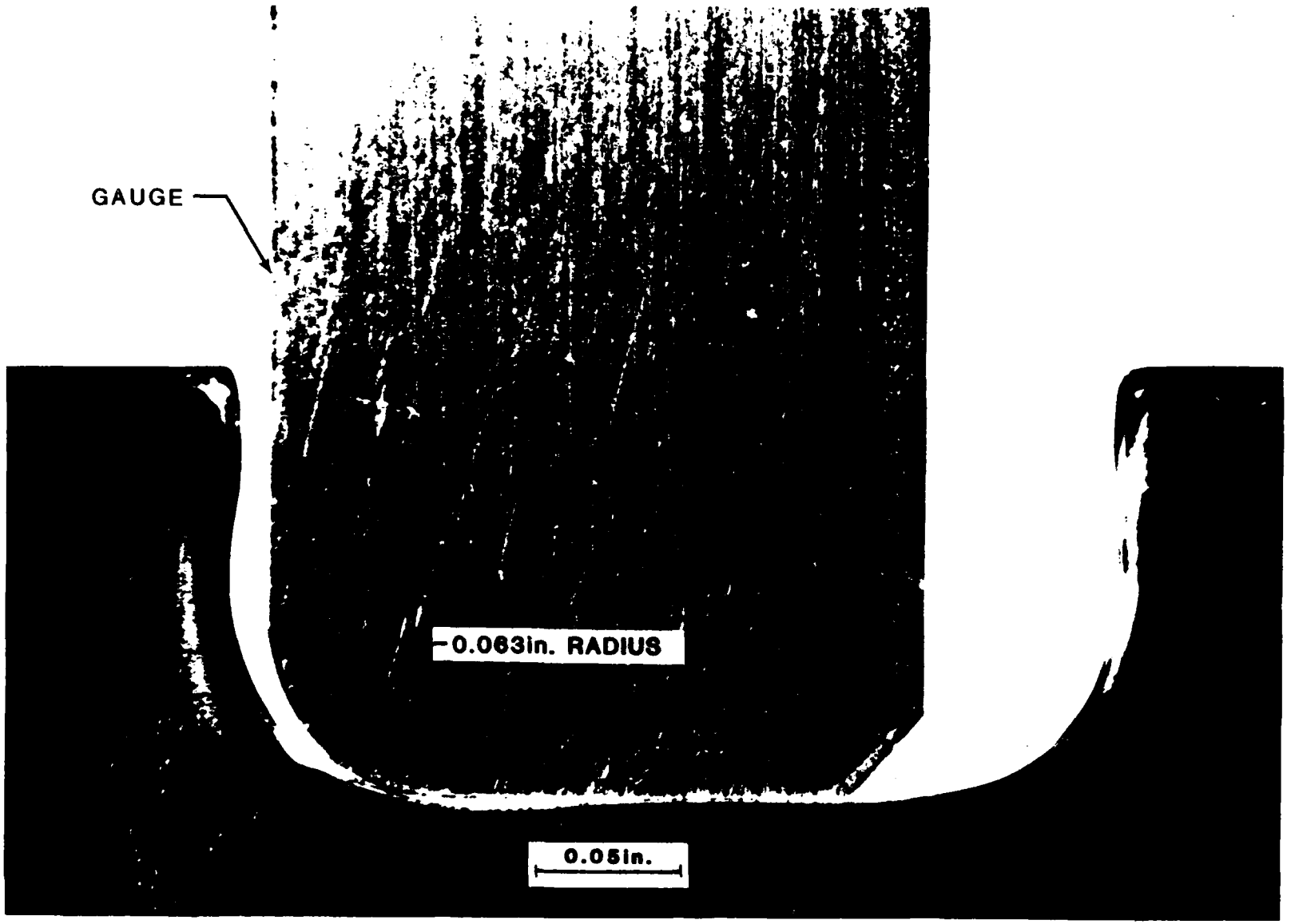

FIGURE 29. SIMULATED ANTIROTATION WINDOW WITH RADIUS GAUGE INSERTED. THE WINDOW CURVATURE IS NOT UNIFORM AND DOES NOT MATCH THE GAUGE CURVATURE.

gauge inserted. Note the nonuniformity in the antirotation window and the difference in the radius from that of the gauge. As will be discussed in a following section, these variations of geometry caused ECP inspection difficulties.

In addition to the set of specimens discussed above, six Ti 6-4 specimens containing fatigue cracks in simulated antirotation windows were obtained from Martin Marietta on a loan basis. These specimens were used in the Air Force program entitled, "Reliability of Nondestructive Inspection of Aircraft Engine Components". Tne specimens were used to obtain ECP data from fatigue cracks in initial experiments. The specimen configuration is similar to that shown in Figure 26 except that the radius measured 0.080 in. The specimen of primary interest contained a 0.020 in. x 0.020 in. fatigue crack.

(2) Experimental Setup

Scans of the antirotation windows in all specimens were made using the laboratory breadboard scanning system described earlier. Figure 30 shows the second-to-third stage seal mounted in the laboratory breadboard scanning system. Additional fixtures allowed the other specimens to be mounted in the scanning system. Two types of scans were made. Using the linear scan path shown in Figure 31, the probe was scanned past the bottom of the antirotation windows and therefore only a simple scanning motion was required. The second arrangement involved a contour scan (Figure 32) in which an ECP probe was placed inside the antirotation window. The contour scan was accomplished by rotating the probe about the window radius starting at 35° from the reference position and ending at the radius tangency point. The

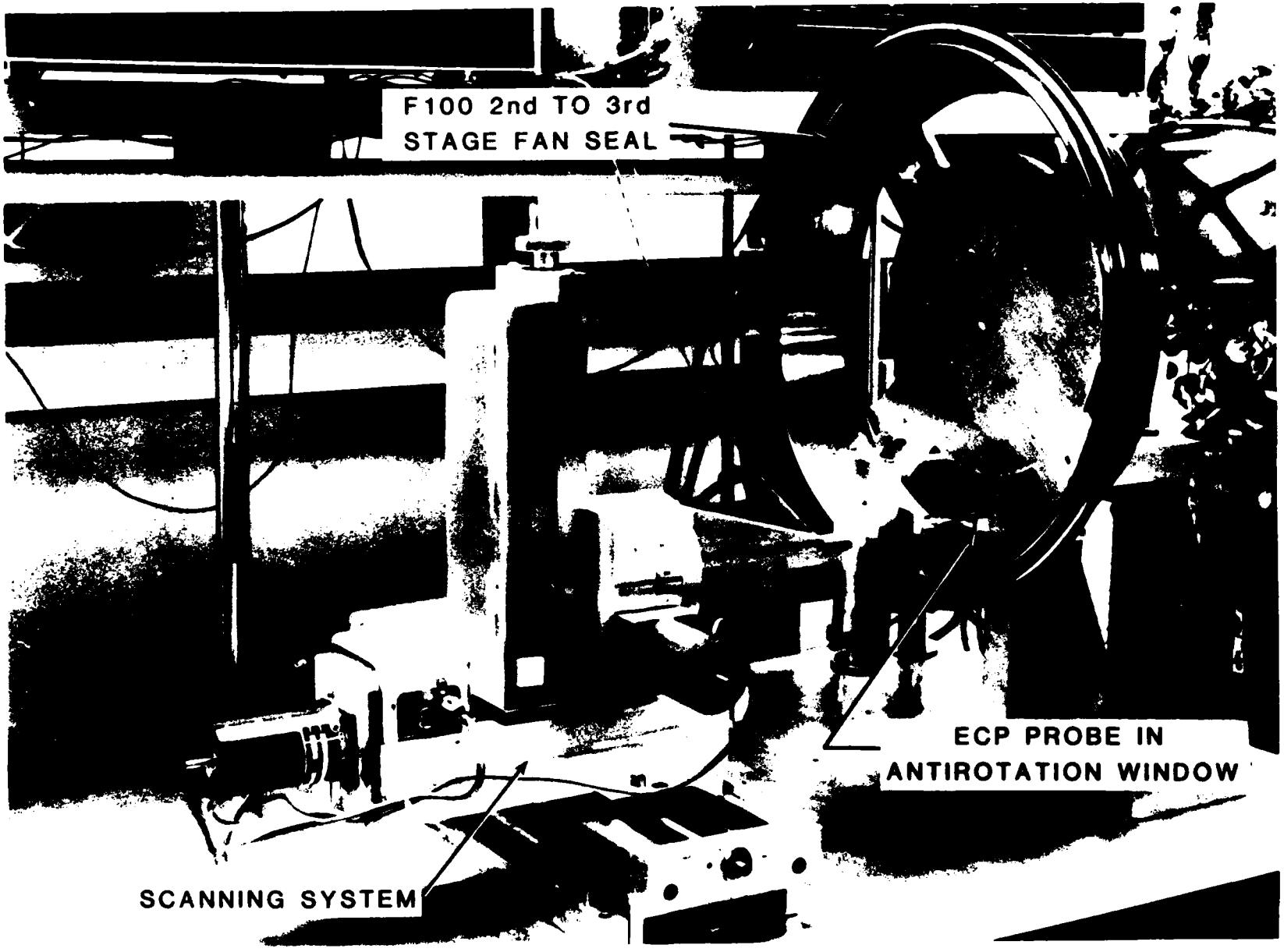

FIGURE 30. ECP LABORATORY BREADBOARD SCANNING SYSTEM WITH F100 SECOND-TO-THIRD STAGE FAN SEAL IN PLACE

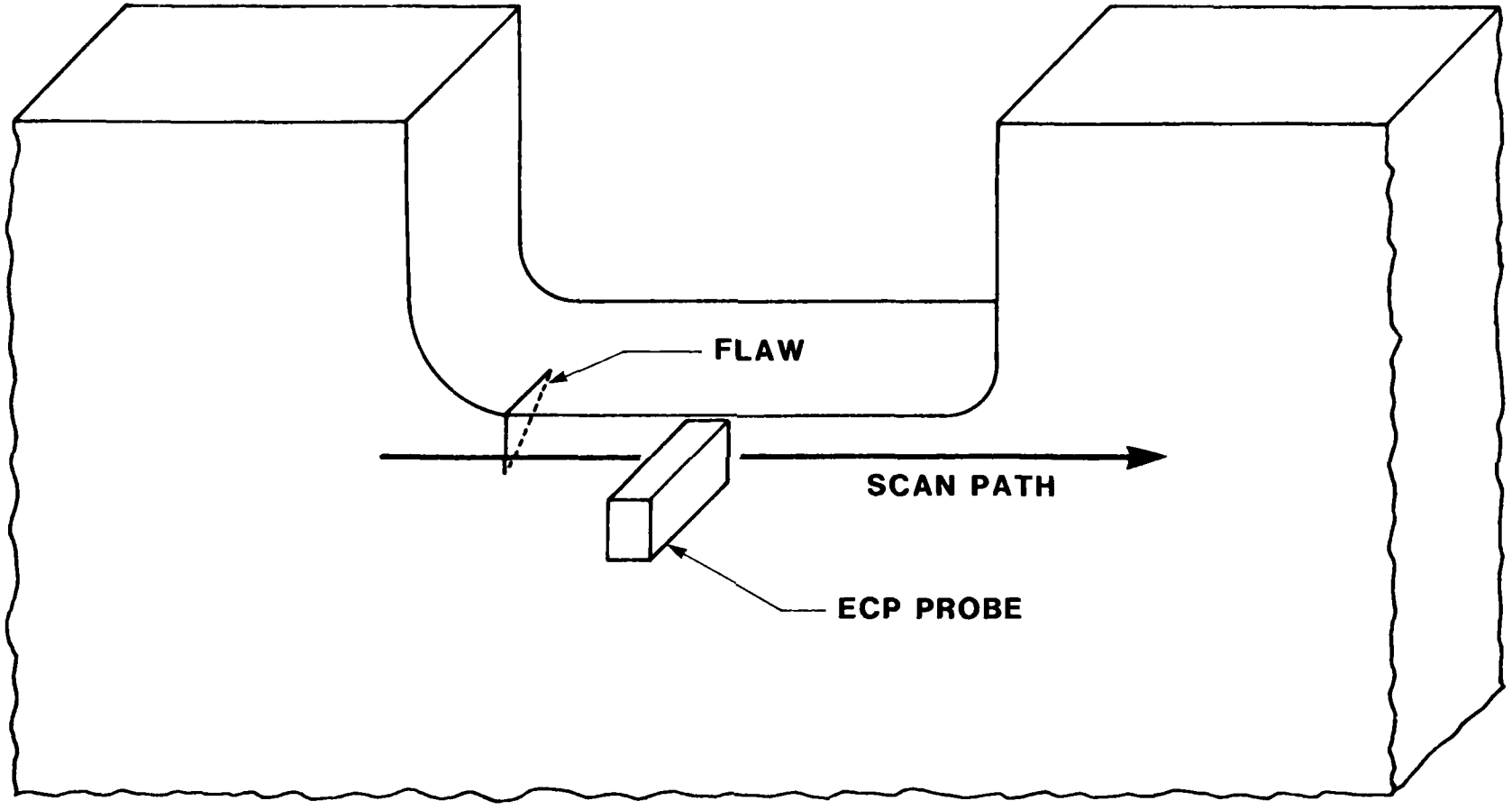

FIGURE 31. CONFIGURATION FOR LINEAR SCANS OF ANTIROTATION WINDOWS

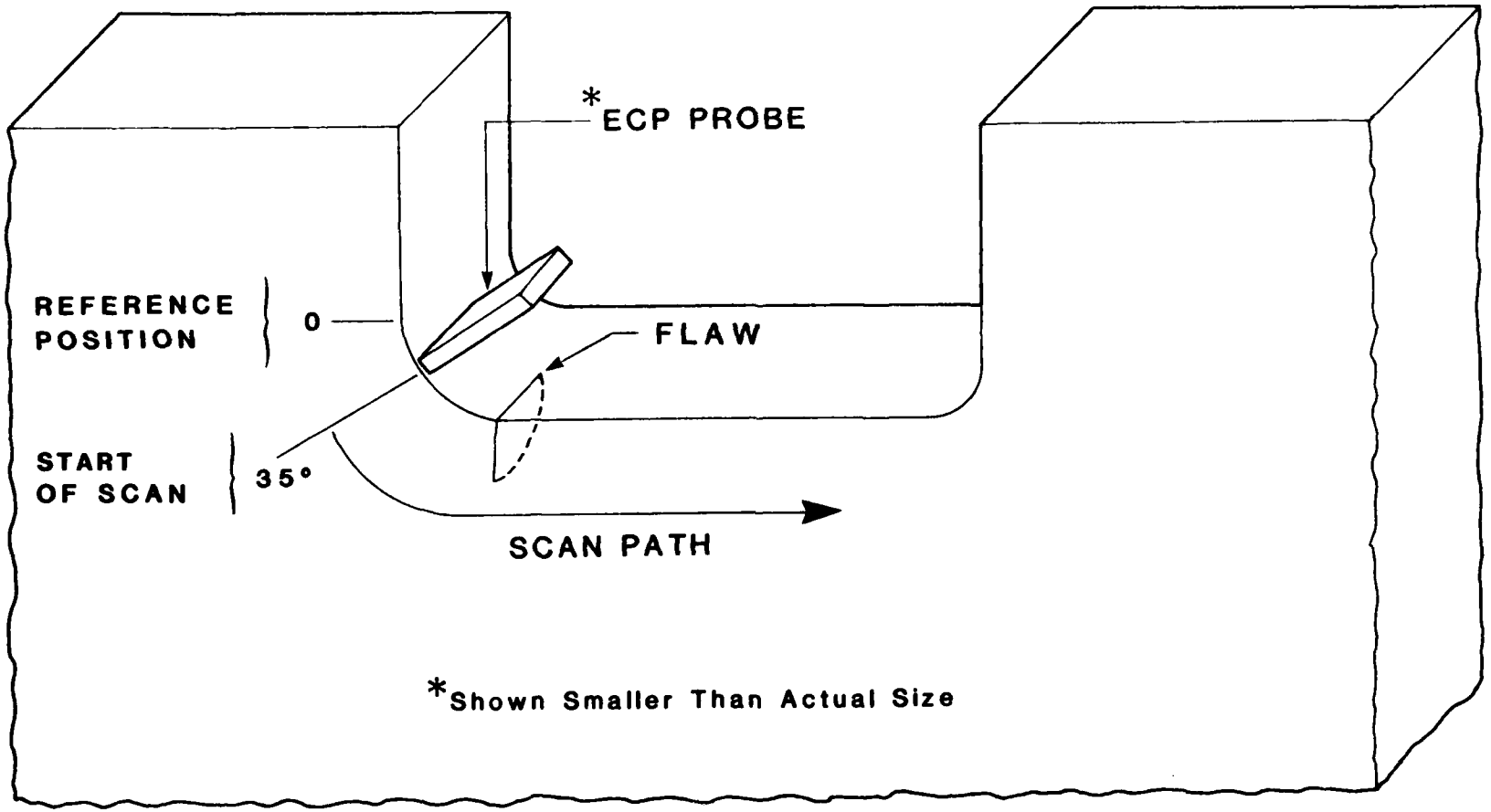

FIGURE 32. CONTOUR SCAN CONFIGURATION FOR ANTIROTATION WINDOWS

probe was then translated linearly along the bottom of the window to the midpoint. This approach allowed an approximately constant relationship to be maintained between the probe orientation and the window geometry.

(3) Experimental Results

(a) Linear Scans

Initial evaluations to optimize the ECP probe for corner flaws and to determine the inherent sensitivity of the ECP method without the influence of specimen geometry were performed on the straight edge of the Type II specimen shown in Figure 27. The probe was scanned linearly along the specimen edge and over the two EDM corner flaws. Results are shown in Figure 33. Note that an excellent signal was obtained from even the smallest flaw with dimensions of 0.010 in. x 0.012 in. From these results, it was apparent that the desired sensitivity to flaws on the order of the RFC target size was established.

The linear scan approach was then applied to the simulated antirotation windows in the Type II specimen. A signal from a linear scan of windows A through D is shown in Figure 34. It is obvious that a substantial gradient signal is obtained even from the unflawed window (A). Also, some asymmetry caused by probe imbalance is present in the signal as shown by the difference in amplitude of the signal peaks from the leading and trailing edges of the window. The flaw signals from windows B, C and D are superimposed on the gradient signal and result in peaks having a larger amplitude than that from the unflawed window. A threshold line corresponding to the maximum amplitude of the unflawed window gradient signal has been drawn on the figure, and the flaws in windows B, C and D produce a signal amplitude

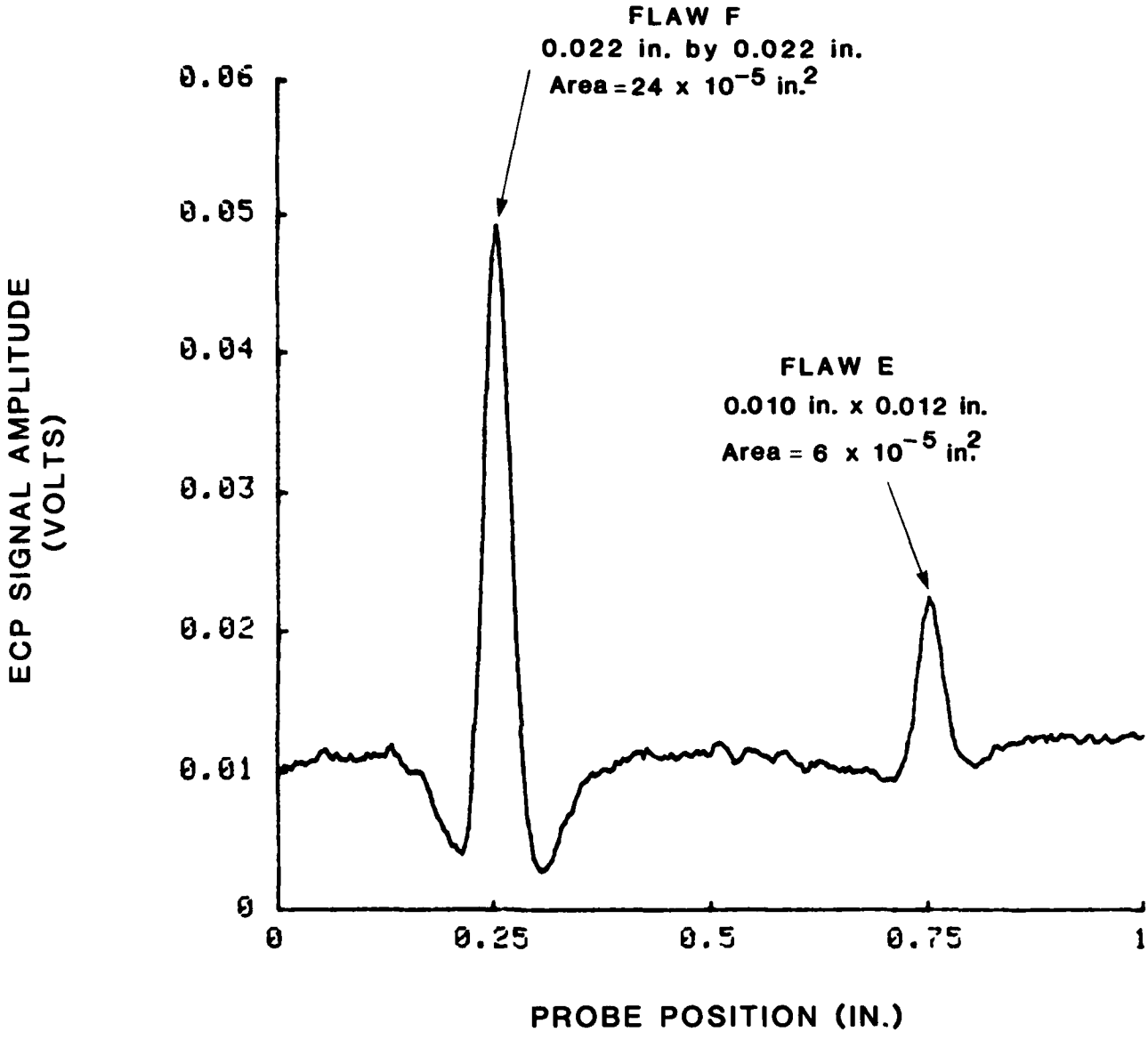

FIGURE 33. ECP SIGNALS FROM CORNER FLAWS IN STRAIGHT EDGE OF TYPE III SPECIMEN

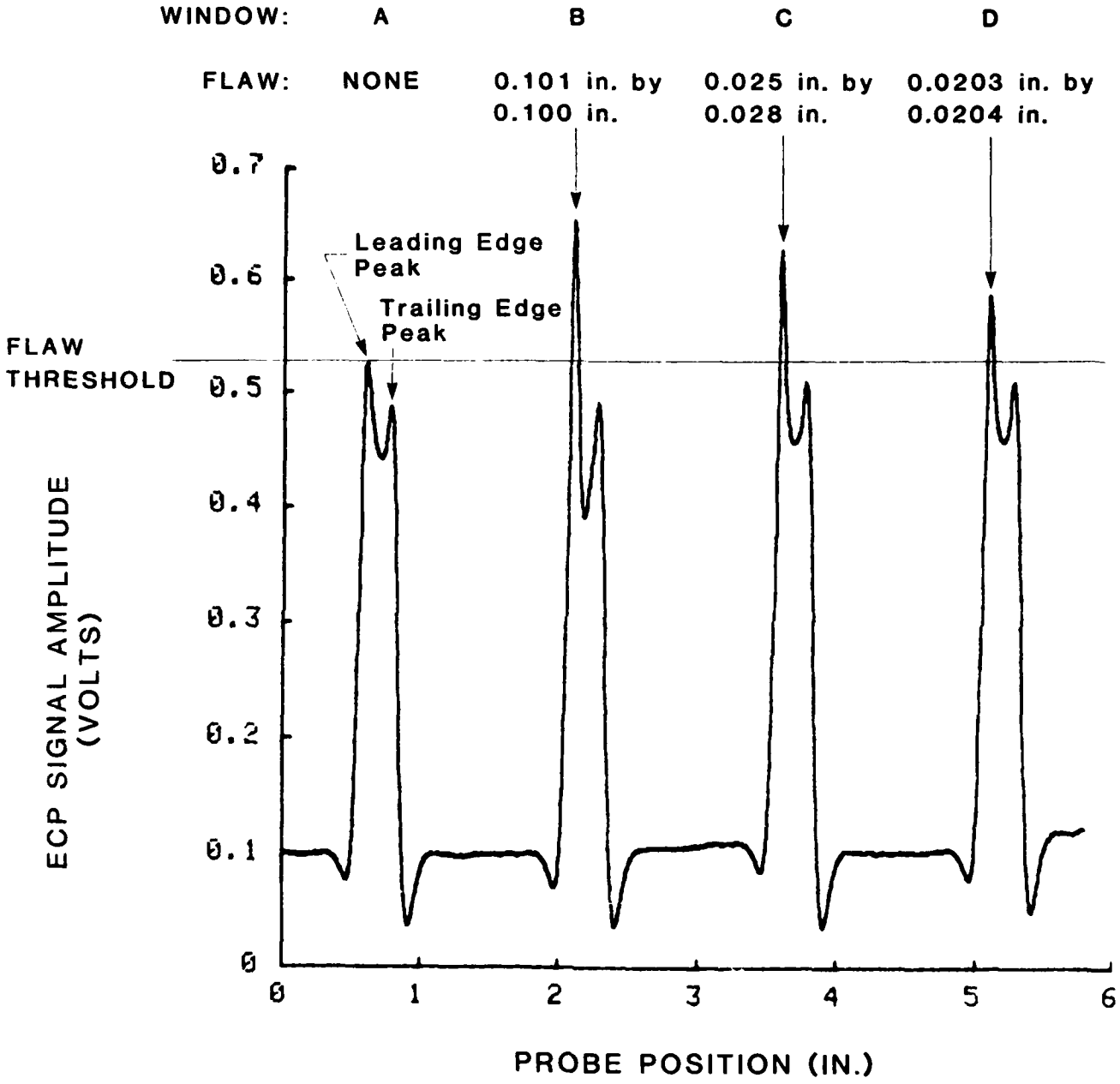

FIGURE 34. ECP LINEAR SCAN SIGNALS FROM SIMULATED ANTIROTATION WINDOWS IN TYPE II SPECIMEN

exeeding this threshold. Thus, even the smallest flaw (0.0203 in. x 0.0204 in.) can be distinguished above the signal gradient.

After completing evaluations on the Type II specimen, the linear scan approach was applied to the antirotation windows in the Type I specimen (second-to-third stage seal). Similar results were obtained as shown in Figure 35. Here, scans of an unflawed window and a window containing a quarter penney shaped EDM slot with a 0.020 in. radius are shown on the same figure. A threshold line has been drawn corresponding to the maximum amplitude of the unflawed window gradient signal. The presence of the flaw causes the signal on the right to exceed this threshold. The signal from the remaining unflawed window in this seal produced a similar response to the signal shown on the left. However, the signal from the window containing the EDM slot with a 0.015 in. radius was not readily distinguishable from the unflawed window signals.

ECP evaluations on the Type III specimens which contained both fatigue cracks and EDM slots did not produce results as definitive as those from the Type I and II specimens. This was due to the fact that the flaws were located in the antirotation window radius instead of at the radius tangency point, and that there were significant variations in the window geometry (see section II.6.b.1). Selected results from the type III specimens are given in Appendix E.

The linear scan approach for antirotation window inspection using ECP requires minimal setup and only simple scanning motions; however, substantial gradient signals are produced even from antirotation windows which contain no flaws. For flaws having a nominal size of 0.020 in. x 0.020 in., and which are located at the window radius tangency point, the flaw signals

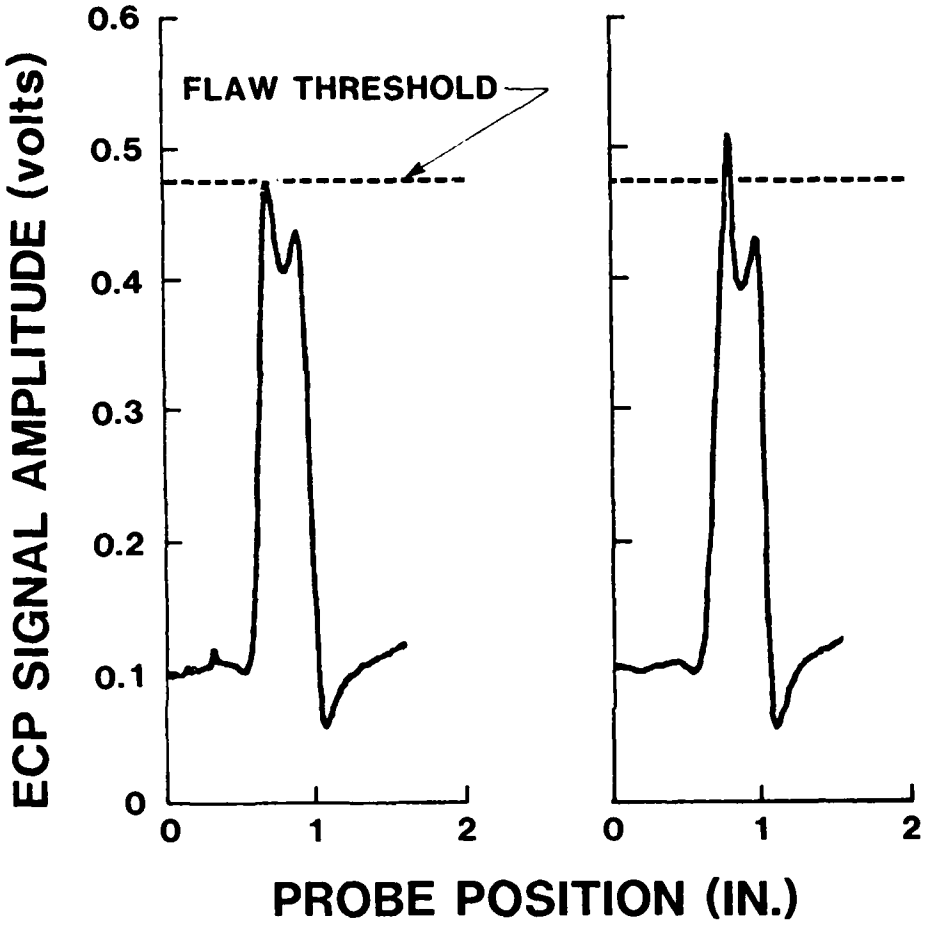

a. Window With No Flaw

b. Window With 0.020 in. Radius EDM Slot

FIGURE 35. ECP LINEAR SCAN SIGNALS FROM ANTIROTATION WINDOWS IN F100 SECOND-TO-THIRD STAGE SEAL (Type I Specimen)

exceed a threshold set at the maximum signal level of the unflawed window gradient signal. Flaws of this size which are located in the radius instead of at the tangency point do not produce signals which exceed the threshold, although subtraction of an unflawed window gradient signal from the flawed window signal yields a recognizable flaw signal (see Appendix E). The linear scan approach is affected somewhat by variations in window geometry; however, the effect does not appear to be severe.

(b) Contour Scans

As discussed in the previous section, linear scans of the antirotation windows, while being relatively simple to implement, produced substantial gradient signals even from windows which contained no flaws. For this reason, additional investigations were undertaken in an effort to reduce the gradient signal from unflawed windows. This was accomplished using contour scans in which a miniaturized ECP probe was used to scan the inside of the antirotation window geometry. The contour scans were accomplished as shown, previously, in Figure 32 by first rotating the probe about the window radius and then translating the probe linearly along the bottom of the window to approximately the midpoint. In this manner a more nearly constant relationship between the probe orientation and the part was maintained compared to the linear scans. Due to probe size constraints the scan was initiated at 35° from the reference position at the radius upper tangency point as shown in the illustration.

The contour scan approach was first evaluated on the Type II specimen. Scans of unflawed window A and window D which contains a 0.0203 in. x 0.0204 in. EDM slot are shown in Figure 36. Although a gradient signal is

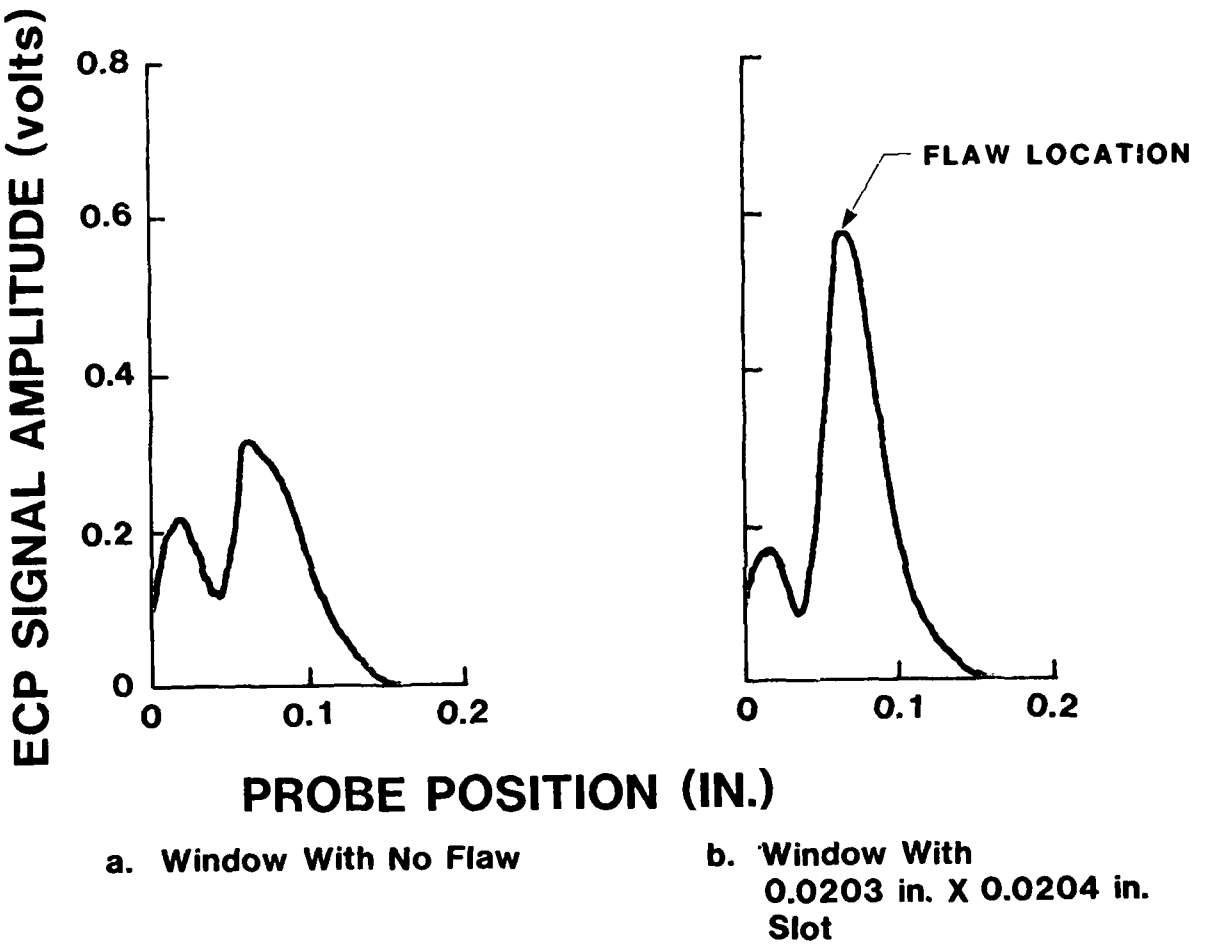

FIGURE 36. ECP SIGNALS FROM CONTOUR SCANS OF SIMULATED ANTIROTATION WINDOWS IN TYPE II SPECIMEN

still obtained from the unflawed window, the window containing the flaw produces a much more recognizable indication from the flaw than was obtained previously with the linear scans.

The contour scan approach was also evaluated on a fatigue crack specimen which was borrowed from Martin Marietta Corporation. The radius in this specimen was nominally 0.08 in. instead of 0.063 in. as in the Type II specimens. A comparison of signals from an antirotation window containing a 0.020 in. x 0.020 in. fatigue crack and an antirotation window continuing a 0.0203 in. x 0.0204 in. EDM slot (Type II specime) shown in Figure 37. In the fatigue crack specimen the crack is located in the radius (at approximately the 45° position) and not at the tangency point. Thus, the signal peak from the fatigue crack is closer to the beginning of the scan than the EDM slot signal peak. Nevertheless, aproximately the same results are obtained from both the windows containing the EDM slot and fatigue crack of nominally the same size.

Contour scans were also completed on the antirotation windows in the second-to-third stage seal (Type I specimen). All four antirotation windows in the seal were scanned. Two windows contained quarter penny shaped EDM slots with 0.015 in. and 0.020 in. radii, respectively, and the remaining two windows were unflawed. The flaws were located at the window corner radius tangency point. Signals from the two flawed windows and one unflawed window are shown in Figure 38. ECP signals from the two flawed windows (solid lines in the figure) show a distinct flaw indication as compared to signals from the unflawed window (dashed lines). Note that the gradient signal from the unflawed window has a different shape from that of the simulated antirotation windows shown previously in Figure 36. This difference in

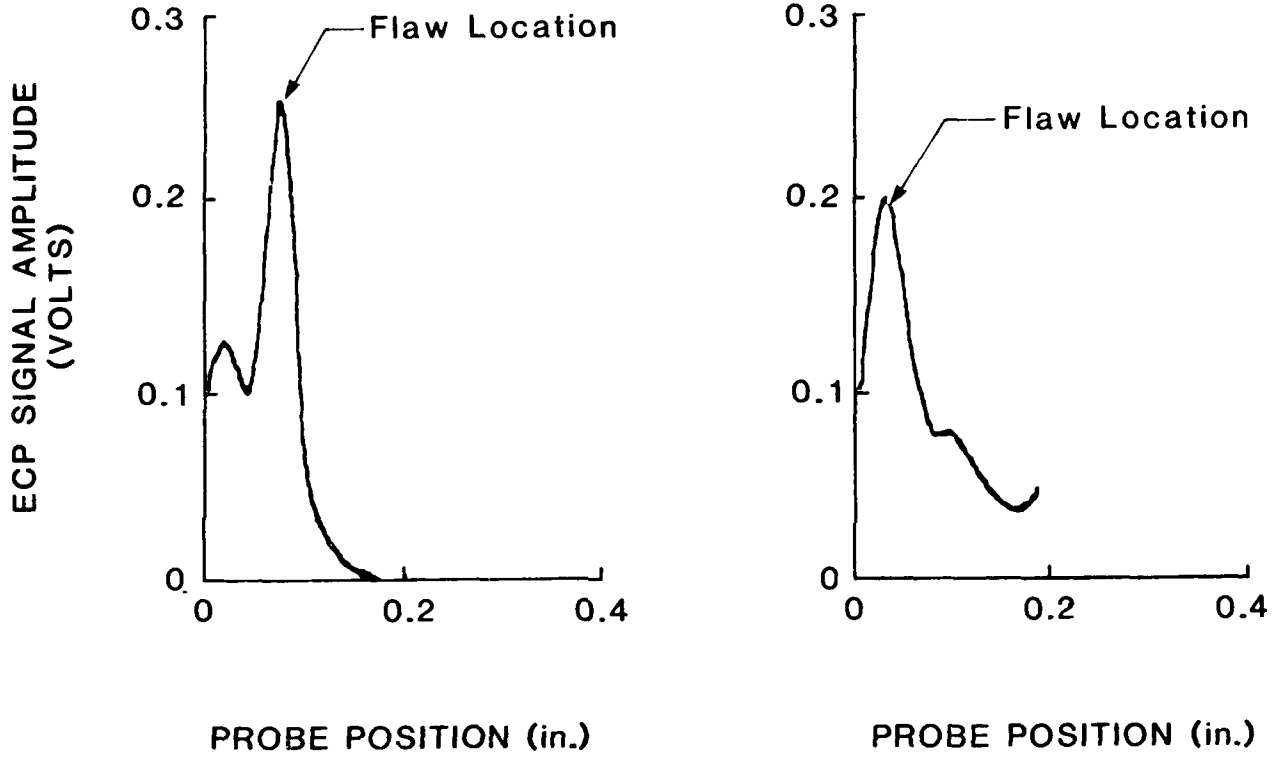

FIGURE 27. ECP SIGNALS FROM CONTOUR SCANS OF SIMULATED ANTIROTATION WINDOWS HAVING AN EDM SLOT AND A CRACK OF NOMINALLY THE SAME SIZE. THE SIGNAL AMPLITUDES DO NOT CORRESPOND TO THOSE IN THE PREVIOUS FIGURE SINCE AN EARLIER VERSION OF THE ECT PROBE WAS USED HERE.

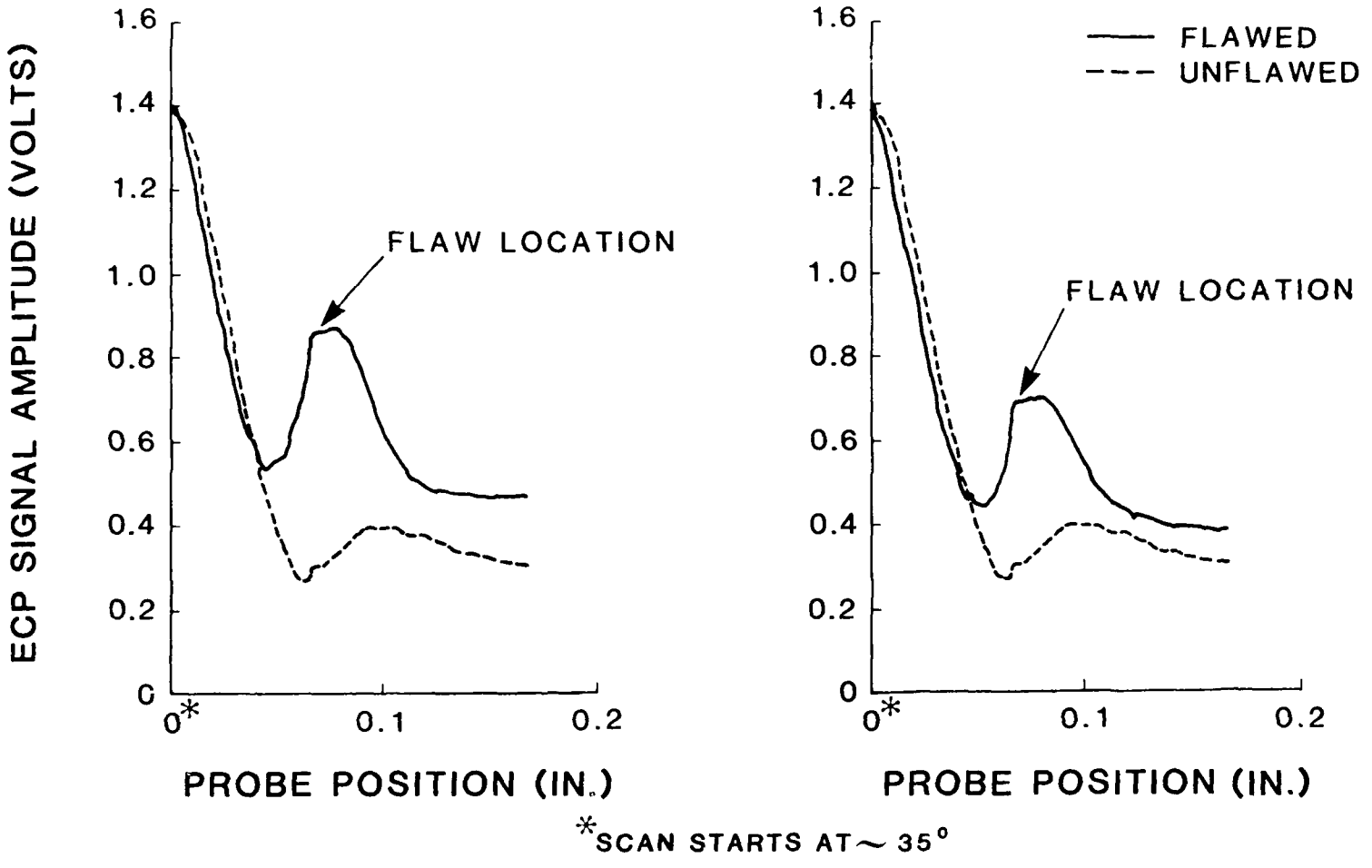

*SCAN STARTS AT ~ 35°

A. WINDOW WITH 0.020 IN. RADIUS SLOT AND UNFLAWED WINDOW

B. WINDOW WITH 0.015 IN. RADIUS SLOT AND UNFLAWED WINDOW

the signal gradient is due to the fact that the simulated windows are machined into a flat specimen while the windows in the seal are positioned close to an area where the seal geometry differs from that of a flat plate.

In Figure 38 it is readily apparent that the ECP signals from the flawed windows differ significantly from signals from the unflawed window. It is also apparent, from Figure 39, that signals from the unflawed windows are nearly identical. Therefore, at least for this seal, variations in ECP signals due to possible differences in window dimensions did not significantly influence the signal shape and, therefore, flaw detectability.

In summary, it can be concluded that the linear scanning approach is easier to implement than a contour scan and is less sensitive to variations in the window geometry, although the signal amplitude from flaws is relatively small when compared to the overall gradient signal obtained from unflawed windows. The contour scan significantly reduces the gradient signal from unflawed windows, and the flaw signal amplitude is much larger compared to the gradient signal than was the case for linear scans. Thus, using the contour scan, both the 0.020 in. and 0.015 in. flaws in the second-to-third stage seal anti-rotation windows were detected while only the 0.020 in. flaw was detectable using the linear scan.

Also, it was noted that the linear scan is most sensitive to detection of flaws at the radius tangency point while the contour scan is sensitive to flaws located anywhere in the radius. Although variation in window geometry was not a problem on the second-to-third stage seal, variations in the window geometry in the Type III specimens showed that if the geometry variations are too severe the ECP gradient signal obtained from a contour scan can be changed dramatically in shape and amplitude. Thus, one factor which

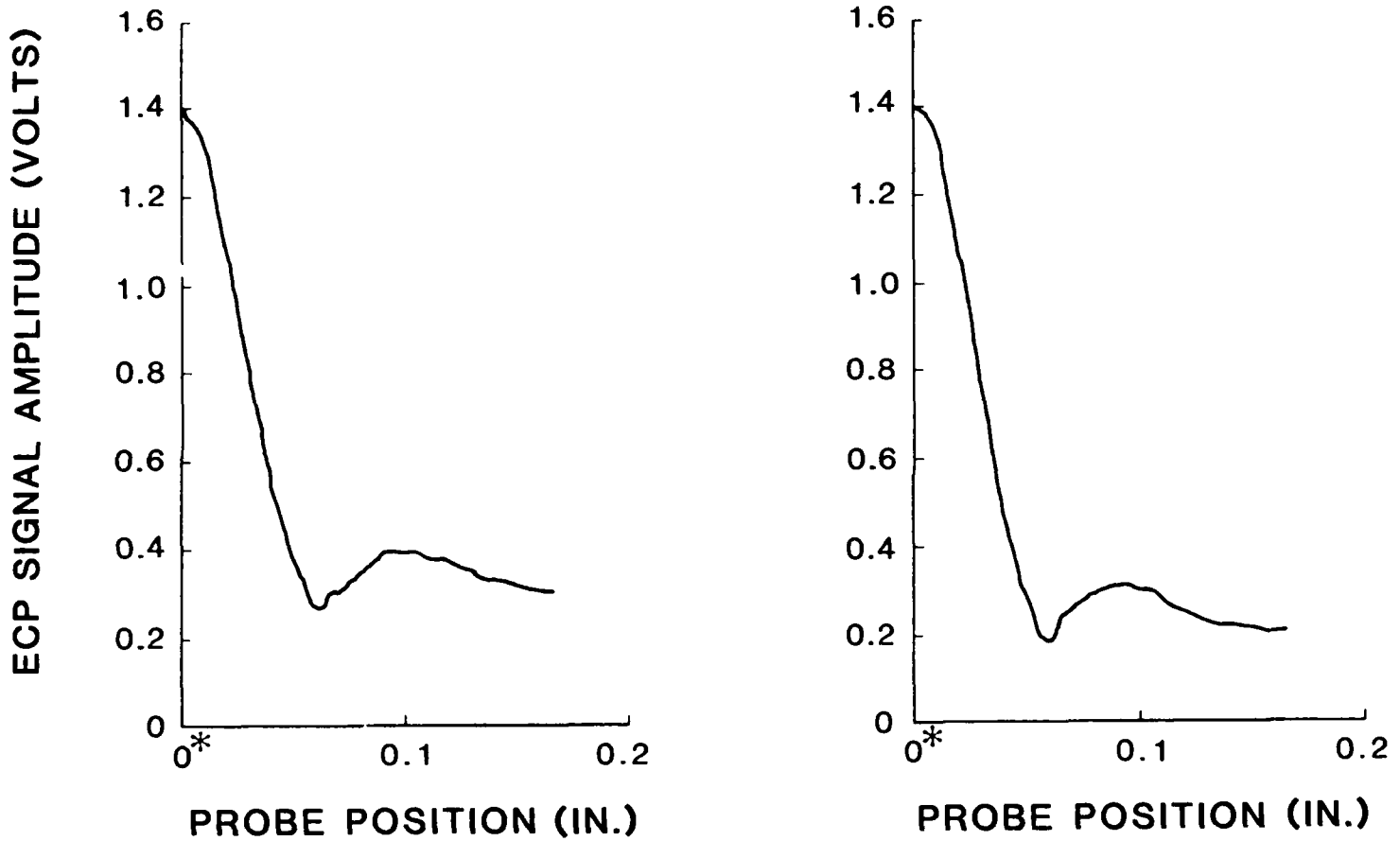

FIGURE 30. ECP SIGNALS FROM CONTOUR SCANS OF TWO UNFLAWED ANTIROTATION WINDOWS IN SECOND-TO-THIRD STAGE SEAL (Type I Specimen)

may limit the applicability of contour scans to the antirotation windows is that the surface inside the window could be roughened significantly by engagement with the mating part on the adjacent disk which protrudes into the antirotation window when the engine is assembled. This may produce a higher background noise level and reduce detectability of smaller flaws. Another factor to be considered is that while the antirotation windows in the F100 second-to-third stage seal have a relatively large radius (0.06 to 0.08 in.), the windows in other seals have much smaller radii (nominally 0.025 in.) which would make implementation of a contour scan much more difficult. Thus, while the contour scan offers superior flaw sensitivity under ideal geometry conditions, practical considerations such as part-to-part variations in geometry, the presence of surface irregularities, and ease of implementation would seem to favor the linear scan in most applications.

c. Balance Flange Scallops

(1) Specimens

The ECP method was demonstrated on balance flange scallops in the F100 first stage fan disk (Type I specimen). The scallops are visible on the fan disk in Figure 13. The scallops consist of semi-circular shaped cutouts (0.5 in. radius) through the thickness of the balance flange. Corner EDM slots were cut into the edge of two scallops to simulate fatigue cracks. It was intended that the EDM slots would have a quarter-penny shape, however, the actual dimensions on both the face and the edge of the scallop showed a slight deviation from this shape. The slot dimensions were 0.020 in. x 0.023 in. and 0.013 in. x 0.015 in.

(2) Experimental Setup

The scallops were scanned using the laboratory breadboard system

and the same probe that was used for the contour scans of the antirotation windows. This probe was placed inside each scallop and rotated about the scallop radius as shown in Figure 40. Due to the size of the probe housing, an arc of only 100° was scanned.

(3) Experimental Results

The ECP probe was scanned as described above and signals obtained from the two scallops containing the EDM flaws are shown in Figure 41. Figure 41a is a scan of the scallop containing the larger flaw which measured 0.020 in. x 0.023 in. and it is obvious that a very strong ECP signal is obtained from the flaw. A scan of the scallop containing the 0.013 in. x 0.015 in. EDM slot is shown in Figure 41b, and again a prominent ECP signal is obtained from the flaw. It is apparent from these results that the ECP method is readily adaptable to inspection of the balance flange scallops and that flaws smaller than 0.013 in. x 0.015 in. can be detected.

7. Preliminary Assessment of Probability of Detection

An accurate analysis of probability of detection requires much more inspection data than can be accumulated under an exploratory development program such as the present project. To obtain reliable statistics one needs several repeat scans over each of numerous parts under conditions representative of the actual inspection environment. The data that form the basis for the analysis presented in this section do not meet these criteria, nor were they intended to do so, because analysis of the statistical aspects of ECP flaw detection lies beyond the scope of this project.

It is, nevertheless, possible and useful to make preliminary estimates of the probability of detection based on data obtained from blade slots during the course of the project. Such an exercise provides preliminary numerical

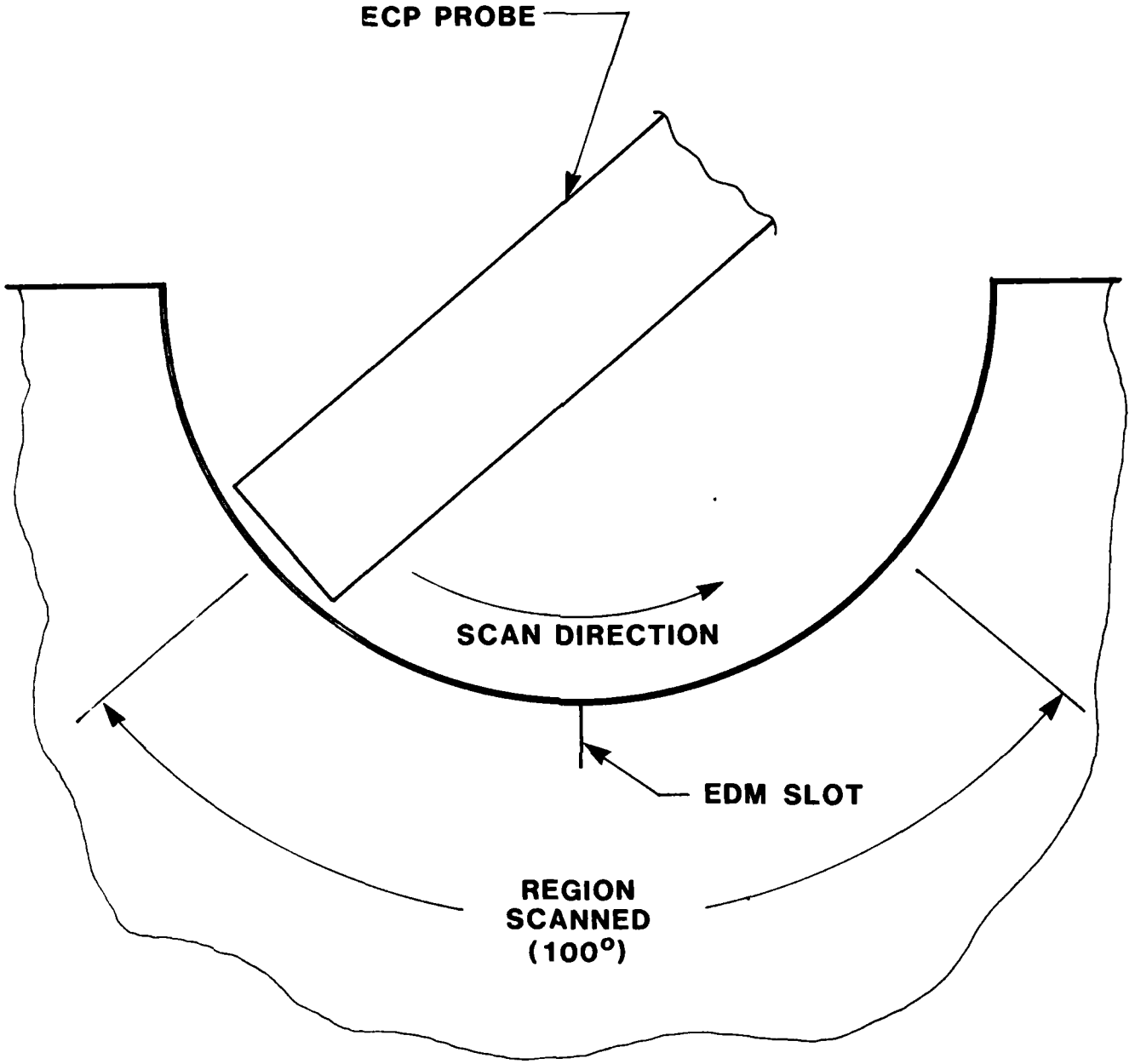

FIGURE 40. SCAN CONFIGURATION FOR BALANCE FLANGE SCALLOPS IN FIRST STAGE FAN DISK

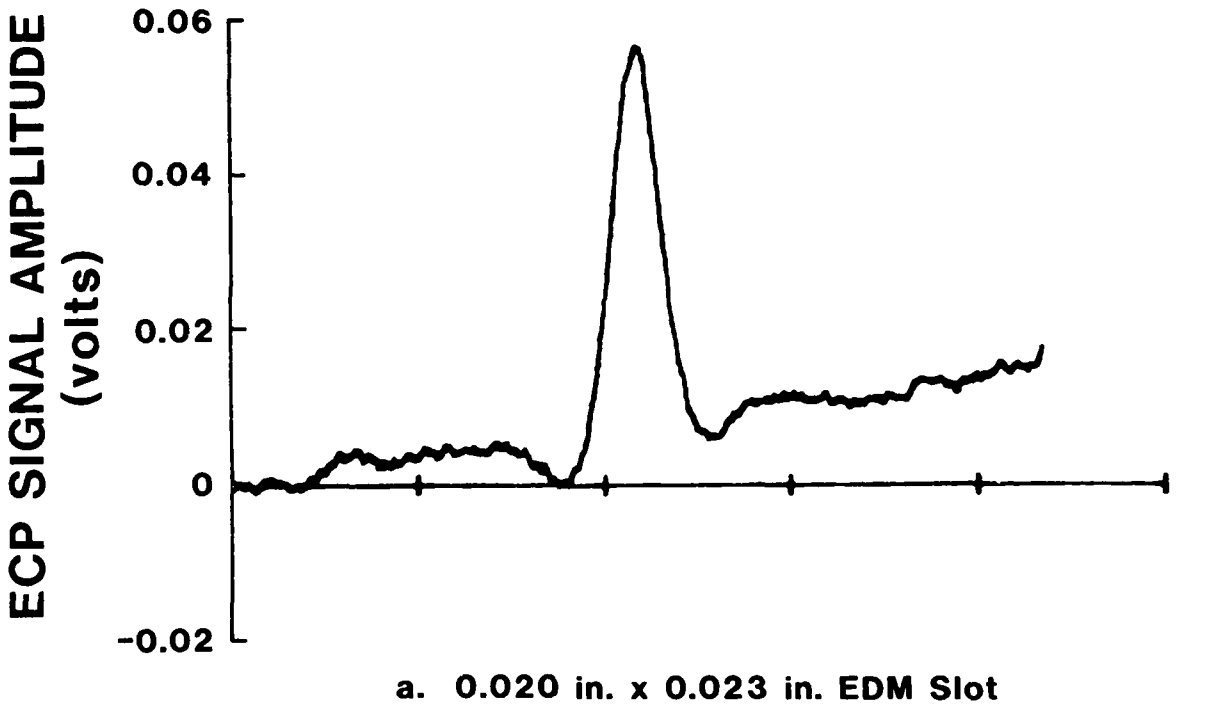

a. 0.020 in. x 0.023 in. EDM Slot

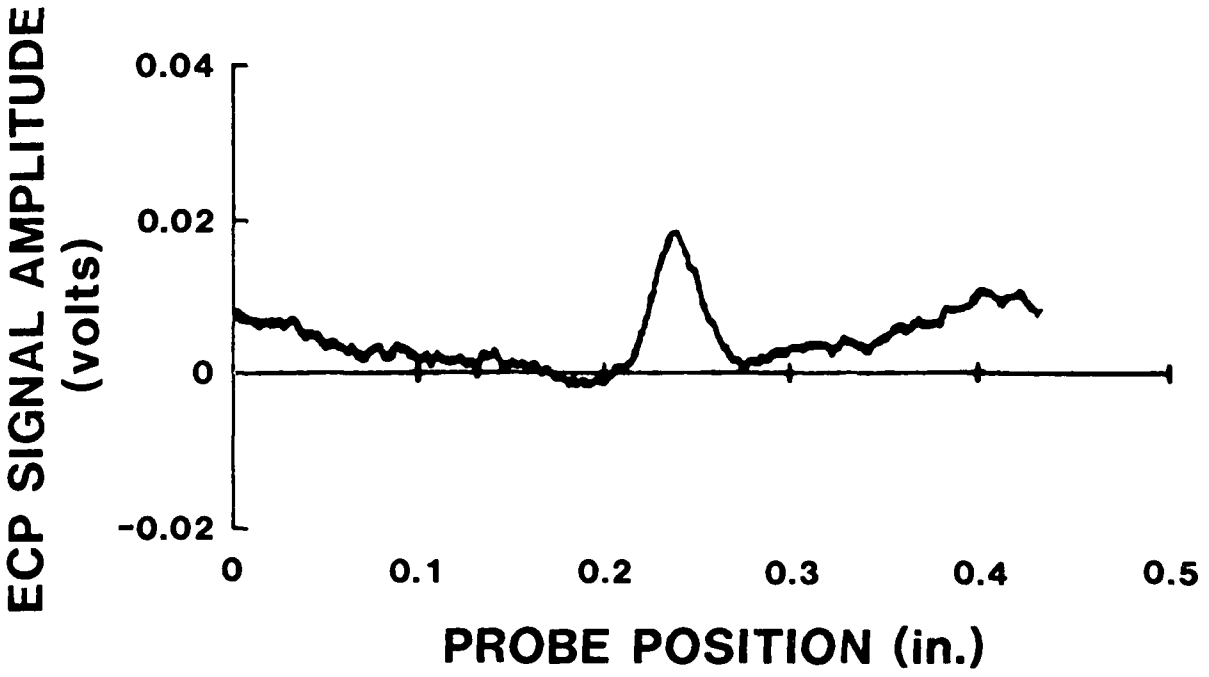

b. 0.013 in. x 0.015 in. EDM Slot

FIGURE 41. ECP SIGNALS FROM EDM SLOTS IN FIRST STAGE FAN DISK BALANCE FLANGE SCALLOPS

data on the tradeoffs among spacing between scan tracks, false alarm rates and flaw detection probabilities, which should prove useful in assessing the potential for RFC applications and in planning further statistical studies. In addition, the analysis serves as an example of how one would use a more extensive data base to determine the statistics of ECP flaw detection.

The subsections that follow contain a brief review of the basic concepts of flaw detection statistics, a description of the data used in the present study, an explanation of the approximations made necessary by the limited data base, and, finally, a presentation and discussion of the results of the present study.

a. Statistical Analysis of Flaw Detection

Despite all efforts to insure repeatability, experimental measurements of flaw signal amplitudes are never exactly the same, in the strict mathematical sense, over a set of repeated scans of the same flaw. Instead, the signal amplitudes thus obtained form a distribution of values ranging from a minimum to a maximum and having some mean, or average, value. If one were to calculate the number of times a given amplitude was observed divided by the total number of scans, and then plot the resulting data as a function of signal amplitude, the curve obtained would be the probability density function for signal amplitudes from that particular flaw size. A similar probability density function for noise or background signals can be defined in much the same way. Two such probability density functions, one for the flaw signal and the other for noise, are shown schematically in Figure 42.

In an inspection situation one would hope that the probability density function (PDF) for flaw signals would lie well to the right (in the sense of Figure 42) of the PDF for noise, so that a given signal amplitude could be

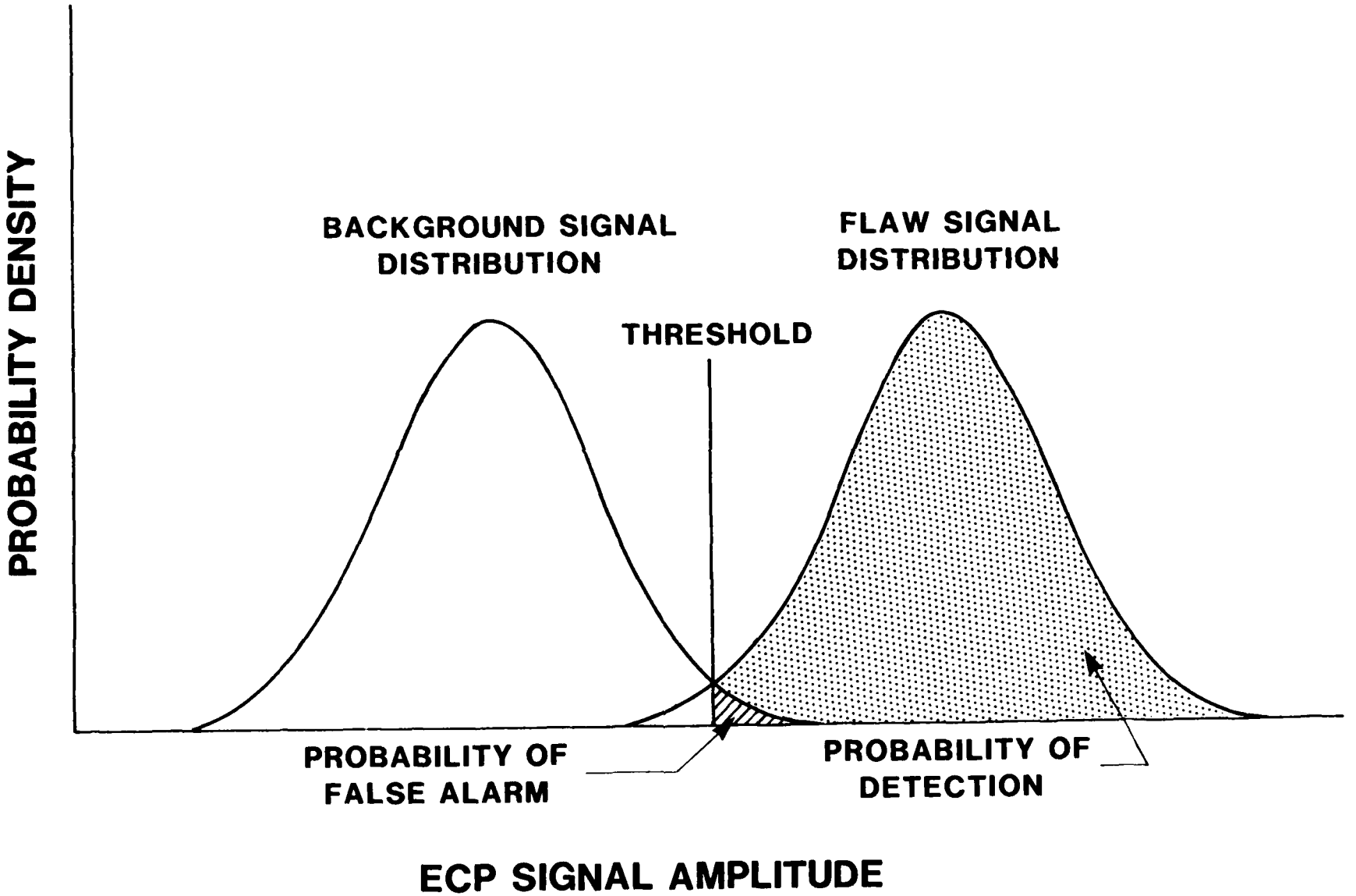

FIGURE 42. SCHEMATIC ILLUSTRATION OF PROBABILITY DENSITY FUNCTIONS FOR SIGNALS AND BACKGROUND NOISE

unambiguously interpreted as either a flaw signal or noise. In such an ideal case all flaws would be detected and there would be no false alarms from background signals that appear to indicate the presence of a flaw.

In practice this ideal situation is realized only for very large flaws in the presence of very weak noise signals. Much more often the PDF's for flaw signals and noise overlap to some extent, as indicated by the overlap of the two bell-shaped curves in Figure 42. It is the extent of overlap, or, more precisely, the areas under the PDF curves in the overlap region, that determine the reliability of the inspection method. This is because what one usually does in a situation where signal and noise PDF's overlap to a significant extent is to decide, first of all, how often one can tolerate false indications of the presence of a flaw. This decision determines a threshold value for signal amplitude, below which signals will be interpreted as noise and above which signals will be interpreted as flaw indications. The area under the noise PDF to the right of the threshold value is then the probability that background noise will give a false indication of the presence of a flaw. At the same time the choice of a threshold value also determines the probability of flaw detection, because the area under the flaw signal PDF to the right of the threshold is the probability of detection. It also determines the probability that flaws will be missed, which is equal to the area under the signal PDF to the left of the threshold. Thus the extent of overlap of the flaw signal and noise PDF's, and the choice of a threshold amplitude for flaw detection, play a critical role in determining the reliability of an NDE method.

b. Signal and Noise Data for Blade Slots

For the purpose of this analysis, signal and noise amplitudes are

defined as peak-to-peak voltages as indicated in Figure 43. The initial set of flaw signal data was obtained by recording the amplitudes measured in 30 repeated scans directly over the 0.0105 X 0.0058 in. flaw. The resulting PDF is that shown as a histogram on the right side of Figure 44. The smooth curve is a Gaussian fit to the PDF determined from the mean and standard deviation of the data. Noise data were obtained from scans in unflawed regions in each of 30 blade slots in the disk. The amplitude recorded for each scan was the maximum noise signal observed in a 1.0 in. scan length. The PDF resulting from these data is that shown on the left side of Figure 44.

The distributions shown in Figure 44 represent the best possible flaw detection situation because signal data were obtained from scans directly over the flaw where the amplitude is greatest. In a practical situation, of course, one does not even know if flaws exist, much less their exact locations. What is done, therefore, is to scan the piece in a raster-like fashion, as in Figure 45, with the distance between scan tracks determined from statistical data to give an acceptable probability of detection and false alarm rate. Under such conditions the scan track-to-flaw distance can be assumed to be equally likely to be any distance from zero (directly over the flaw) to one-half the spacing between scan tracks.

To obtain data representative of a practical inspection procedure, additional flaw signal data were obtained for scan tracks displaced in 0.001 in. increments from 0.0 in. to 0.007 in., each repeated 10 times. Data from the displaced scans (0.001 in. to 0.007 in.) were given twice the weight of data from scans directly over the flaw to account for the fact that in an actual inspection the flaw is equally likely to be on either side of the scan track. The full set of data thus approximates the distribution of signal

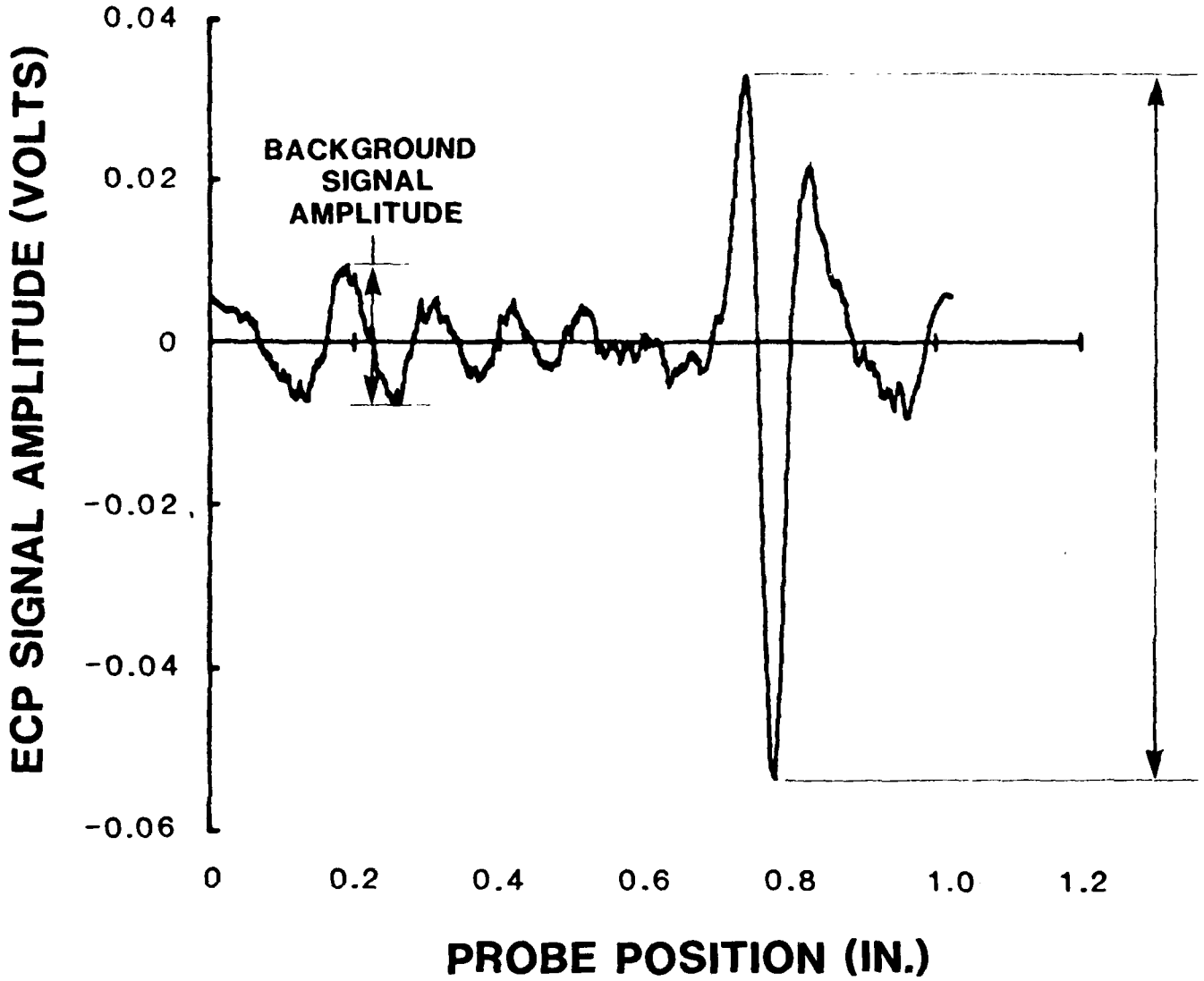

FIGURE 43. DEFINITION OF FLAW AND BACKGROUND SIGNAL AMPLITUDES

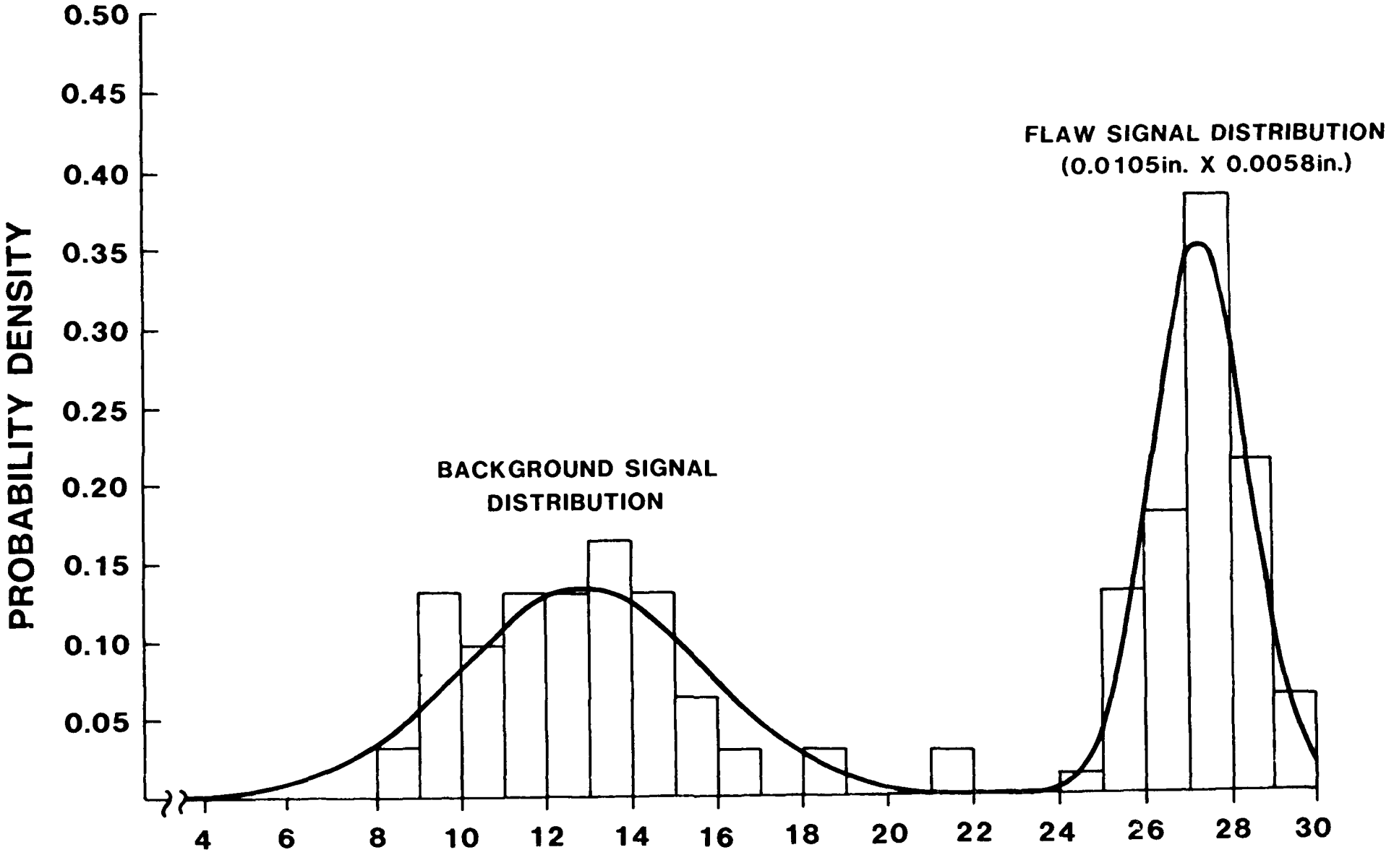

FIGURE 44. SIGNAL AND BACKGROUND PROBABILITY DENSITY FUNCTIONS FOR BLADE STUDY

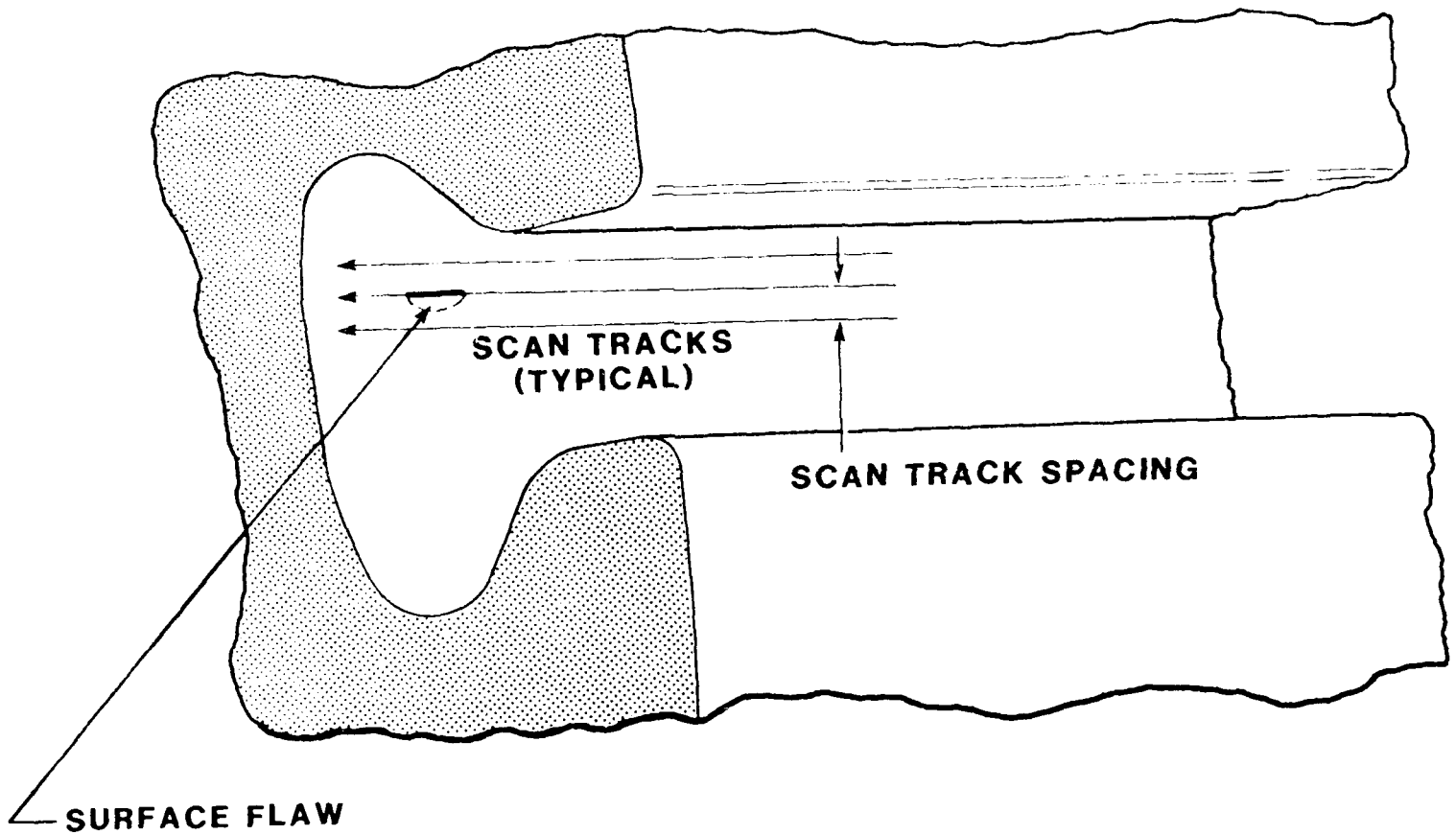

FIGURE 45. SCAN CONFIGURATION FOR BLADE SLOTS

AD-A148 757 EXPLORATORY DEVELOPMENT OF ADVANCED SURFACE FLAW DETECTION METHODS(U) SOUTHWEST RESEARCH INST SAN ANTONIO TX R E BEISSNER ET AL. SEP 84 SWRI-15-7106 2/2

UNCLASSIFIED AFWAL-TR-84-4121 F33615-82-C-5020 F/G 21/5 NL

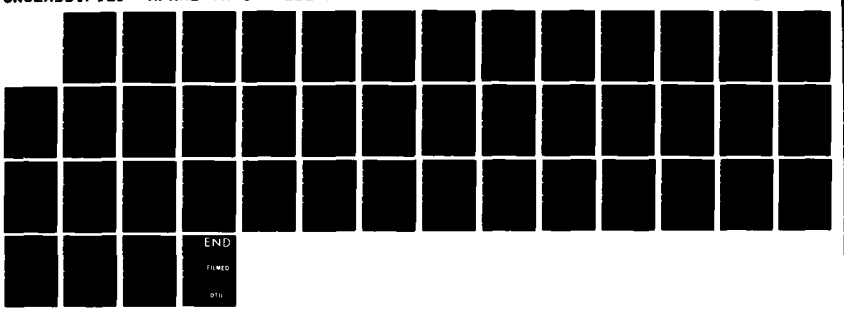

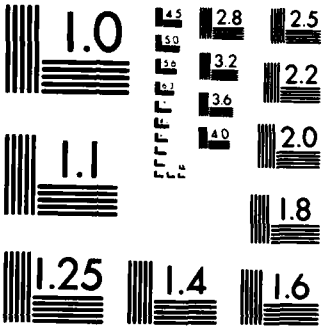

amplitudes obtained from an inspection in which scan tracks are 0.014 in. apart, because the flaw location, which is equally likely to be anywhere in the scan pattern, can then be no more than 0.007 in. from a scan track. The full set of data therefore determines a PDF corresponding to an inspection procedure in which scan tracks are spaced 0.014 in. apart. This PDF is shown as a histogram in Figure 46, along with the corresponding Gaussian fit.

Mean signal amplitudes are plotted as a function of distance from the flaw in Figure 47. From this plot it can be seen that the signal amplitude does not decrease significantly over distances from 0.0 to 0.004 in. from the flaw. Thus, if scan tracks were taken to be 0.008 in. apart, one would expect the corresponding PDF to closely approximate the ideal PDF obtained from scans directly over the flaw. For this reason a second PDF, based on the 5 scan tracks (each repeated 10 times) from 0.0 to 0.004 in. from the flaw, was also generated. The result is shown in Figure 48.

c. Calculations of Probability of Detection

The PDF's shown in Figures 46 and 48 correspond to two different inspection procedures but only one flaw size. To extend the analysis to other flaw sizes, the following approximations were introduced: (1) The standard deviation is independent of flaw size. This means that the shape of the PDF is assumed to be the same regardless of the size of the flaw. (2) The mean signal amplitude is proportional to flaw area. This approximation shifts the PDF to the left or right by an amount proportional to the area of the face of the flaw; it is based on amplitude-area scaling relationship demonstrated in Figure 24 and supported by previous experience[2].

For the calculation of probabilities of detection, false alarm probabilities of 10^{-6}, 10^{-5}, 10^{-4} and 10^{-3} were chosen as representative of the

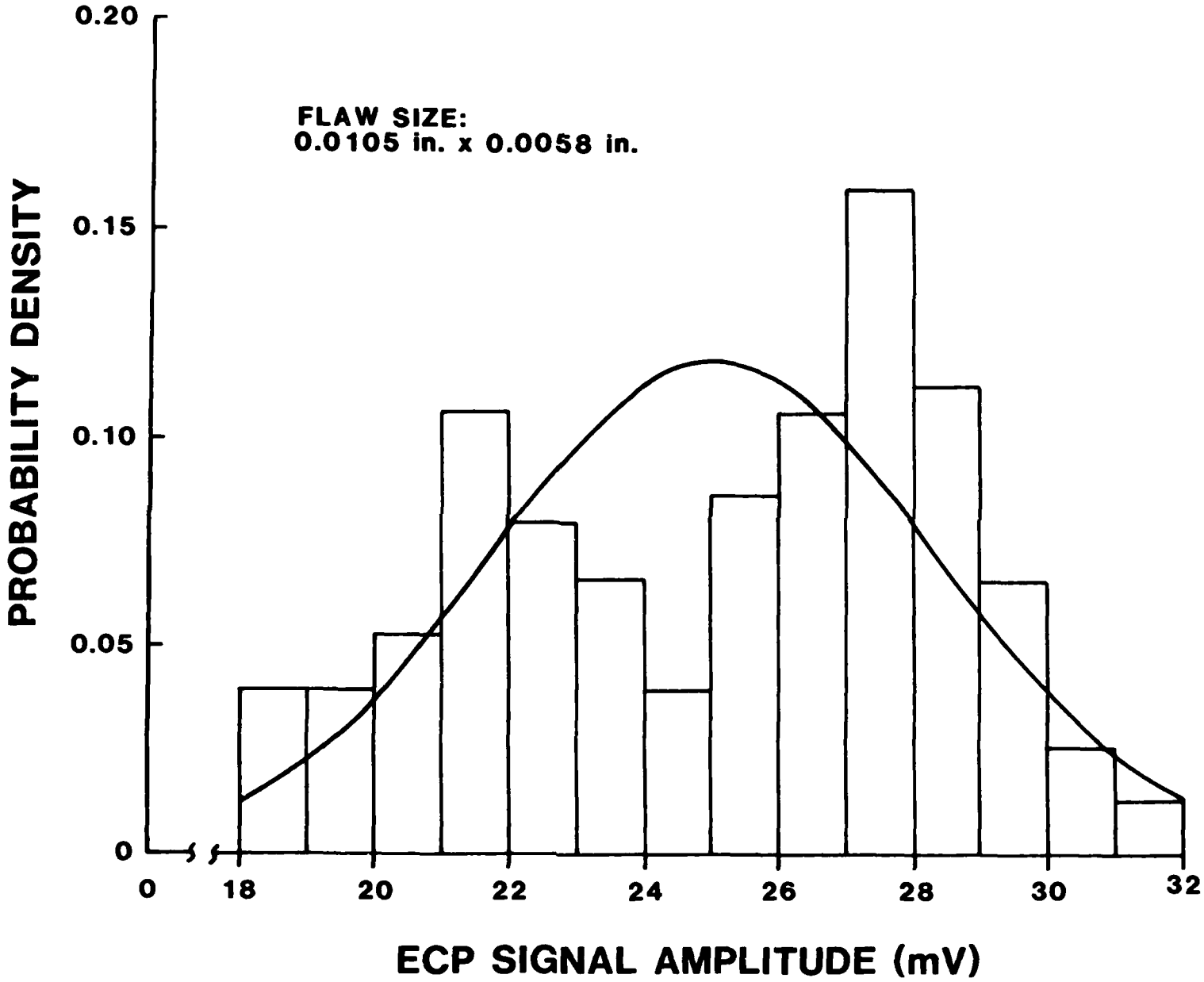

FIGURE 4[illegible]. FLAW SIGNAL PROBABILITY DENSITY FUNCTION FOR A 0.0105 IN. x 0.0058 IN. FLAW WITH 0.014 IN. SCAN TRACK SPACING

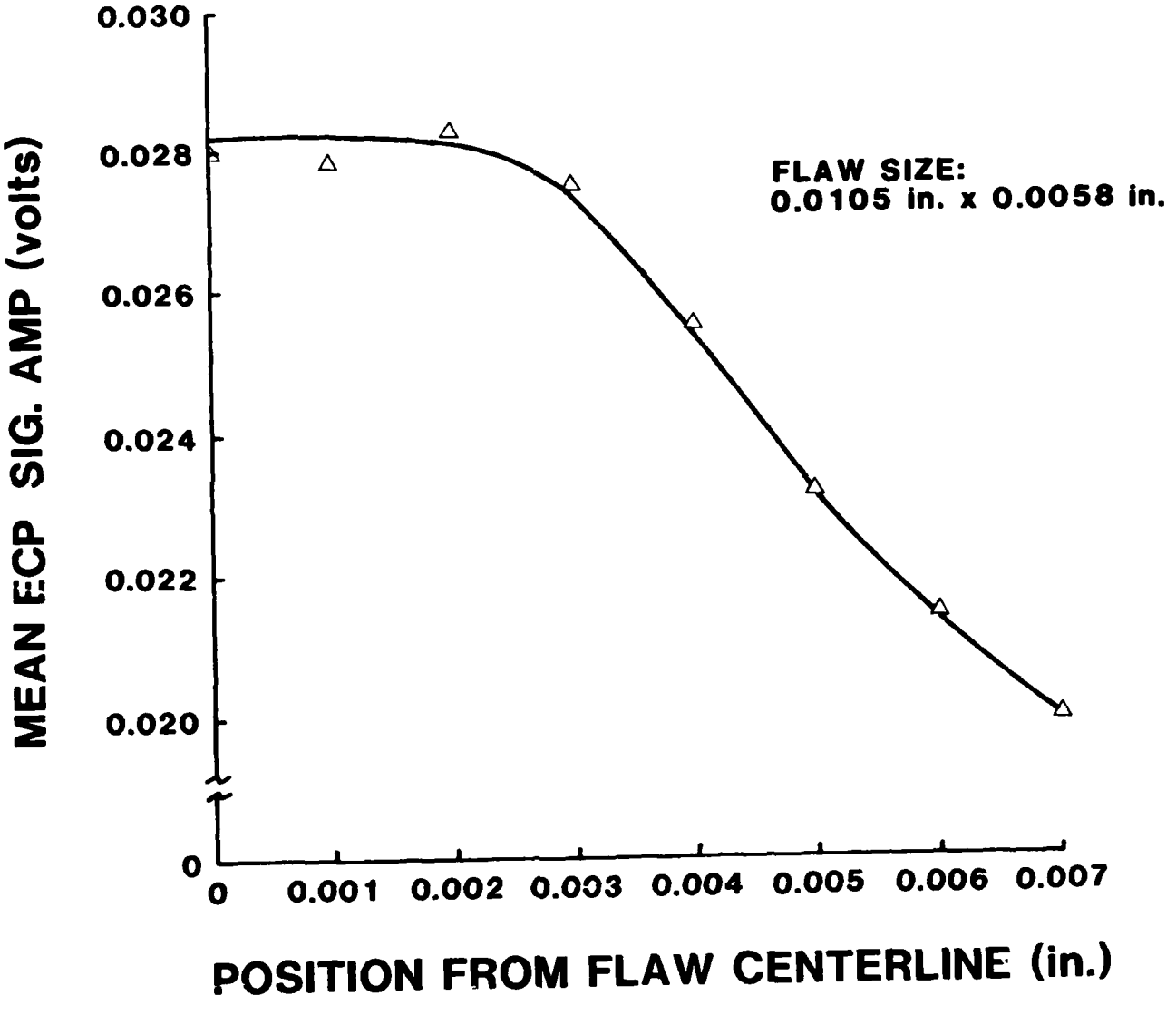

FIGURE 47. MEAN SIGNAL AMPLITUDE FOR A 0.0105 IN. x 0.0058 IN. FLAW AS A FUNCTION OF FLAW-TO-SCAN TRACK SPACING

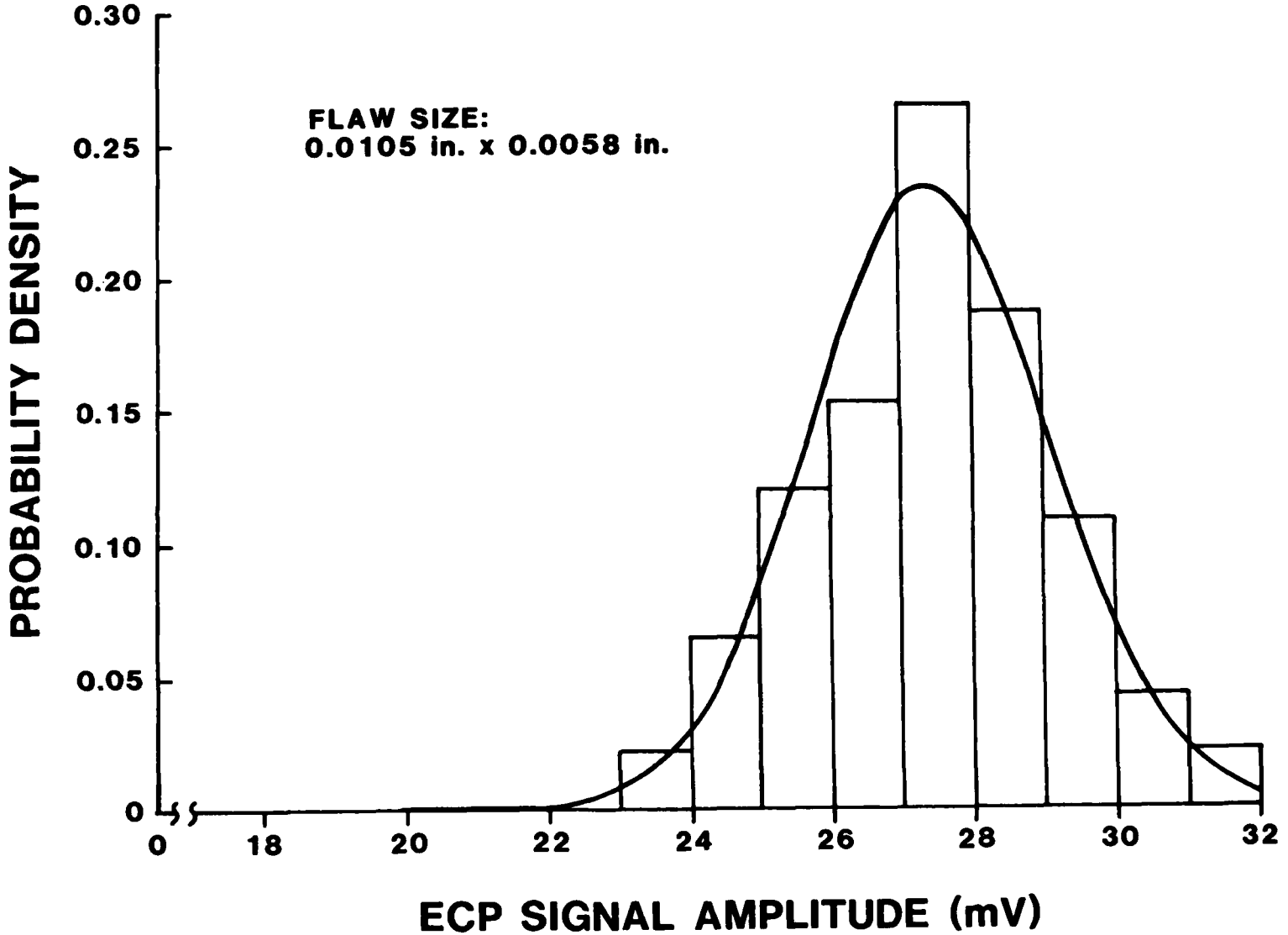

FIGURE 48. FLAW SIGNAL PROBABILITY DENSITY FUNCTION FOR A 0.0105 IN. x 0.0058 IN. FLAW WITH 0.008 IN. SCAN TRACK SPACING

values one might choose for a blade slot inspection. These numbers were then used to determine the four corresponding threshold amplitudes from the noise PDF shown in Figure 44. Probabilities of detection were then calculated as indicated in Section II.7.a for flaw lengths ranging from 0.008 in. to 0.012 in. for flaw signal PDF's corresponding to both the 0.008 and 0.014 in. scan track spacings. Because all detection probabilities were very close to 1.0 for 0.012 in. flaws, there was no need to extend the analysis to larger flaws.

To simplify the computations, Gaussian fits to the PDF's were used instead of actual PDF data for most of the estimates of probability of detection. As a check on the validity of this approximation, additional calculations were performed for the 0.0105 x 0.0058 in. flaw using the actual, experimentally determined PDF data. The results are summarized in Figures 49 and 50, which are plots of all calculated probabilities of detection based on the Gaussian approximation, as a function of flaw size. The results for 0.014 and 0.008 in. scan track specings are shown, on a greatly expanded scale, in Figures 51 and 52, where data obtained directly from the PDF histograms, rather than the Gaussian fits, are also shown along with the scaled data from Figures 49 and 50.

The very sharp rise in the probability of detection data plotted in Figures 49 and 50 means that virtually all flaws with areas slightly greater than that of the 0.010 x 0.005 in. target flaw will be detected with either the 0.014 to the 0.008 in. scan spacing. For flaw lengths in the 0.008 to 0.012 in. range, Figures 51 and 52 show the sensitivity of the probability of detection to the choice of false alarm probability and, comparing the two figures, to the choice of scan track spacing. These figures also show that the

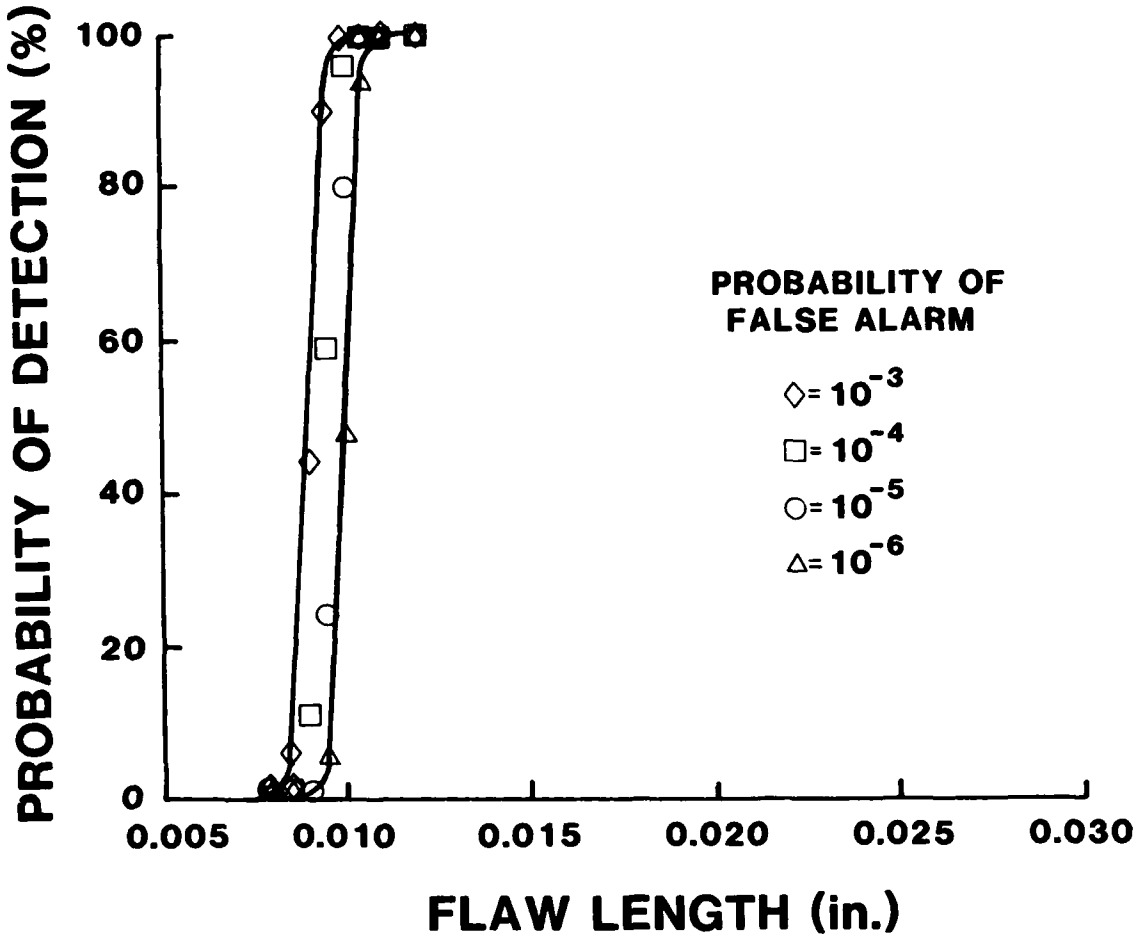

FIGURE 49. PROBABILITY OF DETECTION ESTIMATES FOR A 0.008 IN. SCAN TRACK SPACING IN BLADE SLOT INSPECTION

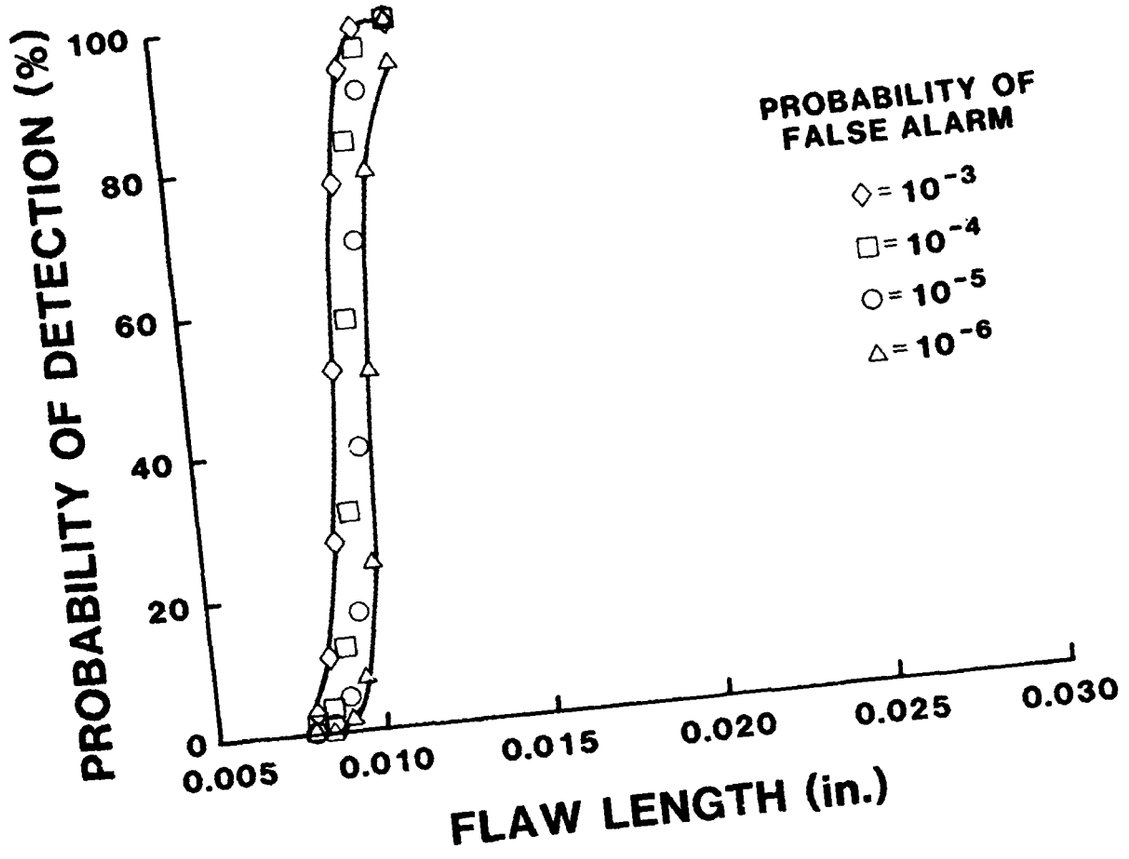

FIGURE 50. PROBABILITY OF DETECTION ESTIMATES FOR 0.014 IN. SCAN TRACK SPACING IN BLADE SLOT INSPECTION

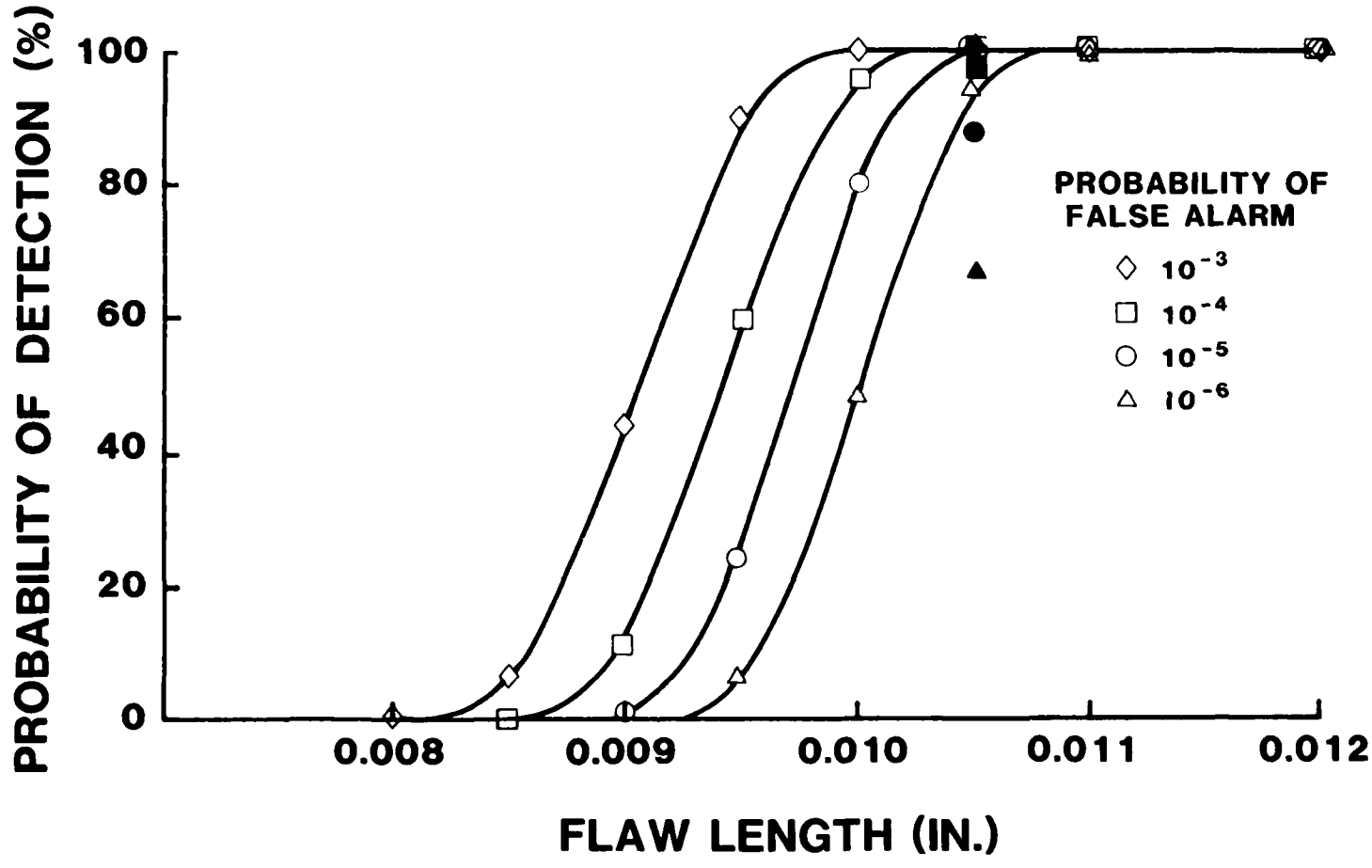

FIGURE 51. PROBABILITY OF DETECTION DETAIL FOR 0.008 IN. SCAN TRACK SPACING. OPEN SYMBOLS ARE BASED ON THE APPROXIMATION DISCUSSED IN THE TEXT; SOLID SYMBOLS ARE BASED ON ACTUAL EXPERIMENTAL DATA.

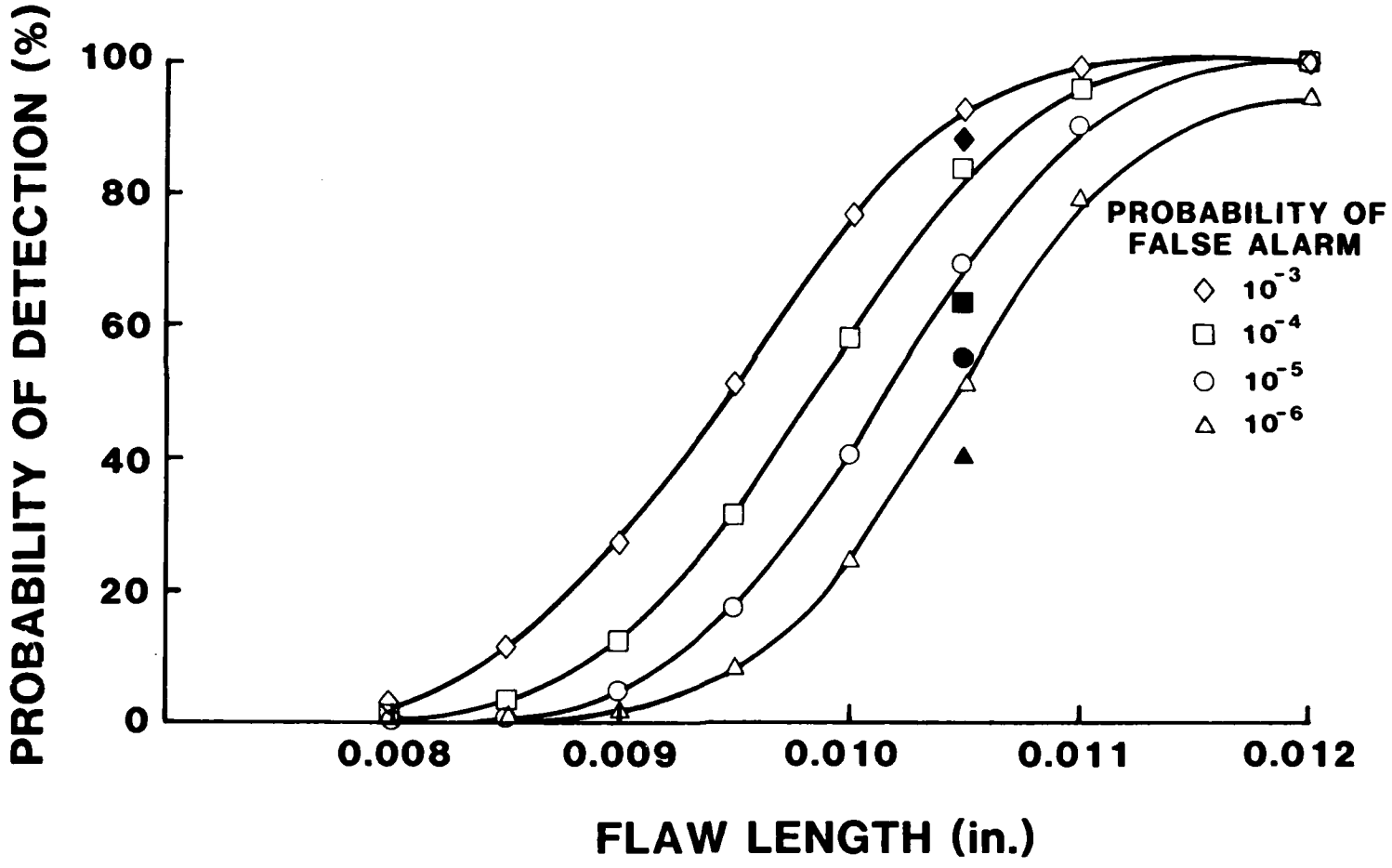

FIGURE 52. PROBABILITY OF DETECTION DETAIL FOR 0.014 IN. SCAN TRACK SPACING. OPEN SYMBOLS ARE BASED ON THE APPROXIMATIONS DISCUSSED IN THE TEXT; SOLID SYMBOLS ARE BASED ON ACTUAL EXPERIMENTAL DATA.

use of the Gaussian approximation to PDF's, which was largely a matter of convenience, tends to give detection probabilities that are somewhat greater than one would obtain from experimentally determined PDF data. Although differences are significant, it was decided that the data set was too limited to warrant further study. Thus, the data presented in Figures 49 through 52 should be regarded as preliminary estimates, with the differences between probabilities of detection as calculated from actual PDF data and Gaussian fits to the data giving some indication of the uncertainty in the estimates. Clearly, much more data are needed for a more accurate assessment of probability of detection.

In spite of such uncertainties, the results of the study are very encouraging because they show nearly ideal performance for flaws only slightly larger than the RFC target flaw size. It is particularly gratifying to note that the experiments were performed under what was considered to be a "worst case" condition in which background noise from the rather rough blade slot surface is greater than might be expected with other engine parts. This point is well-illustrated by a comparison of the blade slot data scan shown in Figure 47 with similar data from a laboratory specimen shown in Figure 20. Signal-to-noise differences in these two scans are quite evident, and it is clear that much better detectability can be achieved in parts with background noise lower than that of blade slots.

8. Assessment of Potential for RFC

In assessing the potential of the ECP method for RFC applications two points must be addressed. The first is compatibility, i.e., the question of whether ECP system requirements are compatible with RFC design. As was indicated earlier, system compatibility was insured by maintaining liaison with

RFC design engineers during development of the ECP system. The specific plan for this liaison is presented in Appendix A and documentation, in the form of answers to a questionnaire on system requirements, is presented in Appendix B.

The second point is more difficult to address as it concerns ECP system performance in the detection of flaws of concern in RFC. All indications are that the ECP system will meet RFC requirements more readily than the present generation of flaw detection equipment. Actual proof of this, however, requires more extensive evaluation of the ECP system in a realistic inspection environment. In other words, the ECP method has passed the first stage of evaluation in the laboratory and appears well-suited to RFC program goals. The method is now ready for the second stage of development and evaluation as a field-worthy system.

SECTION III

CONCLUSIONS AND RECOMMENDATIONS

The principal conclusions drawn from the work reported here are the following:

1. The ECP method has the inherent flaw sensitivity and signal-to-noise characteristics to reliably detect flaws of the RFC target size in F100 engine parts.
2. A practical and efficient scanning and data acquisition system has been demonstrated.
3. Compatibility with RFC system requirements is assured.
4. Flaws of the target size or larger can be detected under worst case conditions of material background noise and complex part geometry.

As the next step in the development of an inspection system for RFC, it is recommended that the ECP method be applied to extensive evaluation with flaws in F100 engine parts that are critical to RFC program goals.

In experiments with blade slots, sufficient flaw signal and noise data were accumulated to make preliminary estimates of the probability of detection as a function of flaw size. It was found, as expected, that noise caused by variations in material properties was the principal limiting factor in the detection of small flaws. Even so, for what was considered to be the worst case in terms of such background noise, experimental results show excellent probability of detection characteristics for flaw sizes of the order of the target flaw size.

As with all NDE methods, however, complex part geometry can inhibit flaw detection by causing spurious variations in the background signal level. In many cases such background variations can be minimized by careful choice of the scan pattern, but the problem is always present to some extent. Still, for the particular complex geometry feature studied here (antirotation windows

in the second-to-third stage fan seal), small flaws were detectble even in the presence of significant, geometry-caused background variations. Thus, the two major constraints that were expected to inhibit flaw detection, i.e., material noise and complex geometries, have been addressed, and flaw detection has been demonstrated successfully, under conditions typical of the most difficult inspection problems presented by the F100 engine RFC components.

Design, assembly and testing of a computer controlled ECP breadboard system has demonstrated that a practical and efficient scanning and data acquisition system, of the type envisioned for RFC, can be realized. In fact, compatibility with RFC has been assured by maintaining liaison with RFC system designers throughout the development of the ECP breadboard. Thus the two major requirements that determine the value of the ECP system to RFC--flaw detectability and system compatibility--have been satisfied.

The ECP method is, therefore, now ready for the next step in it's development, which involves a more extensive evaluation with F100 engine parts. The data obtained in this evaluation should provide an adequate statistical base for the determination of such factors as the optimum tradeoff between false alarm rate and probability of flaw detection, optimum scan spacing, and other parameters that determine the overall efficiency of an inspection. In addition, and equally important, the accumulation of a sufficient amount of data obtained under realistic inspection conditions should serve to convince the user, who must bear the responsibility for inspection and must therefore make the final decision regarding implementation, that the ECP method provides a practical, efficient and reliable technique for finding critical flaws in engine components.

REFERENCES

1. G.L. Burkhardt, C.M. Teller, R.E. Beissner, and J.R. Barton, "Demonstration of the Electric Current Perturbation Technique for Fatigue Crack Characterization in TF33 Turbine Disk Tiebolt Holes," Southwest Research Institute, 1979.

2. R.E. Beissner, C.M. Teller, G.L. Burkhardt, R.T. Smith, and J.R. Barton, "Detection and Analysis of Electric-Current Perturbation Caused by Defects," Special Technical Publication 722, American Society for Testing and Materials, 1981.

3. C.M. Teller and G.L. Burkhardt, "Small Defect Characterization by the Electric Current Perturbation Method," Proceedings of the Thirteenth Symposium on Nondestructive Evaluation, 1981.

4. C.M. Teller and G.L. Burkhardt, "Application of the Electric Current Perturbation Method to the Detection of Fatigue Cracks in a Complex Geometry Titanium Part," Review of Progress in Quantitative Nondestructive Evaluation, 2B, Donald O. Thompson and Dale E. Chimenti, Eds., Plenum Publishing Corp., pp. 1203-1217, 1983.

5. C.M. Teller, G.L. Burkhardt and R.E. Beissner, "An Investigation of Nondestructive Evaluation by the Electric Current Perturbation Technique," SwRI Internal Research Project 15-9221, (1982).

6. J.S. Cargill, et al., "Retirement for Cause Inspection System Design," Pratt & Whitney Aircraft Group, AFWAL-TR-81-4111, Vols. I and II.

APPENDIX A

COMPATIBILITY PLAN

COMPATIBILITY PLAN

This Appendix contains a copy of the compatibility plan prepared at an early stage of the program.

The purpose of this plan is to insure compatibility of the developing electric current perturbation (ECP) inspection instrumentation with the RFC data acquisition and control system design evolving at SRL. The approach consists of maintaining a continuously updated awareness of the SRL system design, projecting the requirements for an ECP instrument as optimization of the method proceeds, and finally indicating considerations for future development of an ECP instrument to insure compatability.

There are three key elements to the plan as follows:

1. Identify the type and extent of the SRL system design information required to determine compatibility.
2. Establish technically effective and economically feasible means for transfer of the necessary design information from SRL to SwRI.
3. Identify those parameters for an ECP instrument anticipated to impact system compatibility.

Information from the above elements should insure compatibility during subsequent development of an ECP instrument and facilitate the anticipation of possible problem areas in interfacing. The remainder of this plan describes the key elements and discusses how they may be accomplished.

Identify SRL System Design Information Required

The types of system functions which will require detailed definition are presented in Figure 1. The architecture of the entire control and data system is required as well as details about each type of function.

Method(s) of Information Transfer

It is desirable, of course, to achieve transfer of the above indicated information through maximum use of already existing lines of contact and communication as well as contractually required documentation. Dr. James E. Doherty, SwRI Program Manager for the RFC program, has been included in the subject program as an internal consultant and system liaison. Additionally, the subject program at SwRI has been placed on the distribution list for reports coming out of SRL on the RFC system development program. SwRI has placed SRL on the distribution list of monthly technical reports for the subject program. SRL has also agreed to include Dr. Teller (or his designate) as a passive observer at selected meetings of the appropriate working group where system decisions are likely to be made. Close, careful coordination will be used between SwRI and SRL in maintaining information transfer to insure minimum impact on both Air Force programs.

Identify Critical ECP Parameters

In order to provide a basis for assessing the control and interfacing compatibility requirements of a future ECP instrument, it is necessary to determine those parameters critical to optimum ECP inspection performance. Such parameters will be identified throughout the optimization and breadboard development efforts under the subject program. With such parameters identified and an adequate definition of the SRL system capabilities, the requirements for compatibility of a future ECP instrument development can be established.

APPENDIX B

ECP SYSTEM REQUIREMENTS

The information in this Appendix was sent to Dr. R.B. Thompson of Ames Laboratory in response to a questionnaire sent by Dr. Thompson on behalf of RFC program concerning compatibility of RFC and ECP system requirements.

SYSTEM REQUIREMENTS FOR ADVANCED NDE TECHNIQUES
(Preliminary Estimates)

Technique: Electric Current Perturbation (ECP)

1. Transducer/Probe Requirements:

Special ECP probes will be required; in some cases, the probes may have to be tailored for particular part geometry considerations.

2. Instrumentation Requirements:

The Mark VI and/or NDT33 must be replaced with special-purpose hardware.

3. Modular Signal Processing:

It is anticipated that the AP500 array processor will provide sufficient real time signal processing capability for ECP inspection.

4. Memory:

From a worst-case analysis based on the inspection of the blade slots in a typical compressor disk, a requirement for one to two megabytes of semiconductor memory is obtained. This memory requirement is based upon the inspection of all slots in one disk and retaining 10% of the data based on exceeding a threshold after initial data processing. It is assumed that all data would be subsequently transferred to permanent memory in the VAX 11/780 prior to initiating inspection of another disk. These memory requirements would be reduced significantly if it is assumed that data for each slot is transferred to the VAX 11/780 after inspecting each slot rather than after each disk.

5. Signal Processing Rate:

It is anticipated that a computational rate for real time evaluation which satisfies EC requirements will be adequate for ECP inspection.

6. Computer Compatibility:

It is anticipated that a prototype design employing the ECP method could be made compatible with the presently planned computer architecture and system interfaces.

7. Manipulator Requirements:

The seven axes specified for the EC manipulator in Figure AI-20-2 of the Summary Report for the RFC/NDE Third Technical Meeting appears to be adequate for ECP inspection. The following precision requirements are anticipated:

Absolute Accuracy

Translation 0.005 in. to 0.010 in.
Rotation 1/4°

Relative Accuracy

Translation 0.001 in.
Rotation 1/4°

If such accuracies are unduly difficult to achieve, some relaxation of requirements may be possible through additional design of more compliant position-seeking subsystems during prototype development.

8. Special Hardware Requirements:

It is anticipated that an air-bearing will be used as part of the EC probe suspension mechanism.

9. Other Comments:

None

APPENDIX C

SUPPLEMENTARY ECP DATA

EQUIVALENCE OF ECP RESPONSE TO SLOTS AND FATIGUE CRACKS

(From C.M. Teller and G.L. Burkhardt, "Application of the Electric Current Perturbation Method to the Detection of Fatigue Cracks in a Complex Geometry Titanium Part," Review of Progress in Quantitative Nondestructive Evaluation, 2B, Donald O. Thompson and Dale E. Chimenti, Eds., Plenum Publishing Corp., pp. 1203-1217, 1983.)

To establish the equivalence of ECP signals from a fatigue crack and a slot, a direct comparison was made between these two types of defects. In prior work,* a 1.30 mm surface length fatigue crack was grown in a smooth Ti 6-4 rod type tensile specimen in a laboratory fatigue machine under stress conditions which produced a true half-penny shaped crack with a 2:1 aspect ratio. The ECP response from this closed fatigue crack was compared to the rsponse from an EDM slot measuring 1.27 mm surface length, 0.65 mm deep and 0.10 mm wide machined in an identical Ti 6-4 specimen.

Plots of ECP signal amplitude vs. position along the defect length are shown in Figure C-1 for both the crack and slot. Identical experimental setups were used for both defects and the absolute signal amplitudes are plotted (i.e. no normalization was used). As seen in the figure, the amplitudes and shapes of the two curves are essentially identical. The overall agreement between signal behavior from the crack and the slot is excellent. Therefore, a slot provides an excellent simulator for determining the ECP response to a fatigue crack with current flow normal to the interface of the defect.

---

* F.N. Kusenberger, G.A. Matzkanin, J.R. Barton, and P.H. Francis, "Nondestructive Evaluation of Metal Fatigue", Interim Report, AFOSR Contract No. F44620-75-C-0042, February 1977.

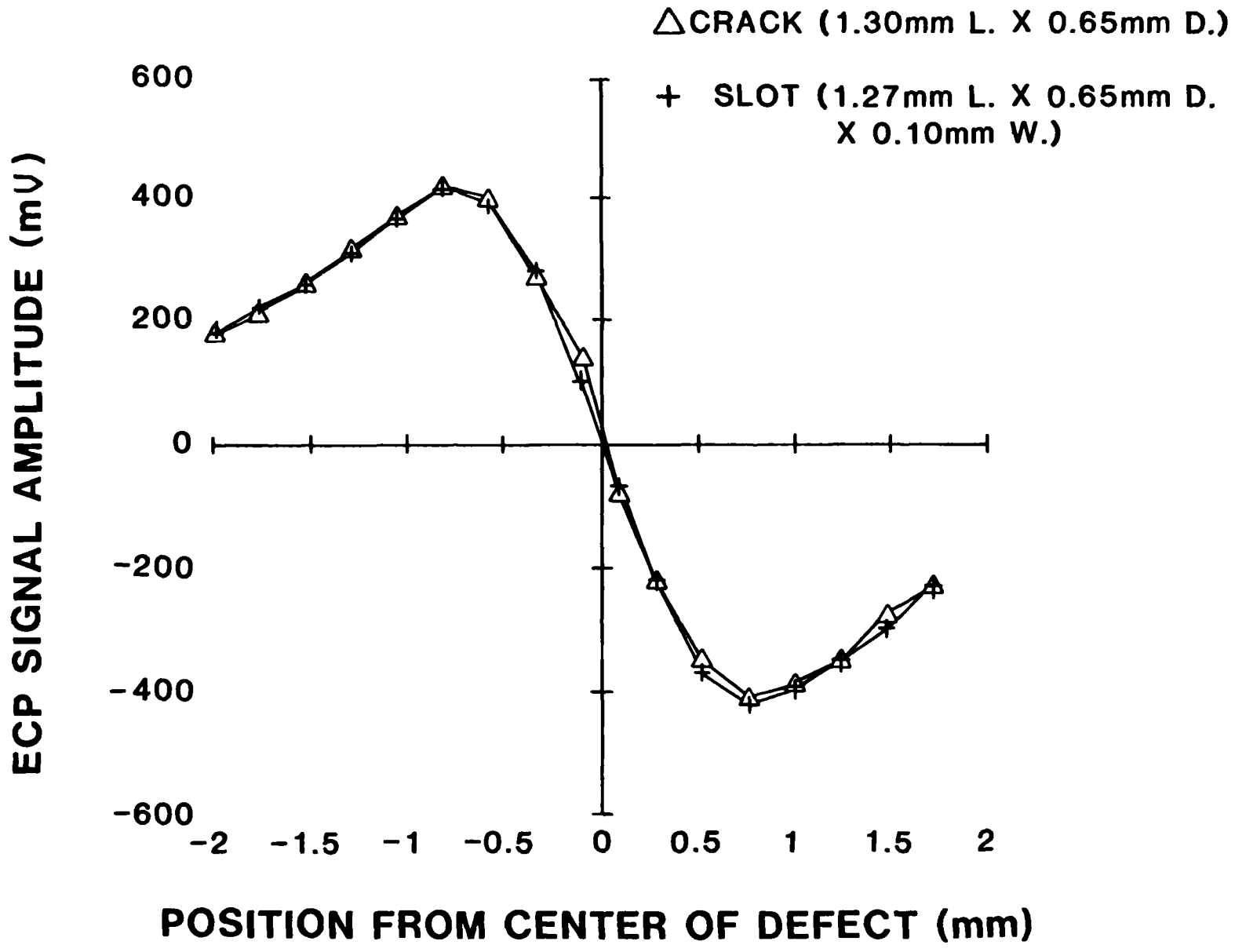

FIGURE C-1. EQUIVALENCE OF ECP RESPONSE FROM AN EDM SLOT AND A FATIGUE CRACK VS. POSITION ALONG THE DEFECT LENGTH

ECP RESPONSE USING DIRECT CURRENT AND ALTERNATING CURRENT

The ECP method is often confused with the conventional eddy current NDE method. Conventional eddy current testing involves the use of an induction coil which is placed above the specimen surface with its axis perpendicular to the surface. This coil is energized with alternating current and in turn induces current flow (eddy currents) in the specimen. The magnetic fields associated with the eddy currents oppose those generated by the coil and alter the coil's impedance. The impedance of the coil is monitored and defects are detected by the coil impedance change which results from a modification of eddy current flow around a defect.

Since coil impedance is strictly an A.C. phenomenon, conventional eddy current methods will not function with D.C. excitation. Therefore, to illustrate a distinction between ECP and eddy current, an experiment was performed to show that the ECP method functions with either A.C. or D.C. excitation.

An experimental setup was established whereby direct electrical contact was made to a flat 6.35 mm (0.25 in.) thick aluminum specimen which contained a 5.08 mm (0.2 in.) long, through-thickness slot.* The specimen was energized with direct current and a single Hall effect sensor was scanned perpendicular to the slot to detect the magnetic field associated with perturbed current flow around the slot.

A second experimental arrangement was established using the same Hall effect sensor and an induction coil (energized with alternating current) to establish current flow in the specimen. The induction coil and sensor were then scanned as a unit over another 6.35 mm (0.25 in.) thick aluminum specimen containing a 5.08 mm (0.2 in.) long, through-thickness slot.

Figure C-2 shows the ECP signals obtained using both direct current and induced alternating current. (Note that since the sensor is a single element instead of two differentially-connected elements, different signal shapes are obtained compared to those shown in previous sections.) Not only does the ECP method function with direct current, but essentially identical signals are obtained with induced A.C. excitation.

Therefore, the ECP method is shown to be distinctly different from conventional eddy current methods and is not dependent on the mode of electric current flow in the specimen.

* C.M. Teller, G.L. Burkhardt and R.E. Beissner, "An Investigation of Nondestructive Evaluation by the Electric Current Perturbation Technique," SwRI Internal Research Project 15-9221, August 1982.

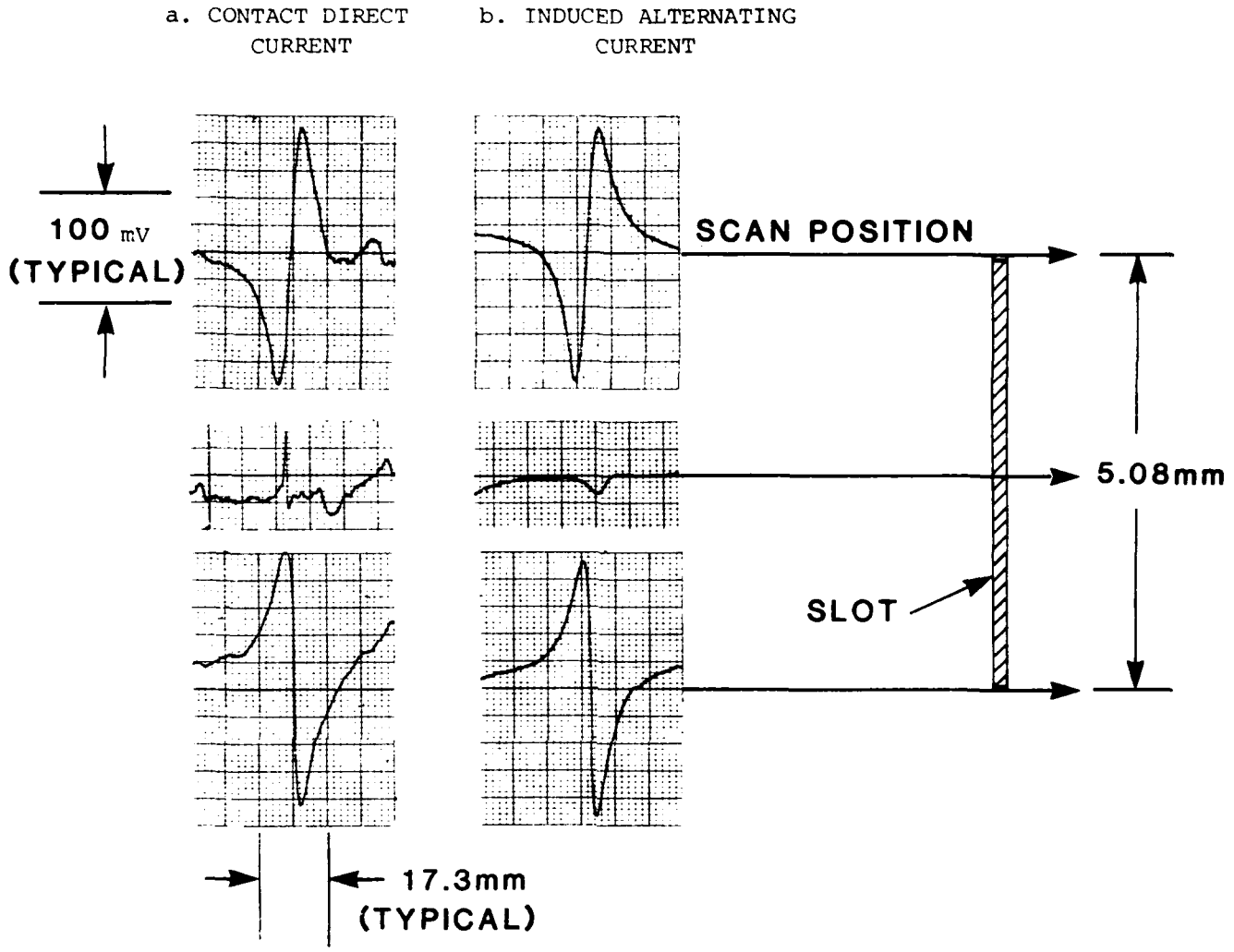

FIGURE C-2. COMPARISON OF ECP SIGNALS PRODUCED BY DIRECT CURRENT AND ALTERNATING CURRENT FLOW INTERACTING WITH A SLOT IN AN ALUMINUM PLATE

RELATIONSHIP BETWEEN ECP SIGNAL AMPLITUDE AND CRACK INTERFACIAL AREA

Comparisons have been made between simple features of ECP signals from an actual fatigue crack and those generated by an analytical model. Experimental results were obtained from a single, half-penny shaped fatigue crack grown to various lengths in a Ti 6-4 rod-type tensile specimen using a laboratory fatigue machine.* (This alloy is very similar in electrical properties to Ti 6-2-4-6.) Fracture of identical specimens containing cracks grown under similar conditions showed that true half-penny shaped fatigue cracks (2:1 aspect ratio) were obtained. Electric current flow was introduced into this specimen by direct contact at each end of the rod, and the perturbations were detected by a separate ECP probe scanned perpendicular to the crack.

Theory and experiment were compared for the ECP signal amplitude as a function of interfacial area of the crack. These data are shown in Figure C-3. It can be seen that the theory predicts an approximately linear relationship between signal amplitude and interfacial area of the crack. Experimental results show very close agreement with theory, thus indicating that crack interfacial area can be estimated by measurement of the ECP signal amplitude.

* F.N. Kusenberger, et al., "Nondestructive Evaluation of Metal Fatigue," Southwest Research Institute, AFO51269-1429TR (AD 688 892).

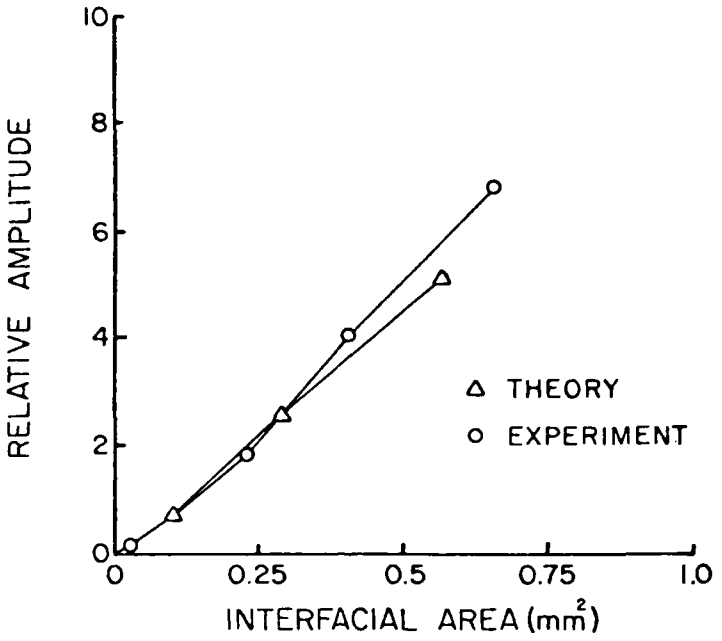

FIGURE C-3. RELATIONSHIP BETWEEN ECP SIGNAL AMPLITUDE AND CRACK INTERFACIAL AREA

APPENDIX D

ENGINEERING DRAWINGS

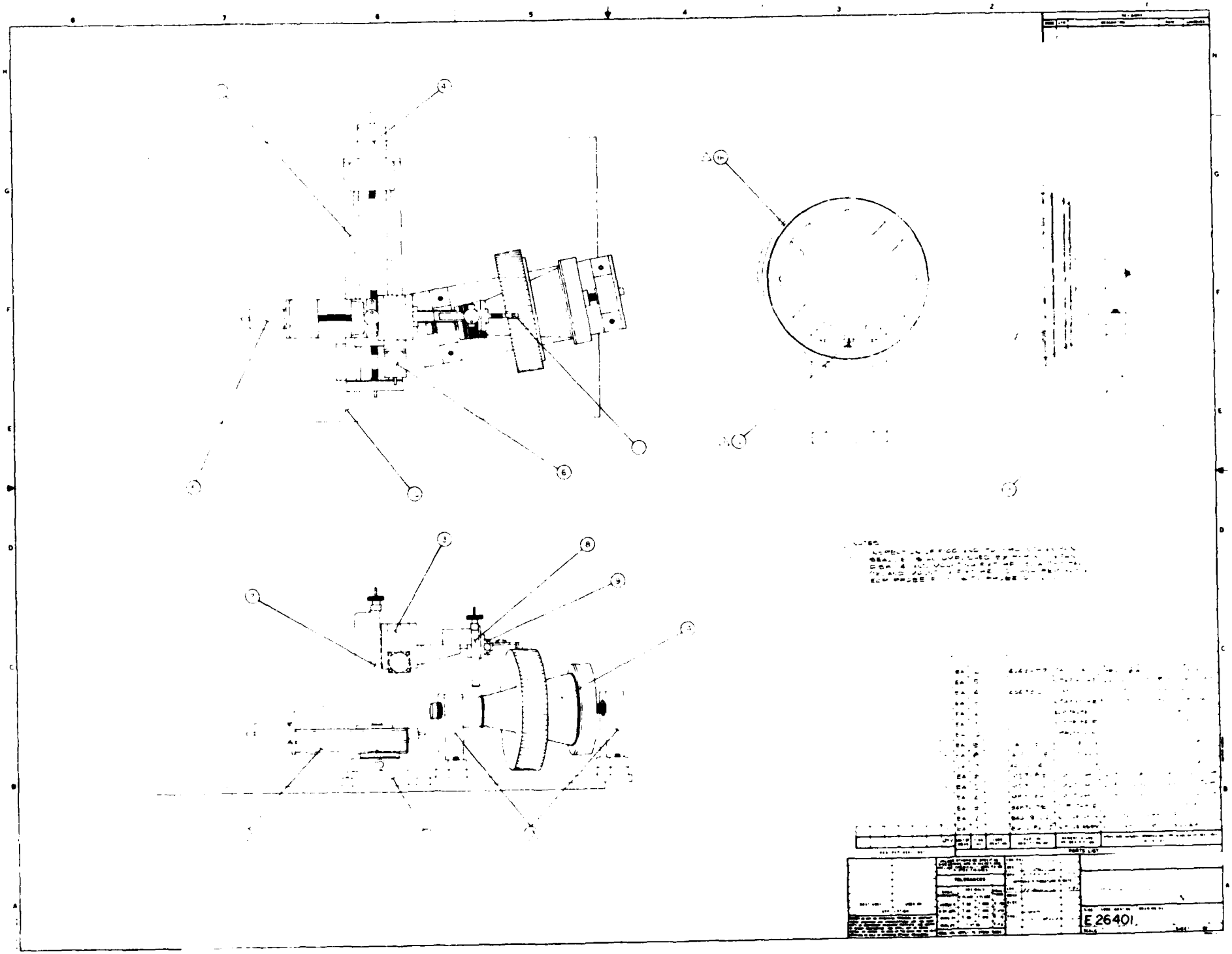

FIGURE D-1. ENGINEERING DRAWING NO. 1

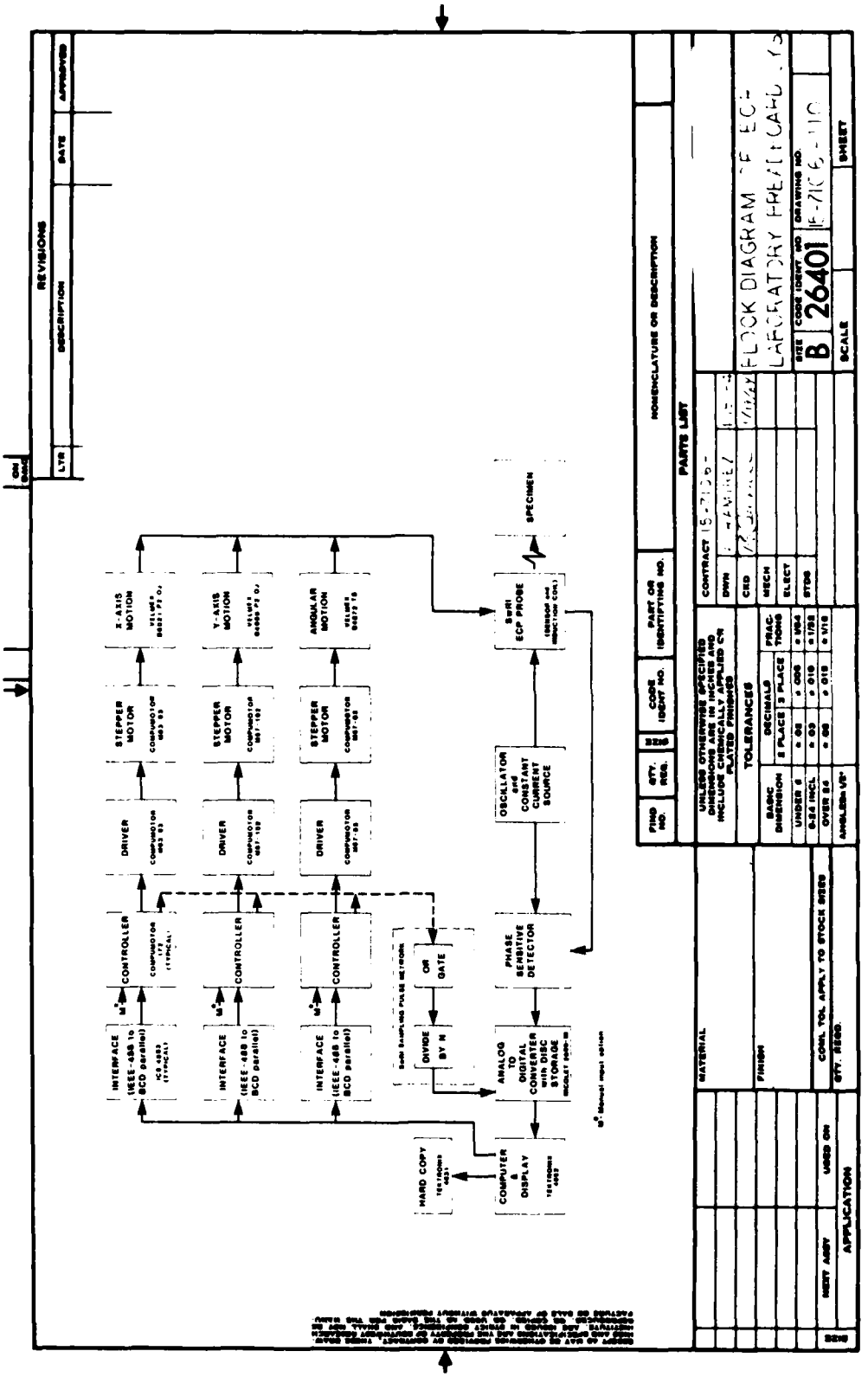

FIGURE D-2. ENGINEERING DRAWING NO. 2

APPENDIX E

ECP RESULTS ON SIMULATED ANTIROTATION WINDOWS IN TYPE III SPECIMENS

Linear Scans

ECP evaluations on the Type III specimens which contained both fatigue cracks and EDM slots did not produce results as definitive as those from the Type I and II specimens. This was due to the fact that the flaws were located in the antirotation window radius instead of at the radius tangency point, and that there were significant variations in the window geometry (see section II.6.b.1).

Figure E-1 shows an ECP signal from a simulated antirotation window with no flaw and a signal from a window with a 0.0247 in. x 0.0195 in. EDM slot. The dashed line on the figure is from the window with the EDM slot. The dashed line on the figure is from the window with the EDM slot. Since the flaw signal was not readily distinguishable, as was the case for the Type I and II specimens, it was necessary to superimpose the two window signals to show the differences. The similarity of the two signals is due in part to the fact that the flaw is in the radius instead of at the tangency point, and the flaw signal is therefore superimposed on the leading edge of the gradient signal instead of the gradient signal peak. The flaw signal is therefore recognizable only as a difference in the leading edge of the two signals. To enhance the flaw signal, the unflawed window gradient signal was digitally subtracted, point-by-point, from the window signal with the flaw, with the result shown in Figure E-2. Here, the flaw signal is prominent even though signals not associated with the flaw are produced by differences in the geometry of the two windows.

ECP data from the 0.020 in. x 0.033 in. area fatigue crack in this same specimen produced a much larger leading edge signal. It is not clear why the crack signal is so much larger than the EDM slot signal since the crack area

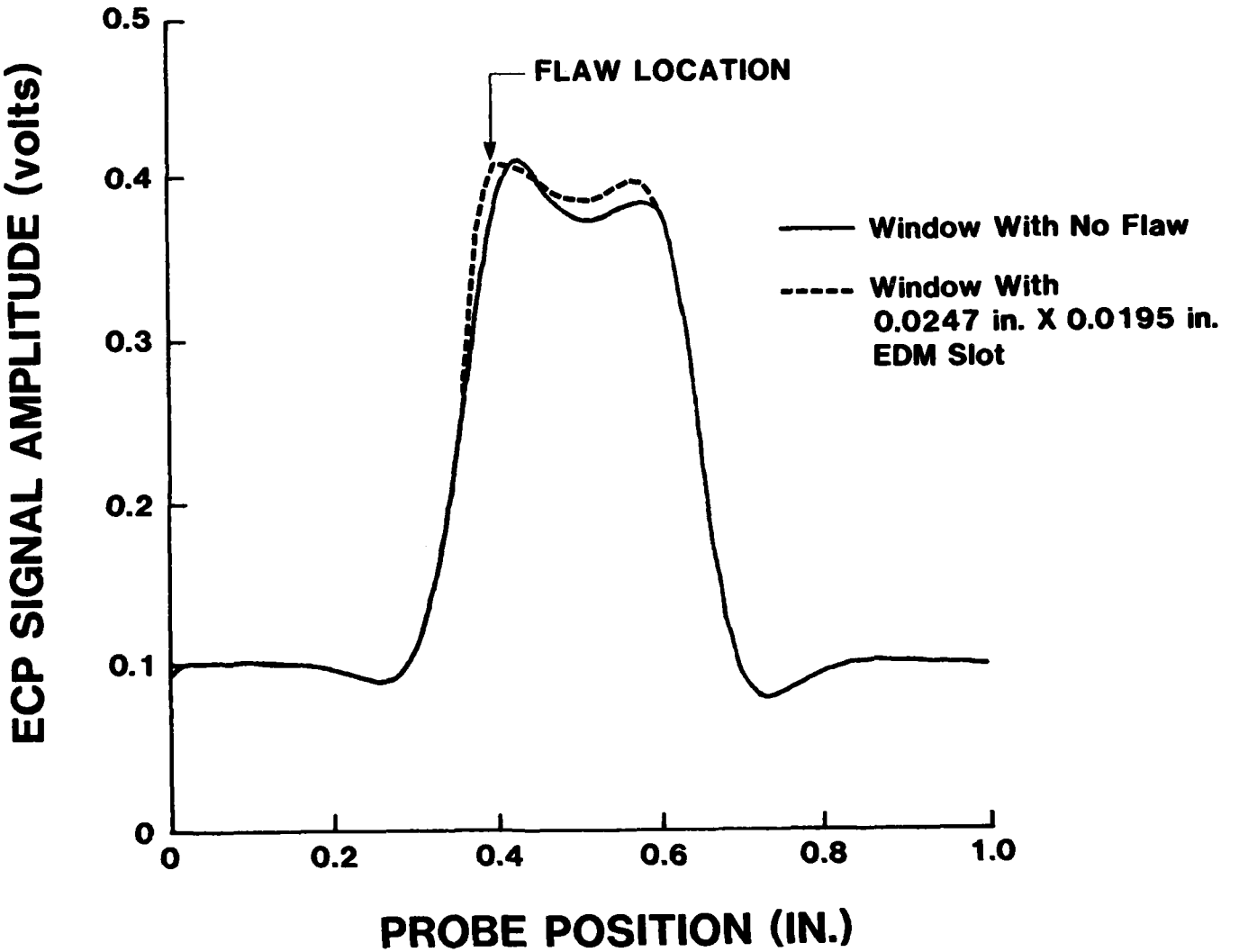

FIGURE E-1. ECP LINEAR SCAN SIGNALS FROM SIMULATED ANTIROTATION WINDOWS IN TYPE III SPECIMENS

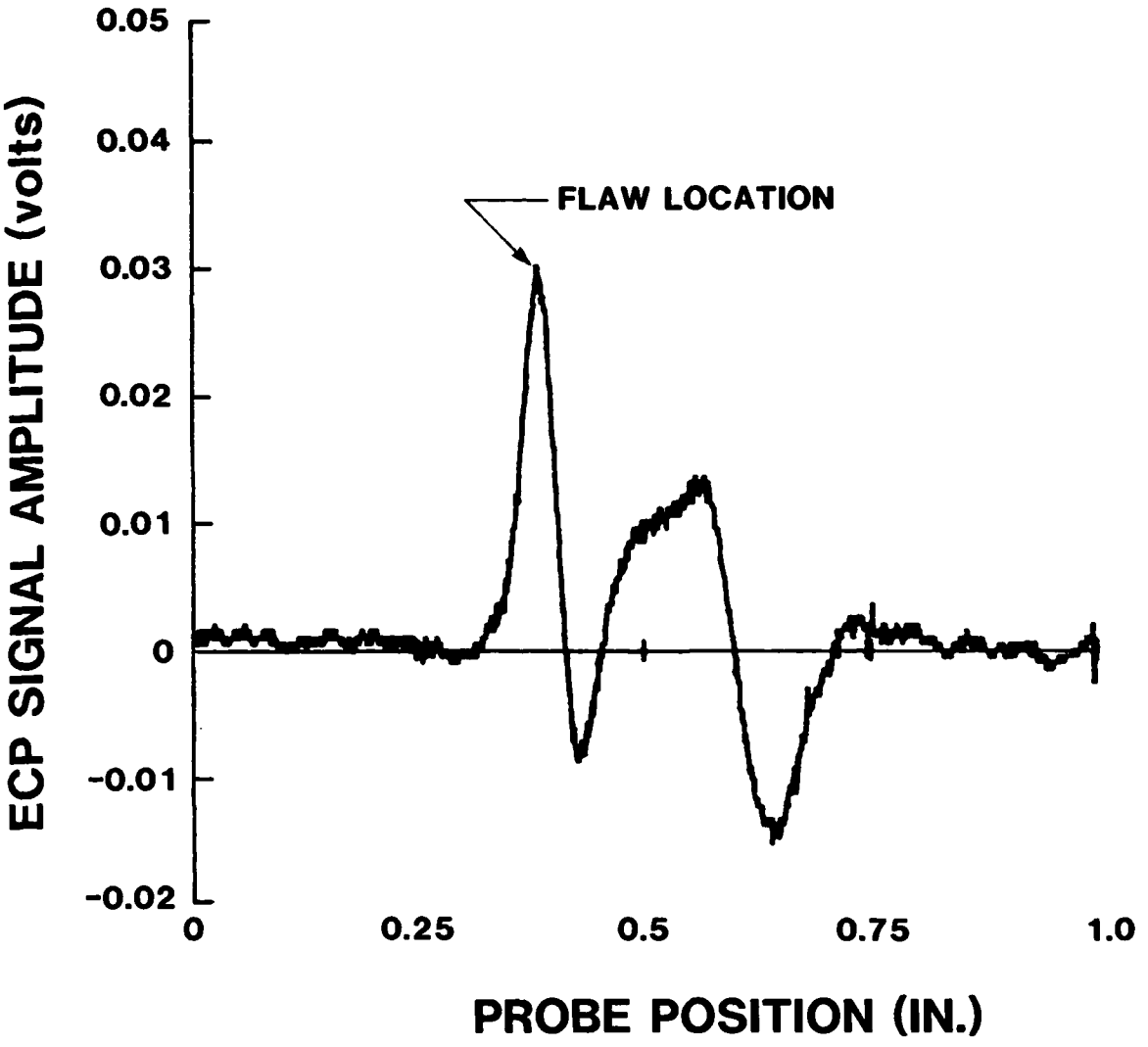

FIGURE E-2. DIFFERENCE BETWEEN ECP LINEAR SCAN SIGNALS FROM SIMULATED ANTIROTATION WINDOWS WITH NO FLAW AND WITH 0.0247 IN. X 0.0195 IN. EDM SLOT

is not that much larger than the EDM slot area. It is possible that the subsurface portion of the crack is larger than indicated by the surface dimensions, or that a difference in window geometry produced a crack-like signal.

ECP data were also obtained from the smaller EDM slots and fatigue cracks in the Type III specimens (Table 4 in main body of report). The smaller flaws, however, were not readily detectable in these specimens.

Contour Scans

The Type III specimens which contained fatigue cracks and EDM slots of similar sizes were also scanned using the contour scan approach. It was intended that these data be used for further comparisons of the ECP response from fatigue cracks and EDM slots. Difficulties were encountered, however, in applying the contour scans to the simulated windows in the Type III specimens because, as was noted earlier, the curved surfaces in these specimens were not circular (see Figure 29), and the average radii in general, were larger than the 0.063 in. radius specified.

An interpretation of why variations in window geometry cause difficulties is illustrated in Figure E-3a and E-3b. Figure E-3a illustrates the ideal geometry in which the window curvature is circular and the center of probe rotation coincides with the center of curvature of the window. In this case, the probe is oriented properly throughout the scan and the liftoff distance on each side of the probe is the same. In Figure E-3b, however, the probe is rotated about the wrong point because the window radius is greater than expected. Proper orientation is not maintained in this case and the liftoff distances on either side of the probe are not equal. If the window curvature is not circular similar orientation errors result.

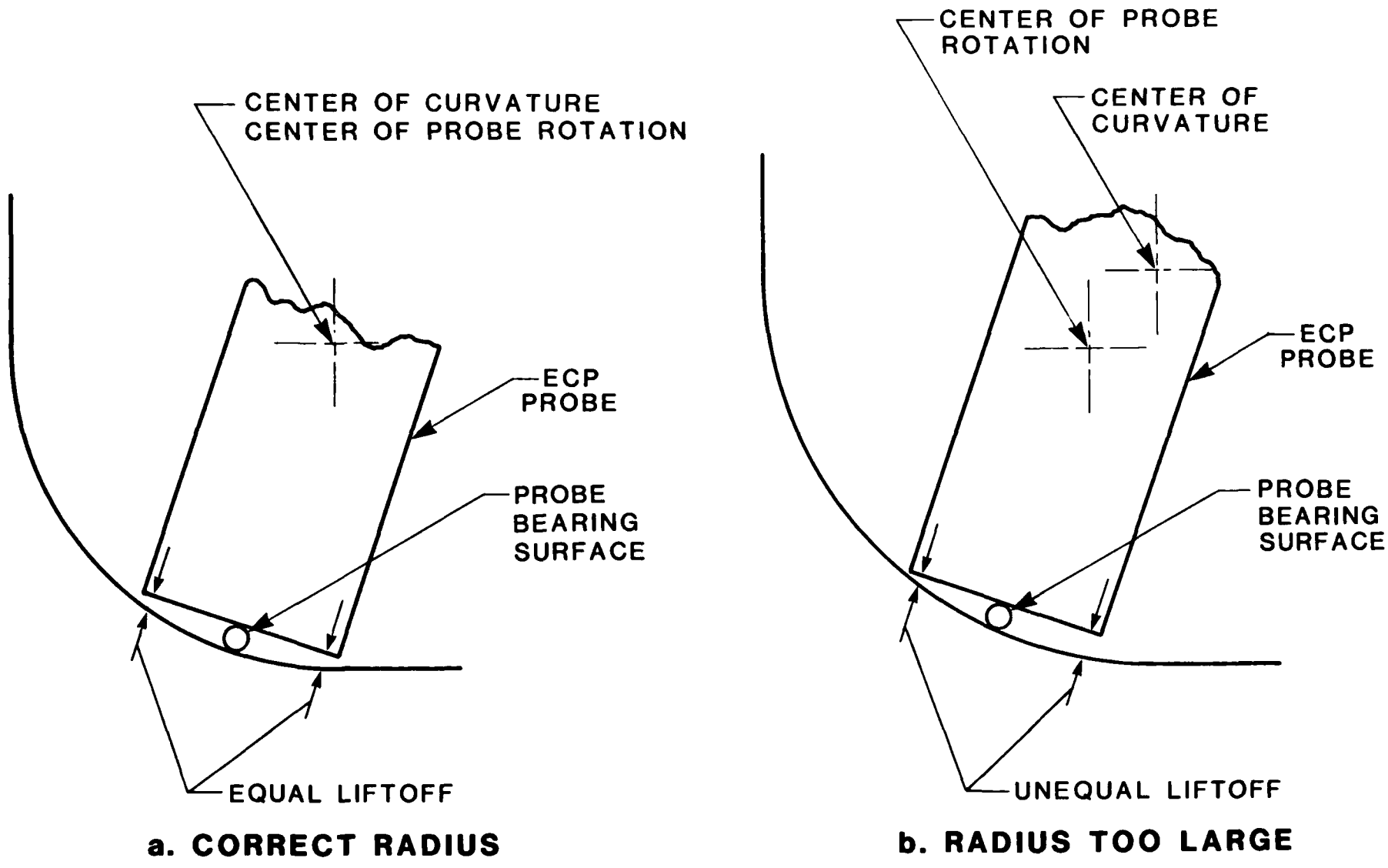

Figure E-3. ECP PROBE SET UP IN ANTIROTATION WINDOWS WITH DIFFERENT RADII. LIFTOFF ON EACH SIDE OF PROBE IS NOT EQUAL IF THE CENTER OF PROBE ROTATION IS NOT THE SAME AS THE CENTER OF THE CURVATURE.

Thus, probe orientation errors caused by the variations in window geometry in the Type III specimens resulted in large gradients in background signals as the window was scanned, and it was very difficult to distinguish the flaw signals from the gradient signal in any of the fatigue crack specimens.

In order to further understand the problems associated with variations in probe orientation, additional experiments were undertaken using the Type II specimens. In these evaluations, the center of probe rotation was changed with respect to the center of curvature of the radius. This was accomplished by moving the center of probe rotation up to 0.01 in. to the left and to the right of the center of curvature of the radius in the sense of Figure E-3. Thus, unequal liftoff on each side of the ECP probe was generated during rotation of the probe. Although this is not exactly the same as changing the actual window radius, it simulates the type of unequal liftoffs obtained in cases where the window radius does vary.

ECP signals obtained from the contour scans of the window with the probe center of rotation in the correct position are shown in Figures E-4a and E-4b for windows in the Type II reference specimen which contained no flaw and a 0.0203 in. x 0.0204 in. EDM slot, respectively. The signal amplitude from the window containing the EDM slot is approximately 0.6 V while the signal amplitude from the unflawed window is approximately 0.35 V. Only slight variation in the shapes or amplitudes of the signals from these two windows was obtained as the center of probe rotation was moved up to 0.01 in. to the left of the center of curvature. However, when the center of probe rotation was moved to the right, variations in the shape and size of the signal gradient from the unflawed window became more significant. When the center of

probe rotation was moved 0.01 in. to the right (Figure E-4c), the amplitude of the gradient signal (0.55 V) was almost equal to the level of the window signal with the flaw and the correct center of rotation (Figure E-4b. The signal from the flawed window with the probe center of rotation moved 0.01 in. to the right is shown in Figure E-4d and it can be seen that the flaw signal level is slightly greater than that from the unflawed window with this same probe position.

These results indicate that the ECP signal is indeed dependent on the orientation of the probe with respect to the part. The probe is more sensitive to misalignment in some directions than in others, since little variation in the signal was experienced when the probe center of rotation was moved 0.01 in. to the left, while movement to the right by the same amount produced significant variations in the gradient signal.

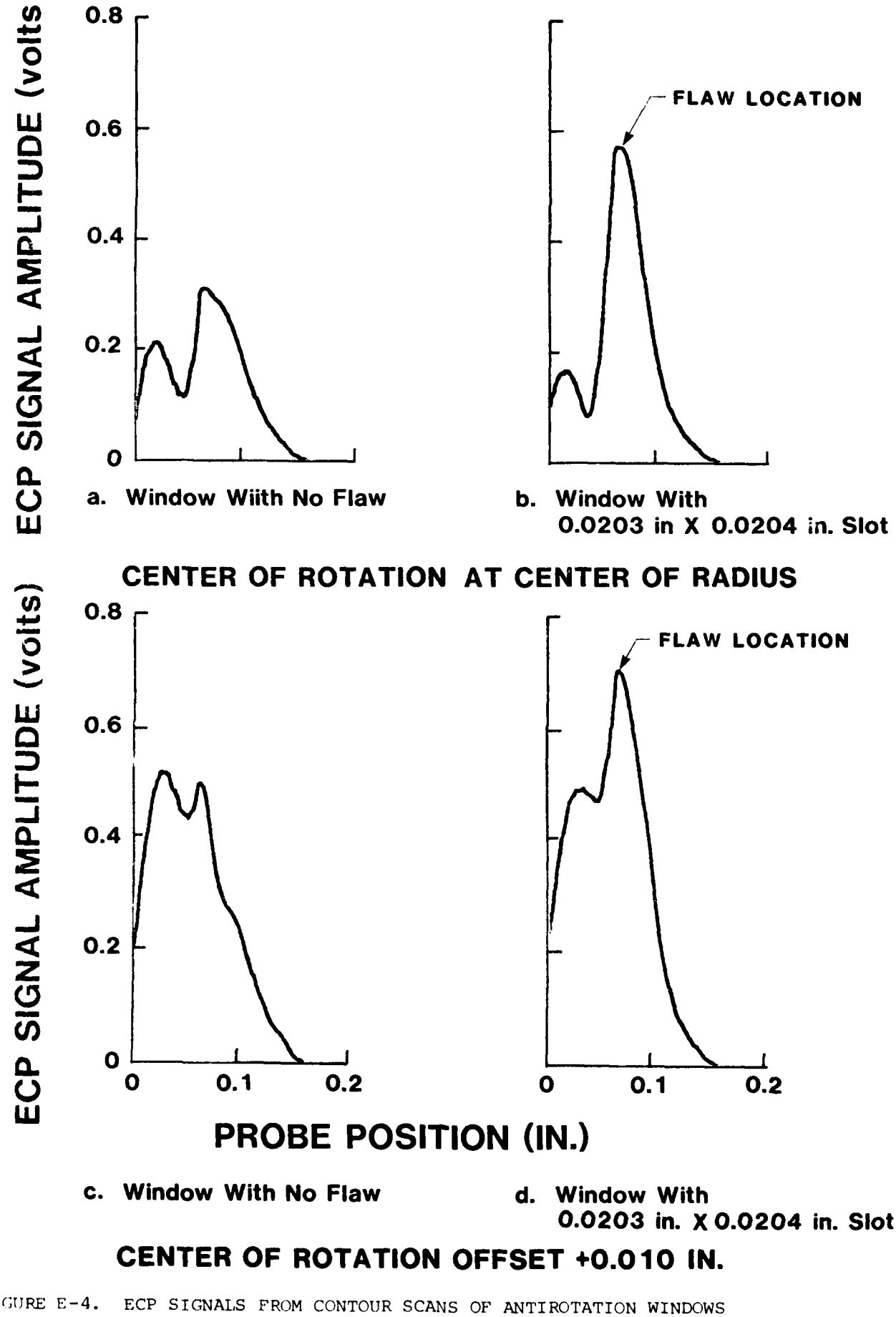

FIGURE E-4. ECP SIGNALS FROM CONTOUR SCANS OF ANTIROTATION WINDOWS IN TYPE II SPECIMEN WITH CENTER OF PROBE ROTATION AT CENTER OF RADIUS AND OFFSET +0.010 IN.

APPENDIX F

ECP PROBE CONFIGURATIONS

Figure F-1a is a schematic illustration of an ECP probe as employed in most applications. The induction coil is a cylindrical winding with axis normal to the specimen surface, much like a conventional, absolute eddy current probe. The sensor, however, is a differential winding, usually on a ferrite core, with axis parallel to the surface so as to minimize sensitivity to the unperturbed magnetic flux. The sensor is normally located just outside the induction coil, as shown in Figure F-1a.

Probes used in blade slot inspection and in linear scans past antirotation windows were of the conventional design shown in Figure F-1a. For window inspections in the linear scan mode, which were the first tests performed under the present program, a previously fabricated induction coil was used and was found to provide adequate sensitivity for flaw sizes of concern. In an effort to improve sensitivity to small surface flaws in blade slots, a probe with a somewhat smaller induction coil was fabricated. Because this second probe proved adequate for blade slot flaws, no further effort wasd devoted to probe optimization for the linear scan and blade slot inspections.

Contour scan inspection of antirotation windows required the development of a miniaturized version of the basic ECP probe. This called for induction and sensor coil windings of smaller dimensions and, in addition, placement of the sensor inside the induction coil to reduce the overall size of the package, as shown in Figure F-1b. This particular configuration, with the sensor offset as far as possible toward one side of the induction coil, had been shown in previous work[5] to provide sensitivity comparable to that obtained with the sensor outside the induction coil in its normal position.

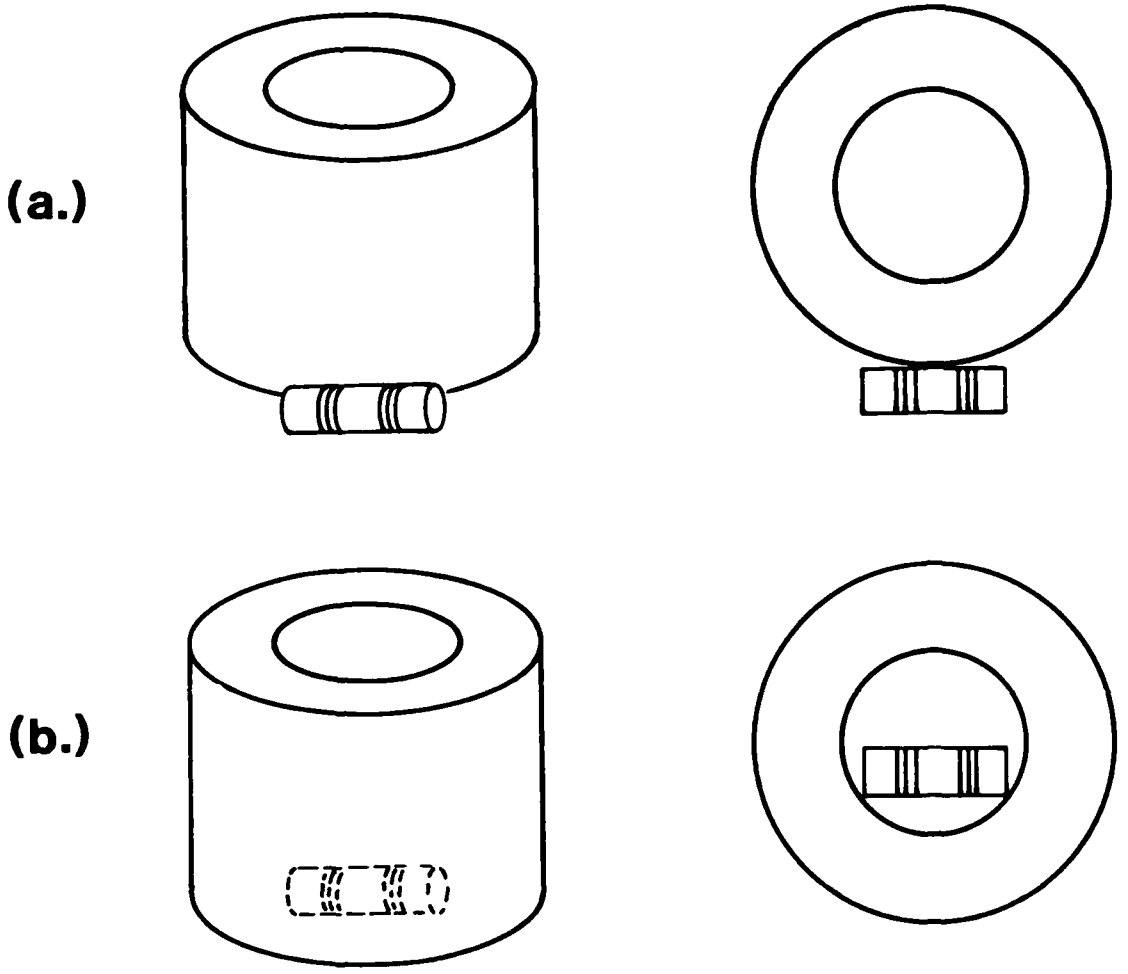

FIGURE F-1. ECP PROBE DESIGNS USED FOR (A) BLADE SLOT AND ANTIROTATION WINDOW INSPECTIONS IN THE LINEAR SCAN MODE, (B) WINDOW INSPECTION IN THE CONTOUR SCAN MODE.

*U.S.Government Printing Office: 1984 — 559-065/20554

END

FILMED

1-85

DTIC